

Progress Report

TO

IOWA STATE HIGHWAY COMMISSION

WATER VAPOR

SODIUM MONTMORILLONITE INTERACTION

Iowa Highway Research Board Project HR-97

Iowa Engineering Experiment Station Project 505-S

October 1965

by

G. L. Roderick

and

T. Demirel

IOWA STATE UNIVERSITY
of Science and Technology / Ames, Iowa



IOWA
ENGINEERING
EXPERIMENT
STATION

WATER VAPOR SODIUM MONTMORILLONITE INTERACTION

by

G. L. Roderick and T. Demirel

ERRATA

<u>Page</u>	<u>Paragraph</u>	<u>Line</u>	<u>Wrong</u>	<u>Right</u>
Abridgement-1	2	2	13 figures	12 figures
1	1	1	The investigation	The interaction
17	3	1	Hendricks and Jefferson	Hendricks and Jefferson
34	figure 8	Ordinates of 2nd and 3rd figures	$\frac{p}{q(p_0 - p_0)}$	$\frac{p}{q(p_0 - p)}$

WATER VAPOR - SODIUM MONTMORILLONITE INTERACTION

by

G. L. Roderick and T. Demirel

SYNOPSIS

The investigation of water vapor with sodium montmorillonite was investigated with X-ray diffraction and sorption isotherm (gravimetric method) experiments. Expansion of the montmorillonite occurs in three increments. The data suggest interlayer water builds up in a laminar fashion. The hysteresis of sorption isotherms is apparently due to the formation of a thixotropic structure and to attractive interlayer forces. BET parameters from adsorption isotherm data reflect adsorption only on external surfaces. Free energy data, computed from adsorption isotherm data, and X-ray data allow separation of the free energy change on adsorption into two components: one for adsorption on external surfaces, and one for adsorption on and separation of internal surfaces. The data also permits the estimation of swelling pressures exerted by sodium montmorillonite due to the uptake of interlayer water from the vapor phase.

WATER VAPOR - SODIUM MONTMORILLONITE INTERACTION

by

G. L. Roderick and T. Demirel¹

INTRODUCTION

Clay-water systems are of prime importance in the engineering usage of soils, as for example in the prediction of bearing capacity, skin friction on piles, or settlement. Past research on these matters has emphasized mechanical aspects of soil-water systems. It has been recognized, however, that some problems such as secondary consolidation, swelling pressures and cohesion are not solvable by a mechanistic approach. Therefore, it appears that a more fundamental knowledge of the clay-water system is essential for understanding and predicting the soil mechanics behavior of clays.

The objectives of this study were to obtain some fundamental knowledge of the sodium montmorillonite - water system from successive adsorption-desorption isotherms of water vapor on the montmorillonite, and from X-ray diffraction data obtained during adsorption and desorption.

¹ Assistant Professor of Civil Engineering, University of Rhode Island, and Associate Professor of Civil Engineering, Iowa State University, respectively

EXPERIMENTAL

Material

Sodium montmorillonite was chosen as the material for this investigation since the expansive clays are the most troublesome in soil engineering practice. Also, this choice provided the opportunity to study the phenomenon of interlayer adsorption of water.

The homoionic sodium montmorillonite sample was prepared from a commercially available Wyoming bentonite, Volclay-SPV produced by the American Colloid Company, by ion exchange as described in detail elsewhere (1, 2).

Methods of Investigation

Sorption isotherm study

Sorption isotherms of water vapor on sodium montmorillonite were determined by gravimetric method (3). Fig. 1 is a schematic representation of the adsorption apparatus. Bulb "A" was the permanent water reservoir vapor source. "B" was a simple mercury manostat-manometer combination for transferring vapor into the adsorption chamber "C" and for measuring vapor pressures. Mercury in "B" could be raised or lowered through air trap "D" into the mercury reservoir "E". All glass parts were pyrex; all stopcocks were mercury-sealed, and high vacuum silicone grease was used at all joints. A McBain-Bakr quartz spring balance "F" was suspended into the adsorption chamber from a mercury sealed ground glass stopper, and a thin walled glass tubing sample

holder "G" was suspended from the balance hangdown loop. The water reservoir, manostat-manometer and adsorption chamber were immersed in a water thermostat maintained at 24.4°C . The apparatus was connected to a high vacuum system by means of a mercury-sealed stopcock.

The sodium montmorillonite sample, in the sample holder, was dried for several weeks in an evacuated desiccator containing phosphorous pentoxide. The initial sample weight was found to be 158.7 mg with a certified analytical balance. The sample was then placed in the adsorption chamber which, after a brief evacuation, was closed off by the manostat while the triple distilled water in the reservoir was degassed by a repeated freezing-pumping-thawing process. With the reservoir closed off from the system, the adsorption chamber and sample were degassed by pumping at 10^{-5} mm Hg for several days. The manostat was then closed, the vacuum system closed off and the water reservoir opened to allow water vapor into the right side of the system.

After thermal equilibrium at 24.4°C was attained, an initial pressure reading, p_0 , was taken with a cathetometer reading to 0.02 mm, and corrected for temperature, gravity and meniscus. An initial balance reading was made with an optical reader; one division on the reader corresponded to 0.0239 mg of mass increase of the sample. A small increment of vapor was then transferred to the chamber through the manostat arrangement. Twenty-four hours were found to be sufficient time for the system to attain equilibrium. After this period the pressure difference on the manometer and the spring balance extension were

measured. The equilibrium pressure, p , in the chamber was found by making the required corrections on the pressure difference observed and subtracting it from the saturation pressure, p_0 . The balance extension was converted to mass increase and divided by the initial sample weight to give the mass of vapor, q , adsorbed by one gram of montmorillonite. More and more vapor was transferred in the same manner until saturation pressure was attained.

In the vicinity of saturation an additional technique was used. After the vapor transfer, a small amount of condensation was formed in the chamber side of the manometer by cooling with a few cc's of cool water. Before saturation this condensation disappeared rapidly. At saturation the time for disappearance increased to several minutes. The mass of vapor adsorbed just before and at saturation differed by less than 0.1%.

The desorption isotherm was obtained by condensing more and more vapor back into the water reservoir by cooling it with water. The sample was pumped at relative pressures, p/p_0 , below 0.3.

The adsorption apparatus, optical reader and cathetometer were all securely mounted on a rigid steel frame tied to a heavy soapstone table top to prevent differential movements. The experimental error in determining p/p_0 was calculated to be ± 0.003 for all pressure ranges. The experimental error in determining q was found to be $\pm 3 \times 10^{-5}$ gm/gm at low pressures and $\pm 3 \times 10^{-4}$ gm/gm near saturation pressure.

X-ray diffraction study

The apparatus used in the X-ray study consisted of a Rigaku-Denki

controlled atmosphere high temperature X-ray diffractometer attachment converted to serve as an adsorption chamber. The furnace and its support base were removed and a stainless steel sample holder (Fig. 2) was constructed to take their place. This sample holder could be aligned by using the translation, rotation and inclination controls provided for alignment of the furnace. The arrangement of the water reservoir source for vapor, the manometer for pressure readings, the mercury-sealed stopcock connection between the reservoir and adsorption chamber and the X-ray windows are shown in Fig. 3. The stopcock was fastened securely to a small brass cylinder which was in turn attached to a larger cylinder which fit snugly over the top of the adsorption chamber. A glass tube was attached to the exhaust port coupling by a kovar metal tube and supplied the connection between the adsorption chamber and the portable vacuum system.

The X-ray windows were made of 0.02 mm aluminum foil backed by a 1/2 mil "Mylar" polyester film. If the aluminum foil alone were used pinhole leaks developed in the windows during the experiment.

The adsorption chamber temperature was controlled by circulating water at constant temperature through the cooling tubes provided in the top and bottom portions of the apparatus. The constant temperature water was also circulated through a cooling coil fastened in a water filled dewar flask such that, when in position, the coil surrounded the water reservoir. In Fig. 3 the flask is shown to the left of the apparatus. The constant temperature water source was thermostatically

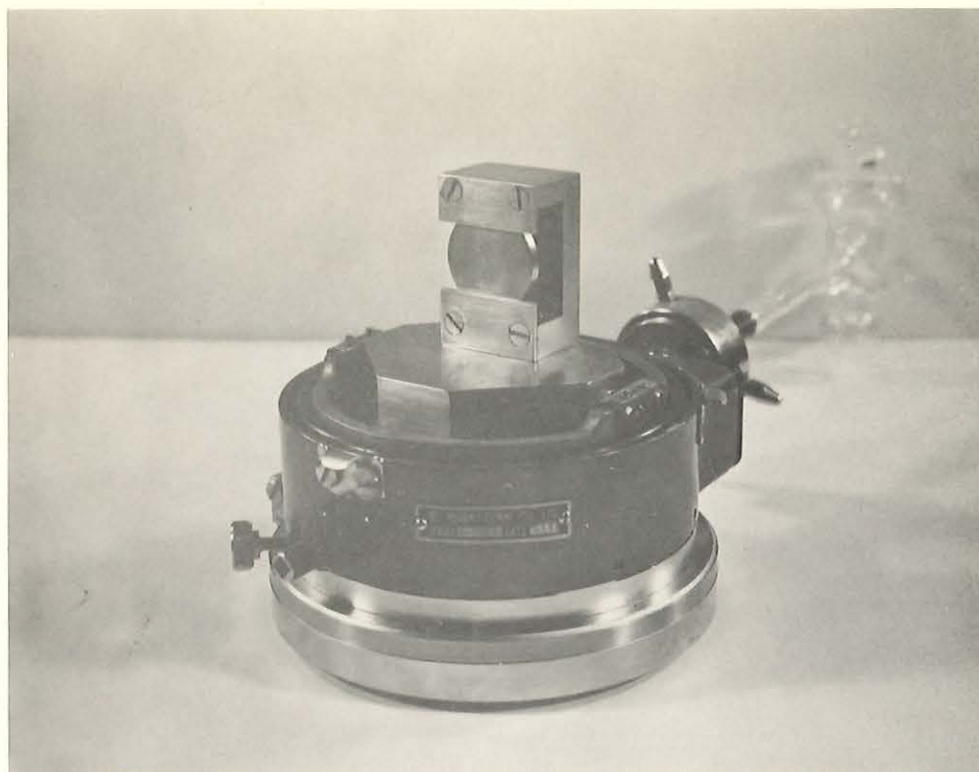


Fig. 2. Sample holder for the X-ray diffraction study

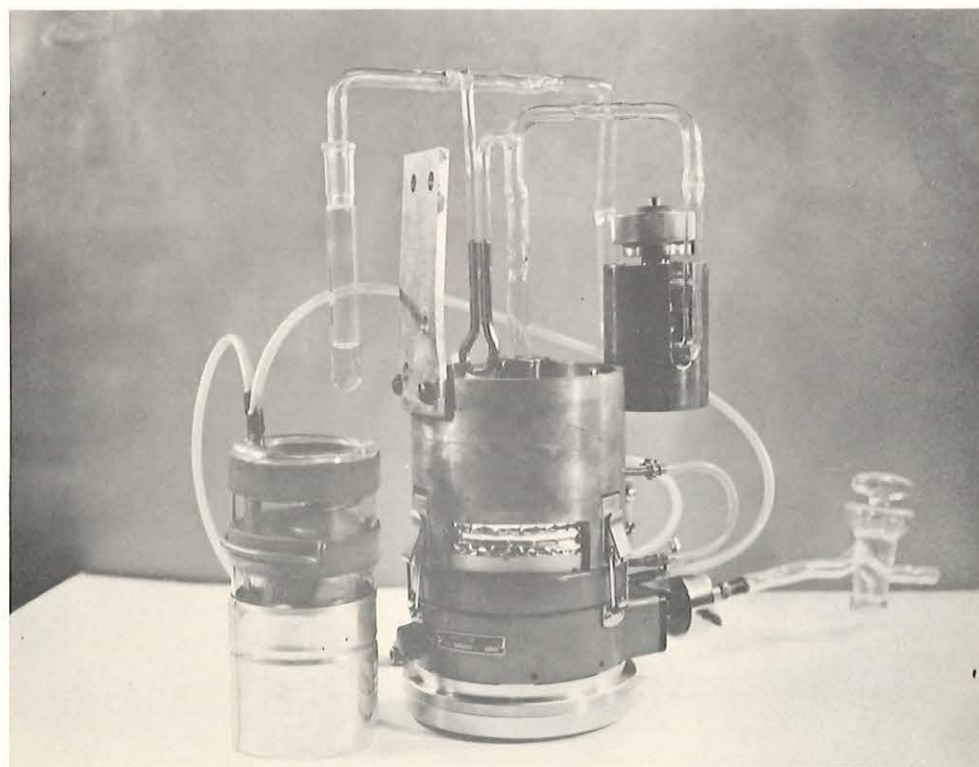


Fig. 3. Apparatus for the X-ray diffraction study

maintained at 22.99°C . The measured temperature in the dewar flask enclosing the water reservoir was 23.2°C during all readings.

A suspension of the sodium montmorillonite was pulled, by a water aspirator, through a 30 mm diameter medium porosity fritted glass disc so that a thin layer of the clay was deposited on the disc. The sample was dried in an evacuated desiccator containing phosphorous pentoxide. It was then placed in the sample holder and the top cover of the apparatus was positioned. The triple distilled water in the reservoir was degassed by a repeated freezing-pumping-thawing process. The stopcock was kept closed while the sample was pumped for several days to 10^{-4} mm Hg. The connection between the adsorption chamber and the vacuum train was cut and sealed; the apparatus was connected to the constant temperature water circulation system, placed on the General Electric XRD-5 Diffractometer and the sample aligned. When thermal equilibrium was attained the sample was X-rayed with copper $K\alpha$ radiation and five traces of the initial $9.82 \overset{\circ}{\text{A}} 001$ peak obtained. A manometer reading was taken, with a micrometer slide cathetometer reading directly to 0.001 mm, and corrected for temperature, gravity and meniscus.

After getting initial peak and pressure readings, the stopcock was partially opened to allow a small increment of water vapor into the chamber. After a period of 24 hours the pressure difference and the new peak position were observed. Each new peak position was recorded five times. In this manner more and more water vapor was

transferred to the chamber until the saturation pressure was reached. Desorption was accomplished by condensing vapor back into the water reservoir by cooling it with ice water until a p/p_0 of 0.3 was reached, and by freezing with a dry ice-acetone mixture to a p/p_0 of 0.03. The vacuum system was used to pump out the last increment.

The experimental error in determining p/p_0 was calculated to range from ± 0.007 at low pressures to ± 0.003 near saturation.

PRESENTATION AND DISCUSSION OF RESULTS

X-ray Diffraction Study

The first order basal spacings and the widths of the observed diffraction peaks obtained for two cycles of adsorption-desorption of water vapor on sodium montmorillonite are plotted against the relative pressure at which they were observed in Fig. 4. The points plotted are the average of five observations for each determination. The accuracy with which individual observations could be made depended on the size of the diffraction angle and on the sharpness of the peaks obtained, which varied with the relative pressure. The average variation from the average value for five observations of the basal spacing were less than ± 0.10 Å, with a maximum variation of ± 0.25 Å at small angles; for line widths the variations were from ± 0.01 to ± 0.10 degrees. The line widths of the diffraction peaks obtained were taken as the peak width at half-maximum intensity (4).

A shift of the adsorption curve for the second cycle from the

position of that for the first may be noted on Fig. 4. The same behavior was observed with an earlier sample used in incompletd runs. The first adsorption curve followed the present one very closely up to a p/p_0 of 0.70 when a leak developed in the X-ray window. Another incomplete run with the same sample showed a shift to a position between those shown in Fig. 4, somewhat closer to the curve for the second run. After solving the leakage problem a new sample, from which the present data was obtained, was placed in the apparatus.

Figure 4 shows the initial average basal spacing was not attained on desorption, indicating some water was left entrapped in the interlayer regions. Perhaps this remaining water, with the accompanying greater average spacing, affected the platelet interactions such that separation of the layers could more readily occur, as shown by the second curve started after a brief period of degassing..

Since the initial adsorption curves for two samples were very nearly the same, and since the procedure for reaching the initial sample condition was the same as in the adsorption isotherm study, discussions in this report will be based primarily on the initial adsorption curve for X-ray data.

Hendricks and Jefferson (5) have shown that theoretically the X-ray diffraction from a powder should show basal spacing varying continuously with water content. Hendricks et al. (6) found this to be so in their study. The data of the present study, Fig. 4, shows that the change in average basal spacing takes place in a continuous but non-uniform

manner with changes in relative pressure. The continuity is apparently due to the simultaneous existence of varying numbers of molecular layers of water between clay platelets. The line width versus relative pressure data substantiates this conclusion. The variations in widths of the observed diffraction peaks are in part due to the lack of constancy of interlayer spacing (4, p. 517) and give an indication of the relative amount of layers at the various spacings (7). Minimum line widths correspond to basal spacings on the flat portions of the curve of Fig. 4, and indicate that most of the clay platelets are nearly at the observed spacings.

Data for the desorption runs were not extensive enough to determine the shapes of the desorption curves of Fig. 4 as well as could be done with adsorption data. The data for basal spacings and line widths were fairly close for the two cycles and the desorption curves were sketched using the data for both cycles.

The quality of the intensity of diffraction peaks obtained did not permit more than a rough analysis. In general, the intensity increased as more water vapor was adsorbed and the basal spacing increased. This is consistent with the observations of others (8, 9).

Comparison with data of other investigators

Figure 5 presents the basal spacing versus relative pressure data of Hendricks et al. (6), Mooney et al. (10), Gillery (11), Demirel (1) and Messina (12) for various sodium montmorillonites. Considerable

scatter of the reported data is apparent. The solid curves trace the first adsorption-desorption cycle of the present study. This loop encloses most of the data presented.

Mooney et al. (10) used the data of Hendricks et al. (6) and their own to determine the stepwise curve presented in Fig. 5. Hendricks et al. used initially dry samples (dried over phosphorous pentoxide in vacuum), which were exposed at 30°C to water vapor, at various relative humidities ranging from 0.05 to 0.90 for a week or longer to attain equilibrium. Mooney et al. used samples taken from their adsorption apparatus during desorption at 20°C. In their first paper Mooney et al. (13) found that the desorption isotherms were reproducible provided the adsorption curve was carried up as high as the final steeply-rising section. In their second paper (10, Fig. 4) the first point of their desorption curve for sodium montmorillonite is at a p/p_0 of about 0.95. Since this is in the range of the final steep portion of the adsorption curve, perhaps they began desorption before saturation pressure was attained. Figure 4 of the present study shows that an additional increment of layer separation occurs at relative pressures above 0.95; at 0.95 the basal spacing observed was 15.6^o Å. If Mooney et al. began their desorption at a relative pressure of 0.95, their curve should begin at this spacing. Figure 5 shows that the initial flat portion of their desorption curve is at 15.5^o Å. The low position of their desorption curve as compared to that of the present study may, therefore, be due to failure to attain saturation pressure and the final increment of

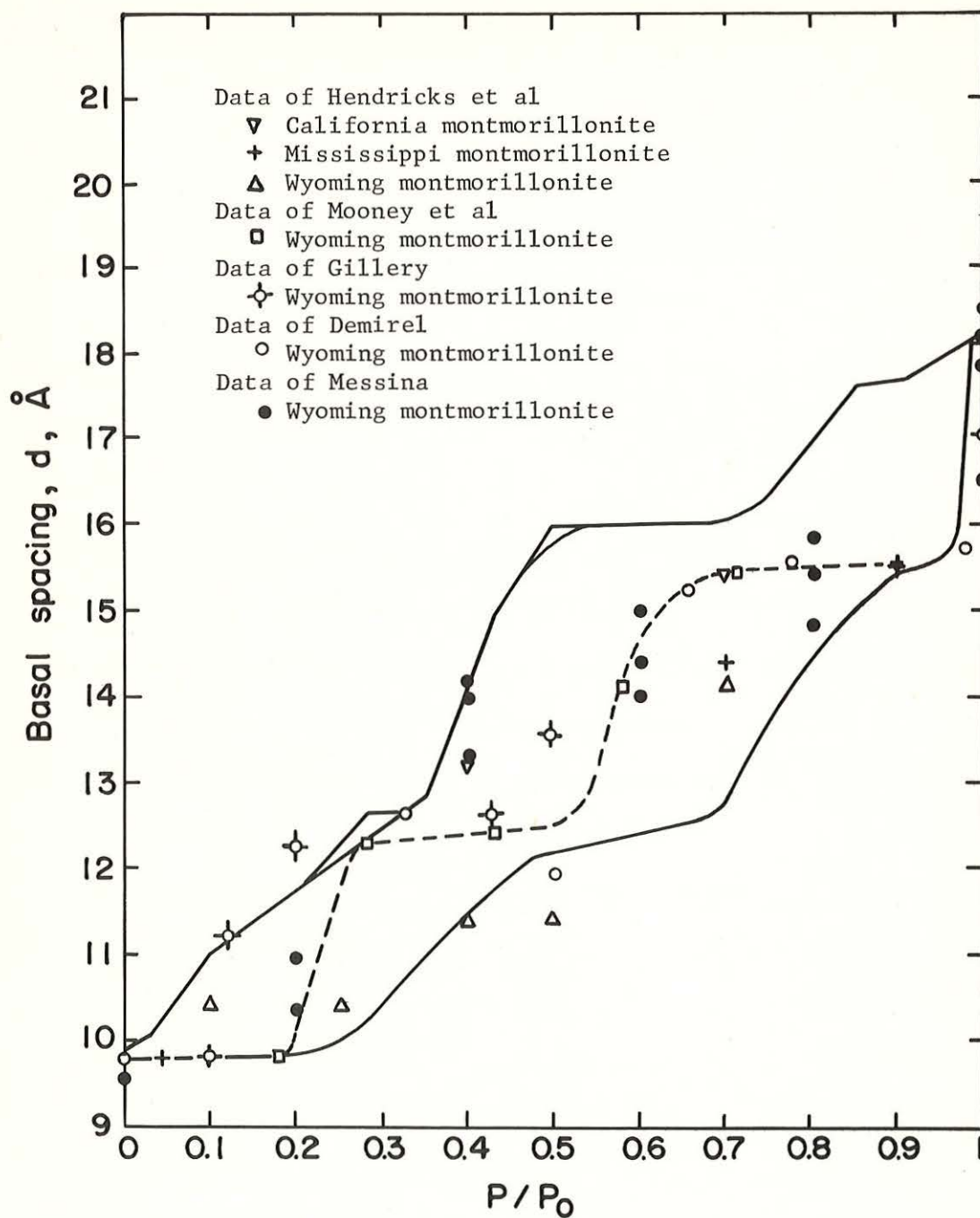


Fig. 5. Variations of first order basal spacings with relative pressure for sodium montmorillonites reported by various investigators

expansion on adsorption. This, as well as the shift in the adsorption curve due to insufficient desorption as discussed earlier, would seem to demonstrate the importance of the initial conditions of the samples.

The methods of controlling and determining relative pressures and temperature varied considerably for the investigations cited (1, 6, 10, 11, 12). This may account, to some degree, for the scatter in the reported data. Demirel (1) equilibrated his samples, at room temperature, over appropriate saturated salt solutions in vacuum desiccators, and maintained the proper relative humidity by placing a plexiglass hood over the sample and appropriate solution during exposure to X rays. Considering the differences in procedure, the data of Demirel is in good agreement with the adsorption data of the present study. Since the material used in the two studies was the same, this would seem to demonstrate the importance of the source of the material and the method of preparation.

From comparison of the X-ray data presented in the literature it was concluded that the major factors responsible for the scatter observed are: a) the initial conditions of the sample at the start of the test; b) the source and method of preparation of the material; and c) whether data is collected during adsorption or desorption. In correlating X-ray results with other methods of investigation care should be taken to assure that the material and test conditions are as nearly the same as possible.

Arrangement of interlayer water

As adsorption on the internal surfaces of montmorillonites proceeds the molecular layers of water build up either in laminae or in another spatial geometric arrangement. Hypothetical configurations for the water adsorbed on the clay surface have been postulated by several investigators (14, p. 162).

Winterkorn (15) emphasizes the dipole character of water and states, "The large adsorption forces exerted on water molecules by the surface of solid soil particles act similar to externally applied pressures.....". He postulates on the basis of the high pressure side of the phase diagram of water that pressures from adsorption "may liquify solid water or solidify liquid water". Thus, according to Winterkorn the water held on the surfaces of solid soil particles is in a physical state corresponding to either liquid water if the moisture content is high, or to one of the five crystalline forms of ice if the moisture content is low.

Hendricks, and Jefferson (5) hypothesized that an extended hexagonal net of water molecules is hydrogen-bonded to the clay mineral surface. Successive hexagonal nets build up on each other by being hydrogen-bonded to the previous one. Taking $2.76 \overset{\circ}{\text{A}}$ as the thickness of a water molecule (16, p. 464), their hypothesis results in a laminated stacking causing a separation of $2.76 \overset{\circ}{\text{A}}$ for each molecular layer of water.

Macey (17) noted the lattice similarities between the basal planes

of ice and of clay minerals. He suggested the ice structure develops on clay mineral surfaces with the hexagonal molecular configuration of the basal plane of ice. This structure tends to build outward from the surface. Forslind (18) suggested the same ice structure postulated by Macey but based his argument on the Edelman-Favejee structure rather than the Hofmann-Endell-Wilm structure of montmorillonite.

Demirel (1) presented two ways in which the ice structure may develop in the interlayer regions. Using data reported in the literature and his own for various species of homoionic montmorillonites, he found evidence to support the buildup of an ice structure in which the first hexagonal network is shared by two montmorillonite platelets causing a separation of $2.76 \overset{\circ}{\text{A}}$; two hexagonal networks are stacked and held by the two silica surfaces causing a separation of $5.52 \overset{\circ}{\text{A}}$; the third and fourth molecular layers of water fill in between the hexagonal networks forming tetrahedrons with the water molecules of the network. A complete unit cell of ice is formed with the entrance of the fourth molecular layer of water, causing a separation of $7.36 \overset{\circ}{\text{A}}$. The fifth and sixth layers of water enter between the unit cell of ice and the clay surfaces, forming hexagonal networks and causing separations of $10.12 \overset{\circ}{\text{A}}$ and $12.88 \overset{\circ}{\text{A}}$, respectively.

Barshad (19) suggested an arrangement which becomes progressively denser with addition of water. He postulated arrangements for water molecules that would give various increases in basal spacing for each additional molecular layer of water, depending on the position of

water molecules with respect to the basal oxygens of the clay surface and to water molecules of previously adsorbed layers. The first layer would give spacing increases of 2.76 or 1.78 Å; other layers would give increases of 2.76 or 2.09 Å.

The continuity of the basal spacing versus relative pressure curve of the present study has been attributed to the simultaneous existence of clay platelets separated by various molecular layers of water. If all of the interlayer water has been removed at zero relative pressure, a sharp peak will be observed corresponding to the collapsed basal spacing of sodium montmorillonite, about 9.60 Å (20). As the relative pressure increases some water begins to penetrate between some of the clay layers. If it is assumed that at low relative pressures the system consists primarily of layer spacings corresponding to zero and one molecular layers of water between platelets, i.e., that the contributions of layers separated by 2, 3 or more molecular layers of water to the observed diffraction peaks are negligible, then the system may be treated as a random interstratification of two components. At somewhat higher relative pressures the observed peaks may be treated as composite peaks from another random two component system, one component corresponding to one molecular layer of interlayer water and the other to two such layers. This may be extended to higher increments of expansion. As the relative pressure increases, the relative proportions of the two components change and the observed diffraction peaks migrate from the position

of the first pure component, A, toward that of the other pure component, B. According to MacEwan, Amil and Brown (7), in a preliminary analysis there will be no great error in assuming that the peaks move linearly between the two pure component positions. When the distances from the observed peak to the A and B positions are x and y , respectively, the proportion of component A is deduced to be $y/(x + y)$. As the observed peak migrates from the A position it first becomes diffuse and then sharper again as it approaches the B position. Taking the line width to be a function of the nonconstancy of layer separations, we would suspect that a maximum width would correspond to the most random distribution of the two layer separations and that this would occur when the relative proportions of the two components are nearly equal. Although this conclusion may not be strictly true (7), it is felt that assuming the maximum line width corresponds to an A/B ratio of one will be in no greater error than that in assuming the peak migration to be linear.

If it is assumed that : a) the system of the present study may be treated as a random interstratification of two components; b) peak migration between pure component positions is linear; and c) maximum line widths occur when the relative proportions of the two components are equal, the line width and basal spacings data of this study may be used to test possible arrangements for the interlayer water that have been postulated by others. The minimum line widths should correspond to a basal spacing near that calculated from the proposed

arrangement for an integral number of molecular layers of water between clay platelets. If assumptions b and c hold, the maximum line widths should occur at a basal spacing which is the average of those calculated for two successive layers of water between platelets.

The observed basal spacing and line widths for the first adsorption run are plotted against one another in Fig. 6. Using 9.60 \AA as the collapsed basal spacing of sodium montmorillonite, the basal spacings for integral numbers of molecular layers of water between platelets and the averages of each two successive spacings were calculated for the various postulated interlayer water arrangements. At low pressures the values obtained for the laminated structures and the ice-like structure of Demirel (1) showed the best agreement with experimental data; the values calculated for these arrangements are presented in Table I.

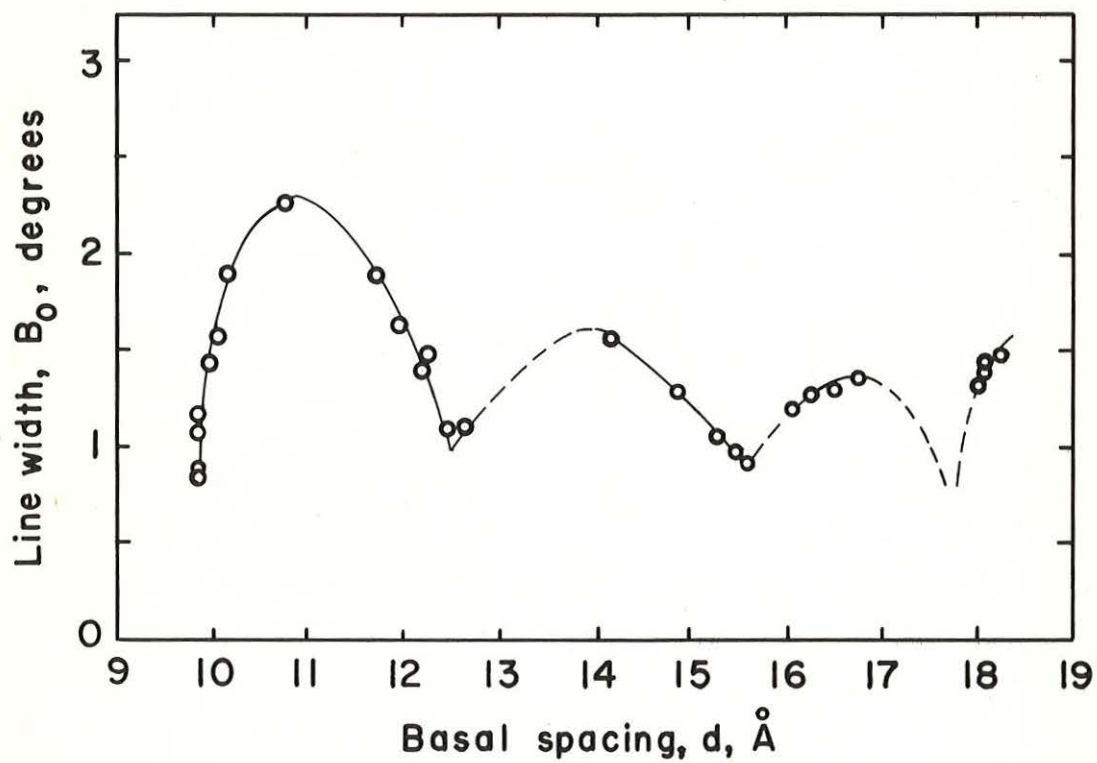


Fig. 6. Variation of line widths with basal spacings of sodium montmorillonite

Table I. Calculated first order basal spacings of sodium montmorillonite

Number of molecular layers of water	Laminated, stacking arrangement of water		Ice-like arrangements of water molecules	
	Calculated basal spacings, Å	Average, two successive spacings, Å	Calculated basal spacing, Å	Average, two successive spacings, Å
0	9.60	10.98	9.60	10.98
1	12.39	13.74	12.36	13.74
2	15.12	16.50	15.12	13.74
3	17.88	19.26	15.12	16.04
4	20.64	22.02	16.96	18.34
5	23.40		19.72	

The first maximum line width occurs at a basal spacing of about 11.0 Å, very near the 10.98 Å average calculated for zero and one molecular layers of water. The first minimum line width occurs at about 12.5 Å, which is close to the calculated value of 12.36 Å for one molecular layer of water. Although the observed data is scarce, the second maximum line width appears to be at about 14 Å which is reasonably near the 13.74 Å average for one and two layers of water. The second minimum line width is at about 15.5 Å, somewhat higher than the 15.12 Å calculated for two layers of water. The higher than expected basal spacings corresponding to the observed line width minima may be due to failure of the assumption of a

two-component system in the region near the peak position for a pure component (all platelets at one spacing). As the peak position approaches that for a pure component the number of platelets at the next increment of expansion increase and most probably their contributions to the observed peak are no longer negligible. Therefore, the system in this region is likely to be one of three rather than two components and the observed minimum line width may well occur at a slightly higher average basal spacing.

The rest of the data plotted in Fig. 6 are not very conclusive. The X-ray data in this region are all in the p/p_0 range of 0.97 to 1.00 and are quite crowded. However, Fig. 6 does show that a probable maximum line width does occur at a basal spacing greater than about 16.7 Å. This is closer to the 16.5 Å average calculated for laminated structures than it is to the 16.04 Å average for the ice structure. The last group of points in Fig. 6 suggest a minimum line width may occur at an average basal spacing of slightly less than 18 Å. Again, this is nearer the 17.88 Å calculated for three molecular layers of water in a laminated structure than it is to the 16.96 Å calculated for four molecular layers of water in an ice structure. More extensive data at high relative pressures are needed for a definite conclusion to be drawn. Smaller increments of vapor transfer at high relative pressures may enhance the line width - basal spacing relationship in this region.

The data of this study gives evidence of the formation of a

laminated arrangement of the interlayer water rather than an ice structure for sodium montmorillonite with up to three layers of water. The arrangement in individual layers of water can not be ascertained from this data. More detailed studies with sodium montmorillonite, and with other materials such as calcium montmorillonite, may give more complete evidence. Also, better data on the intensity of diffraction peaks may be helpful. Other methods of investigation, e.g., nuclear magnetic resonance studies, heat capacity studies, etc. may also enable more definite conclusions to be drawn.

Sorption Isotherm Study

Figure 7 is a plot of the sorption isotherms for three successive adsorption-desorption cycles. The adsorption and desorption branches fall in different regions of the plot, illustrating the hysteresis expected with porous absorbents (3).

The data of the present study show that the adsorption branch is more closely reproduced on successive runs than is the desorption branch. After a p/p_0 value of about 0.28, the adsorption curves for the first and third cycles follow one another very closely, within the experimental error given previously. The desorption curves for these two cycles are not in as good agreement until relative pressures below 0.30 are reached. Neither the adsorption nor desorption branches for the second run, which began at a higher value of q , agree very well with those for the other cycles. If the isotherm for

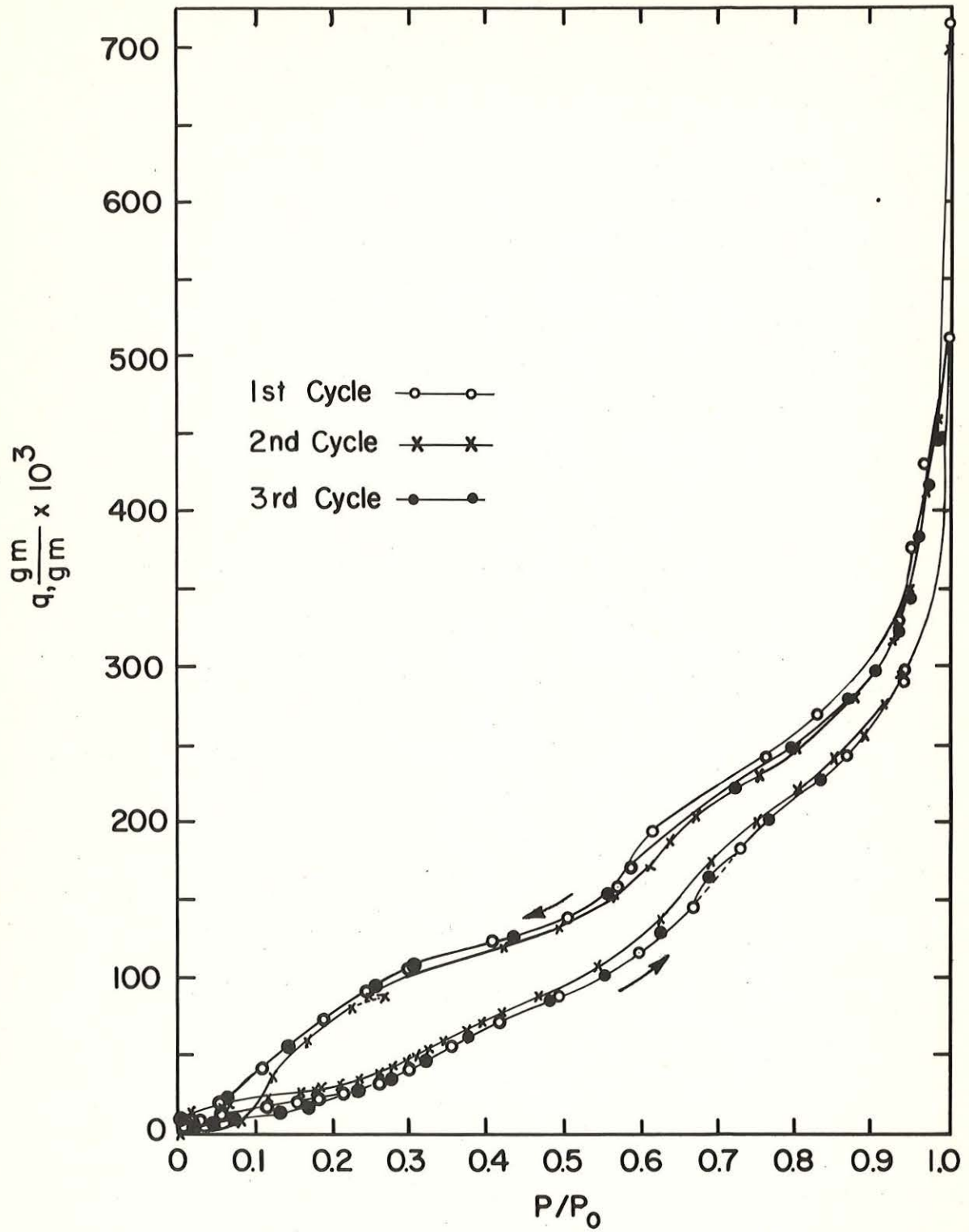


Fig. 7. Adsorption and desorption isotherms of sodium montmorillonite

the second cycle is started at the origin the agreement is much better for adsorption than for desorption. The data suggest that the adsorption branch may be the true equilibrium curve. This would be in agreement with the "ink bottle" theory of McBain (21) and the "open pore" theory of Foster (22), both of which explain the hysteresis on the basis of the shape and arrangement of the pores in which capillary condensation takes place.

Barrer and MacLeod (23) studied the adsorption of various non-polar and polar gases and vapors, including water vapor, by a sodium-rich montmorillonite, and gave an explanation for the hysteresis observed when polar vapors are adsorbed in the interlayer regions. When nucleation of an adsorbate rich phase occurs around the periphery of crystallites it must be associated with strain and interfacial free energies, which slow down the free development of the adsorbate-rich phase until the pressure has exceeded the value for true thermodynamic equilibrium between the vapor and separated montmorillonite layers with and without interlayer adsorbate. On desorption the development of the adsorbate-poor phase in the interlayer region is delayed by strain and interfacial free energy until the pressure has fallen below that for true equilibrium, and a hysteresis loop is observed.

Hirst (24) also developed a similar explanation for hysteresis associated with interlayer adsorption. Attractive forces between layers prevent penetration of the adsorbate until a threshold pressure is reached. These forces are then overcome by forces leading to penetration and the layers separate to admit a layer of adsorbate. On desorption

the layers are initially separated and their attractive interaction weakened while the forces tending to separate them are high. The layers can not come together until the amount of interlayer adsorbate, and thus swelling pressure, are substantially reduced. Therefore, a hysteresis loop is observed.

According to Brunauer (3, p. 409) the adsorption process most probably causes a change in the pore volume which may be either reversible or irreversible. This may result in different pore ar-

rangements in the external surfaces of the montmorillonite and may account for the difference in the adsorption curves prior to a relative pressure of about 0.28 for the first and third cycles. X-ray diffraction data show that at a p/p_0 of about 0.28 the basal spacing begins to increase rapidly with increasing p/p_0 . It is in this region that the adsorption curves begin their agreement, suggesting that the effect of the interlayer surfaces far outweighs that of the external surfaces.

The general shape of the adsorption and desorption isotherms in Fig. 7 is very similar to those presented elsewhere (1, 13, 23, 25). Figure 4 shows that the steeper portion between p/p_0 of 0.25 and 0.45 on Fig. 7 corresponds to the first increment of layer separation. The steeper portion of the isotherm beginning at a p/p_0 of 0.65 corresponds to the second increment of layer separation. The argument proposed by Barrer and MacLeod explains the form of the adsorption isotherm of this study. The initial water adsorbed is mainly confined to the external surfaces of the clay. After an approximate threshold pressure is reached the water molecules penetrate more freely between clay sheets and cause separation. With water vapor, a second stage of interlayer adsorption occurs and is reflected by the second steeper portion of the isotherm. As p/p_0 approaches 1.0, capillary condensation occurs. The X-ray data show that a third increment of layer separation also occurs at high relative pressures.

The desorption isotherms show a pronounced dip in the relative

pressure range of 0.65 to 0.30. This is also shown in data of others (13, 23, 25). Barrer and MacLeod attribute the steep portion of this dip to the removal of interlayer adsorbate; the process occurring at an approximate threshold pressure below that for the adsorption curve. The X-ray data of the present study show that the basal spacing remains nearly constant at $16 \overset{\circ}{\text{A}}$ in the relative pressure range 0.65 to 0.50 corresponding to the steep portion of the dip. This would indicate that the greater portion of the water being desorbed is from the external surfaces.

Barrer and MacLeod (23) observed hysteresis loops for the adsorption-desorption of non-polar gases and vapors on their montmorillonite. Since these adsorbates were adsorbed only on external surfaces, the reasons given for hysteresis with polar adsorbates are not applicable. They suggest that when the clay is lubricated by a film of capillary condensate some of the clay particles are drawn by surface tension forces into a thixotropic structure. This more regular array then retains capillary condensed adsorbate more firmly than would a purely random array. When the film of condensate becomes sufficiently dilute it ceases to lubricate and hold the thixotropic structure together. The array then becomes more random again and must give up the remaining condensate. The desorption isotherm becomes steeper and, with non-polar adsorbates, closes the hysteresis loop.

In view of the X-ray data of the present study, it is proposed

that the above argument may be applied to the desorption of water vapor in the relative pressure range of 0.65 to 0.50. The steep portion of the isotherm in this range is, therefore, due to the destruction of a thixotropic structure with its accompanying release of capillary condensed water. The X-ray data show that removal of the last layer of interlayer water corresponds to a steep portion of the desorption isotherm beginning at a p/p_0 of about 0.30. The hysteresis explanations of Hirst (24) and of Barrer and MacLeod (23) are applicable in this region.

Figure 7 shows that the desorption branches for the first and third cycles do not come back to the initial q value, but that the desorption branch of the second cycle does reach this value. A possible explanation for the more complete desorption for the second cycle is proposed. Figure 7 shows a break in the second desorption curve at a relative pressure of about 0.25. At this point no vapor transfers were made for a period of 18 days, after which it was observed that the sample had desorbed more water and the relative pressure had increased as shown by the shift (dashed line) to a position lower and to the right. Two more days disclosed no additional change. The next vapor transfer caused a shift down and to the left (second dashed line) in one day. Before the 18 days with no vapor transfers it appeared that the second desorption curve was approaching the path followed in the first run and later followed in the third cycle. However, after the idle period the desorption curve

became steeper and the zero value of q was attained with relative ease. On the third run, with no prolonged non-vapor-transfer period, a special effort was made to reach the initial value of q . Even with a final pumping period extending over a period of three weeks the value of q could not be brought substantially lower than that attained on the first run. This suggests that the remaining water was trapped in external pores (such as McBain's "ink bottle" pores) and/or the interlayer regions. X-ray diffraction data, Fig. 4, indicate that at a relative pressure of 0.25 the last layer of interlayer water had started to be withdrawn. This is also shown by the data of Mooney et al. (10) and of Gillery (11) reproduced in Fig. 5. The prolonged period of no vapor transfer may allow for particle rearrangement and for escape of water from pores and interlayer regions which would be blocked off by contraction of the mass on further desorption.

The behavior discussed above for a prolonged non-vapor-transfer period would indicate that equilibrium was not attained in the 24 hour period between vapor transfers, at least in that region of the desorption isotherm. There was a similar non-vapor-transfer period of 20 days, at a relative pressure of 0.70 on the desorption curve, with no significant change in the location of the position observed 24 hours after the vapor transfer, indicating equilibrium was attained in 24 hours.

No relaxation of the type described here was observed for ad-

sorption runs; 24 hours were enough for attainment of equilibrium.

Application of BET Theory

In the low pressure region the Brunauer, Emmett and Teller theory of multimolecular adsorption (26) predicts the adsorption equation will be $\frac{p}{q(p_0 - p)} = \frac{1}{q_m C} + \frac{C - 1}{q_m C} \frac{p}{p_0}$, where q_m is the mass of vapor adsorbed when the solid surface is covered by a monolayer and C is a constant approximately equal to $e^{(E_1 - E_L)/RT}$, where E_1 is the heat of adsorption of the first layer and E_L is the heat of liquefaction of the vapor.

The values of the BET function, $\frac{p}{q(p_0 - p)}$ calculated from the sorption isotherm data, are plotted against p/p_0 in Fig. 8 for the three sorption cycles. Generally, BET plots will have a straight line region only between p/p_0 of 0.05 to about 0.3 (27, p. 481). The curves of Fig. 8 show that a fairly straight line is obtained for the adsorption data between p/p_0 of 0.05 and 0.18. Comparison with the initial adsorption curve for basal spacings, Fig. 4, reveals that at p/p_0 of 0.18 the first increment of interlayer separation is just beginning. Therefore, it was concluded the linear portion of the BET plot represents adsorption taking place predominantly on the external surfaces of the montmorillonite, and the BET parameters q_m and C represent the external surfaces. The values of these parameters are given on Fig. 8.

The present BET plots show a hump at a p/p_0 of about 0.2 and another deflection point at a p/p_0 of about 0.6 to 0.7. The X-ray

sorption runs; 24 hours were enough for attainment of equilibrium.

Application of BET Theory

In the low pressure region the Brunauer, Emmett and Teller theory of multimolecular adsorption (26) predicts the adsorption equation will be $\frac{p}{q(p_0 - p)} = \frac{1}{q_m C} + \frac{C - 1}{q_m C} \frac{p}{p_0}$, where q_m is the mass of vapor adsorbed when the solid surface is covered by a monolayer and C is a constant approximately equal to $e^{(E_1 - E_L)/RT}$, where E_1 is the heat of adsorption of the first layer and E_L is the heat of liquefaction of the vapor.

The values of the BET function, $\frac{p}{q(p_0 - p)}$ calculated from the sorption isotherm data, are plotted against p/p_0 in Fig. 8 for the three sorption cycles. Generally, BET plots will have a straight line region only between p/p_0 of 0.05 to about 0.3 (27, p. 481). The curves of Fig. 8 show that a fairly straight line is obtained for the adsorption data between p/p_0 of 0.05 and 0.18. Comparison with the initial adsorption curve for basal spacings, Fig. 4, reveals that at p/p_0 of 0.18 the first increment of interlayer separation is just beginning. Therefore, it was concluded the linear portion of the BET plot represents adsorption taking place predominantly on the external surfaces of the montmorillonite, and the BET parameters q_m and C represent the external surfaces. The values of these parameters are given on Fig. 8.

The present BET plots show a hump at a p/p_0 of about 0.2 and another deflection point at a p/p_0 of about 0.6 to 0.7. The X-ray

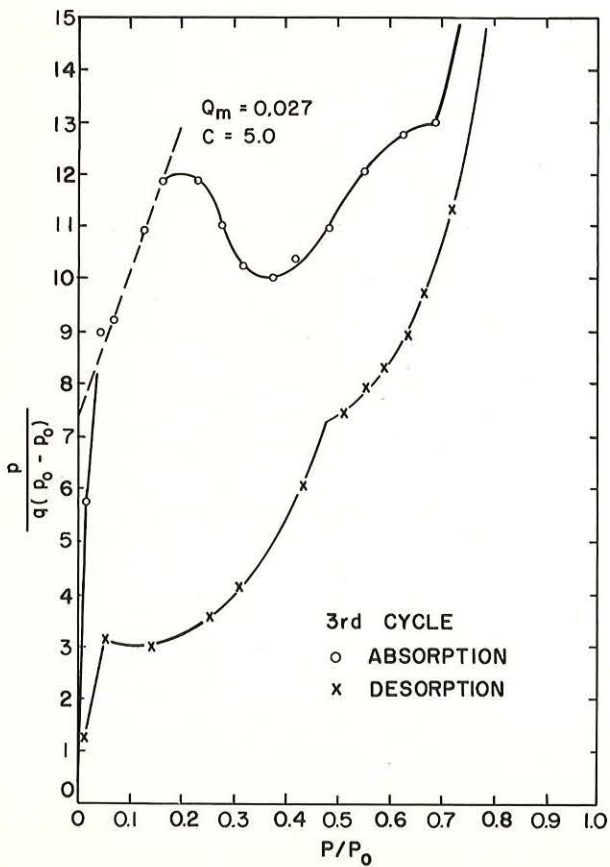
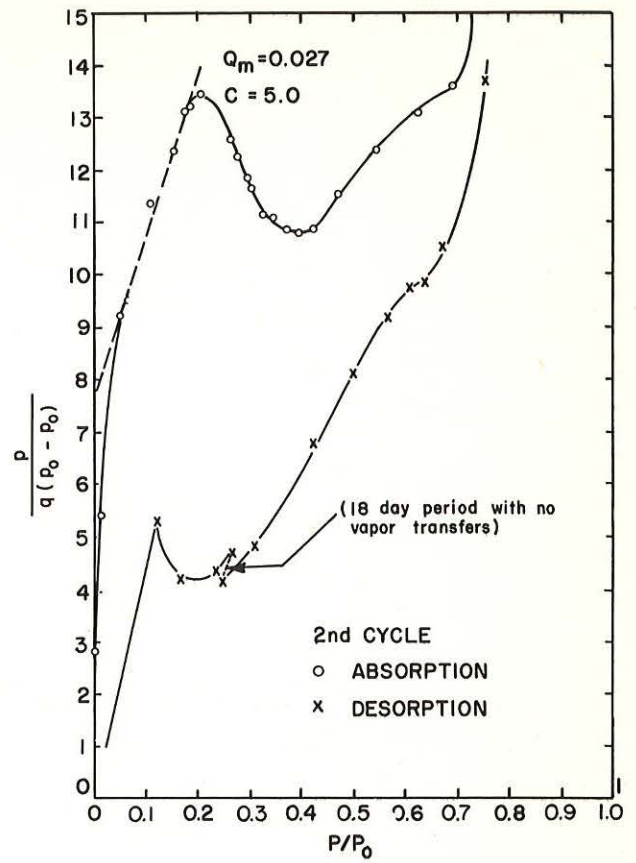
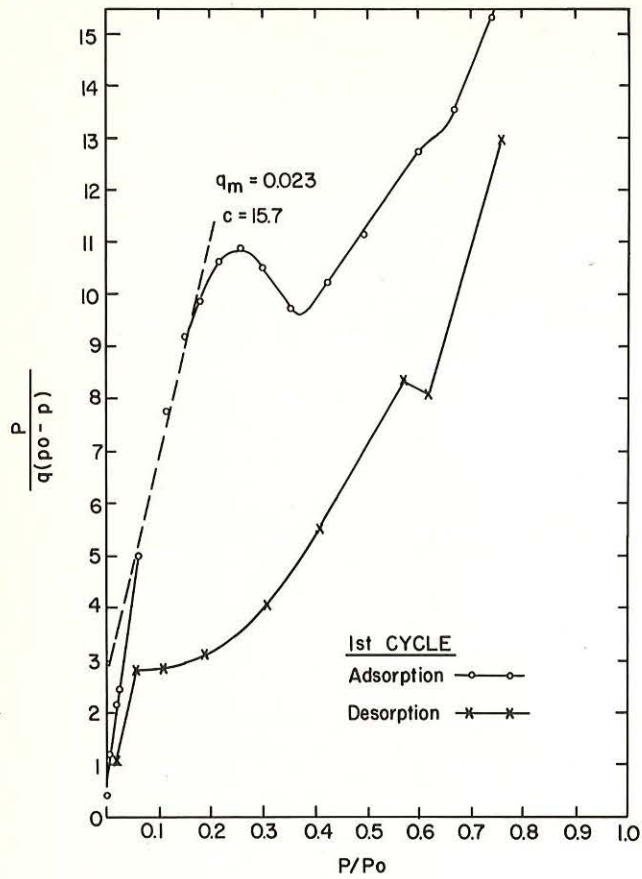


Fig. 8. BET plots of sorption data for water vapor on sodium montmorillonite

data show that these correspond with the initial portions of the first and second increments of expansion. Apparently the behavior is due to expansion making accessible surface areas not initially available for adsorption.

The pronounced hump at a p/p_0 of 0.20 appears to be a characteristic which occurs only with sodium Wyoming montmorillonite (Volclay). The adsorption data of Hendricks *et al.* (6) for sodium Wyoming montmorillonite (Volclay) yields a very similar hump, while their data for sodium Mississippi and California montmorillonites do not. The data of Johansen and Dunning for sodium Wyoming montmorillonite (Volclay) would seem to be an exception; however, their data (25, Fig. 2) show no experimental observations in the p/p_0 range in which the hump occurs. Also, the q_m value of 0.056 obtained from their data is in very good agreement with values of 0.054, 0.058 and 0.055 obtained if the present BET plots in the p/p_0 range of 0.4 to 0.6 are extrapolated back to low pressures. Orchiston's data for sodium Arizona montmorillonite (28) show a high point on the BET plot at a p/p_0 of 0.05. This may represent a behavior similar to that observed much more clearly with the present data, i.e., adsorption on external surfaces before penetration of water between clay layers, and may indicate that expansion begins at an appreciably lower relative pressure than for the Wyoming material.

External surface area

If the area, s , of the adsorbent surface occupied by each water molecule of the monolayer was known, the parameter q_m could be used to determine the external surface area, A_e , per gram of montmorillonite by the expression: $A_e = \frac{Nq_m s}{M}$, where N is Avagradros constant, M is the molecular weight of the adsorbate, and q_m is expressed per gram of adsorbent. If the water molecules are in a closest packing arrangement s is equal to 10.8 \AA^2 . However, other investigators have suggested other spatial geometric arrangements which result in other than closest packing for the monolayer coverage. The arrangement of Hendricks and Jefferson (5) gives an area of about 11.5 \AA^2 ; the basal plane of ice structures of Macey (17), Forslind (18) and Demirel (1) give an area of about 17.5 \AA^2 . External surface areas per gram of sodium montmorillonite, A_e , were computed using each of the above areas for the water molecule and the q_m values obtained from the adsorption data. The results are presented in Table 2. The external area increased somewhat during the first adsorption-desorption cycle; the sorption process may result in different pore shapes and volumes in the external surfaces and in different arrangements of the surfaces, thus making more area available for adsorption. The external areas obtained are larger than those reported by others as determined from nitrogen adsorption, i.e., 41 to 71 m^2/gm by Emmett et al. (29) 33 m^2/gm by Mooney et al. (13), 38 m^2/gm by

Johansen and Dunning (25) and $24.5 \text{ m}^2/\text{gm}$ by Zettlemyer et al. (30). This indicates some portions of the external surfaces are accessible to water vapor but not to nitrogen. Also, the line width data of Fig. 4 show that there may be a small amount of water penetration into interlayer regions.

Table 2. External surface areas per gram of sodium montmorillonite calculated from water vapor adsorption data

Cross-sectional area per water molecule, A^2	External surface area, A_e , m^2/gm		
	First cycle $q_m = 0.023$	Second cycle $q_m = 0.027$	Third cycle $q_m = 0.028$
10.8	83.0	97.4	101.1
11.5	88.3	103.7	107.5
17.5	134.4	157.8	163.7

Heat of adsorption

The C parameters obtained in this study were used to calculate $E_1 - E_L$ values for the first monolayer of water adsorbed on external surfaces. The values, corrected according to Clappitt and German (31), were 3.3, 2.7 and 2.7 Kcal/mole and were in good agreement with values reported elsewhere (1, 28). Calculations from the calorimetric heat of immersion data of Zettlemyer et al. (30) yielded $E_1 - E_L$ values of 3.0 to 3.7 Kcal/mole for the first monolayer on external surfaces.

The heat of adsorption curve presented by Zettlemyer et al. (30, Fig. 4) from their heat of immersion and adsorption isotherm data does not show good agreement with isosteric heat of desorption isotherm data curve of Mooney et al. (13, Fig. 5) from desorption isotherm data. It does, however, show good agreement with the isosteric heat of adsorption data of Takizawa (32) from adsorption isotherms with Niigata bentonite. This may indicate that the adsorption isotherm is nearer the true equilibrium curve than is the desorption isotherm.

Free Energy Changes

Free energy of wetting

The free energy of wetting of sodium montmorillonite may be given as (1): $\Delta F = (\gamma_{sl} - \gamma_{so}) + \alpha \Delta V$, where γ_{sl} is the solid-liquid interfacial tension, γ_{so} the surface tension of the solid in vacuum, α the interlayer surface area per cm^2 of total surface and ΔV the free energy change per cm^2 of interlayer surface due to separation of layers against the force of interaction. ΔF was calculated from the adsorption isotherms by using Bangham's free energy equation (33), which may be expressed as:

$$-\frac{RT}{MA} \int_0^1 \frac{q}{p/p_0} d(p/p_0), \text{ where } R \text{ is the gas constant, } T \text{ the absolute}$$

temperature, M the molecular weight of water and A the specific surface of sodium montmorillonite. Figure 9 presents plots of $\frac{q}{p/p_0}$ versus

p/p_0 for graphical integration of the above equation. From crystallographic

data, A was determined to be $748 \text{ m}^2/\text{gm}$ for the sodium montmorillonite. The error in values of ΔF obtained was estimated to be about $\pm 6\%$. The free energies of wetting thus determined were -40.55 ± 2.43 , -36.15 ± 2.17 and $-37.50 \pm 2.24 \text{ ergs/cm}^2$ for the first, second and third adsorption runs. These values are in good agreement with that of $-34.76 \pm 1.91 \text{ ergs/cm}^2$ determined earlier for sodium montmorillonite (1).

Free energy changes on adsorption

Fu and Bartell (34), in their paper on the surface areas of porous adsorbents, evaluated the integral $-\frac{RT}{M} \int_0^{p/p_0} \frac{q}{p/p_0} d(p/p_0)$ at various values of p/p_0 for the adsorption of vapors on porous solids. When q is the mass of vapor adsorbed per gram of solid, the value obtained is the free energy change, $A\Delta F$ in ergs/gm of solid, for adsorption from a relative pressure of zero to p/p_0 . When $\log(A\Delta F)$ was plotted against $\log(p/p_0)$, two straight line portions were obtained.

In discussing their method, Fu and Bartell state:

"It is also conceivable that, with suitable interpretations, this method can be utilized to study the expansion or deformation of porous materials caused by the adsorption of various vapors".

Sodium montmorillonite is a porous material which undergoes expansion with adsorption of water vapor; therefore, it was felt that an analysis similar to that of Fu and Bartell may be instructive.

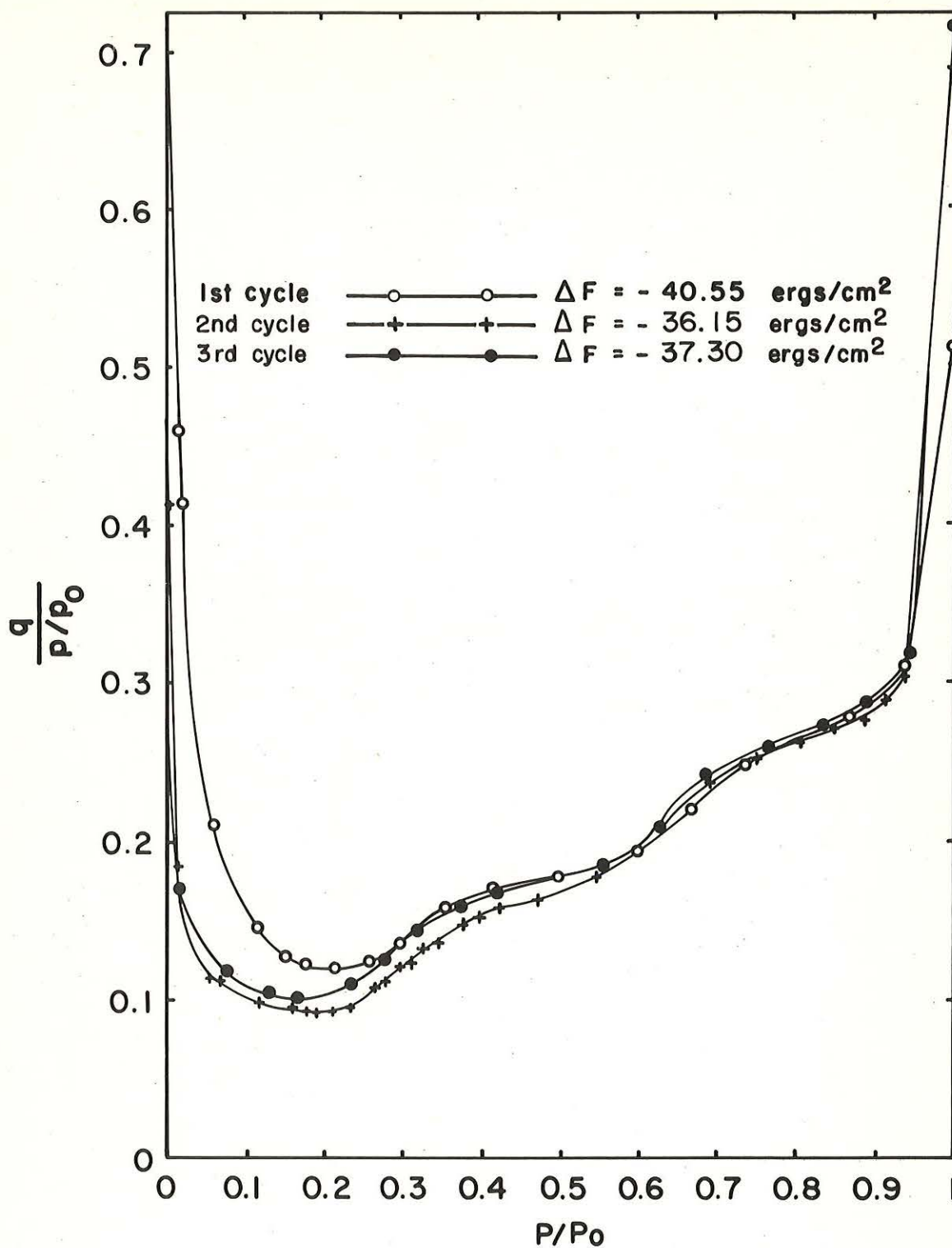


Fig. 9. Plots for integration of Bangham's free energy equation for water vapor adsorption on sodium montmorillonite

The values of the integral

$$-\frac{RT}{M} \int_0^{p/p_0} \frac{q}{p/p_0} d(p/p_0)$$

for increasing increments of p/p_0 , up to and including the saturation point, for the adsorption data of the present study were determined by graphical integration. This was also done with the adsorption data obtained earlier for sodium montmorillonite (1). Values of the integrals, $A\Delta F$, were thus obtained for four complete adsorption runs involving two separate samples of the material.

Plots of $\log(A\Delta F)$ versus $\log(p/p_0)$ are presented in Fig. 10 for each run. Each of the plots display three straight line portions (implying equations of the type $A\Delta F = \alpha(p/p_0)^\beta$ for various portions) rather than the two obtained by Fu and Bartell. The portions of the plots below p/p_0 of about 0.05 are not strictly linear but breaks in the slopes can be observed in the p/p_0 range of 0.045 to 0.055. This is in agreement with the observations of Fu and Bartell. They reported nonlinearity below p/p_0 of 0.05 and attributed it to the decreased accuracy in determining q values at very low pressures.

Comparison of Fig. 10 with the X-ray data for the initial adsorption run reveals that the break in the $\log(A\Delta F)$ plot at a p/p_0 of 0.16 to 0.18 corresponds closely with the beginning of an increase in the basal spacing from 9.8 Å. The break at a p/p_0 of about 0.65 corresponds quite closely with the beginning of a

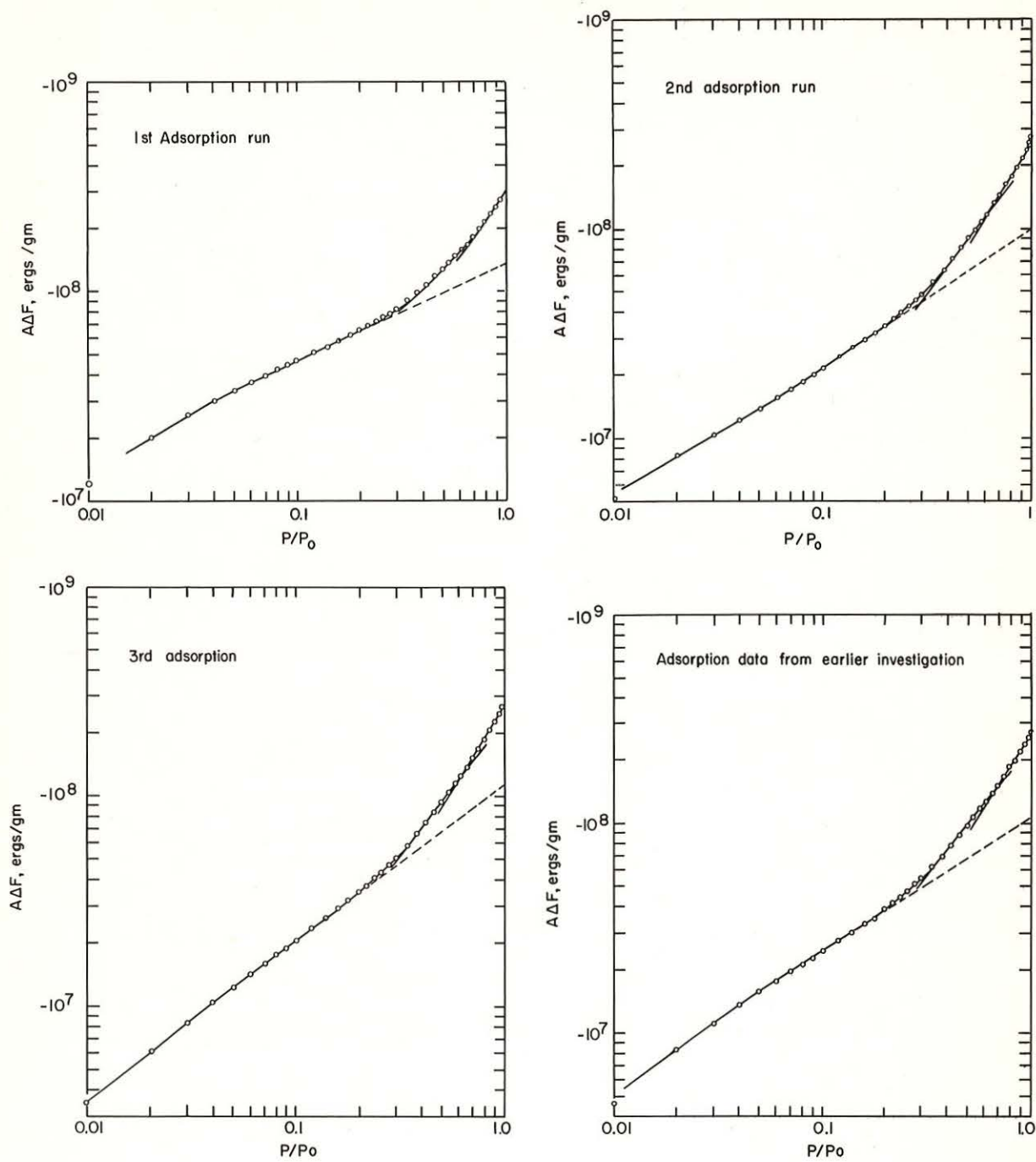


Fig. 10. Log-log plots of free energy change versus relative pressure

second increment of expansion from a basal spacing of 12.5 Å; the break at a p/p_0 of 0.95 corresponds closely with the beginning of the third increment of expansion from a basal spacing of about 15.5 Å. The last two breaks also correspond very well with observed minima in the line width plot of Fig. 4; these minimum line widths indicate the majority of the clay platelets have the basal spacing noted. On the basis of these correlations it was concluded that the portion of the $\log(A\Delta F)$ vs $\log(p/p_0)$ plot below p/p_0 of 0.16 to 0.18 reflects the energy changes due to adsorption on external surfaces only; at higher pressures energy changes due to adsorption on the internal surfaces are included and reflect the energy of interaction between clay platelets. The slope changes apparently reflect the differences in platelet interaction energies at increasing increments of expansion.

In their study Fu and Bartell (34) attributed the change of slope in their plots to capillary condensation in the pores of the adsorbent. In the present system capillary condensation probably occurs in external pores in the higher relative pressure range, but its effect on the energy changes is apparently masked by those caused by adsorption on the internal surfaces. According to Barrer and MacLeod (23) capillary condensation of water between montmorillonite particles does not occur until the relative pressure approaches 1.0.

The relation between the free energy change and separation of clay platelets is shown quite well in Fig. 11. The values of $A\Delta F$ for the first adsorption run are plotted against platelet separation h , at the same p/p_0 ,

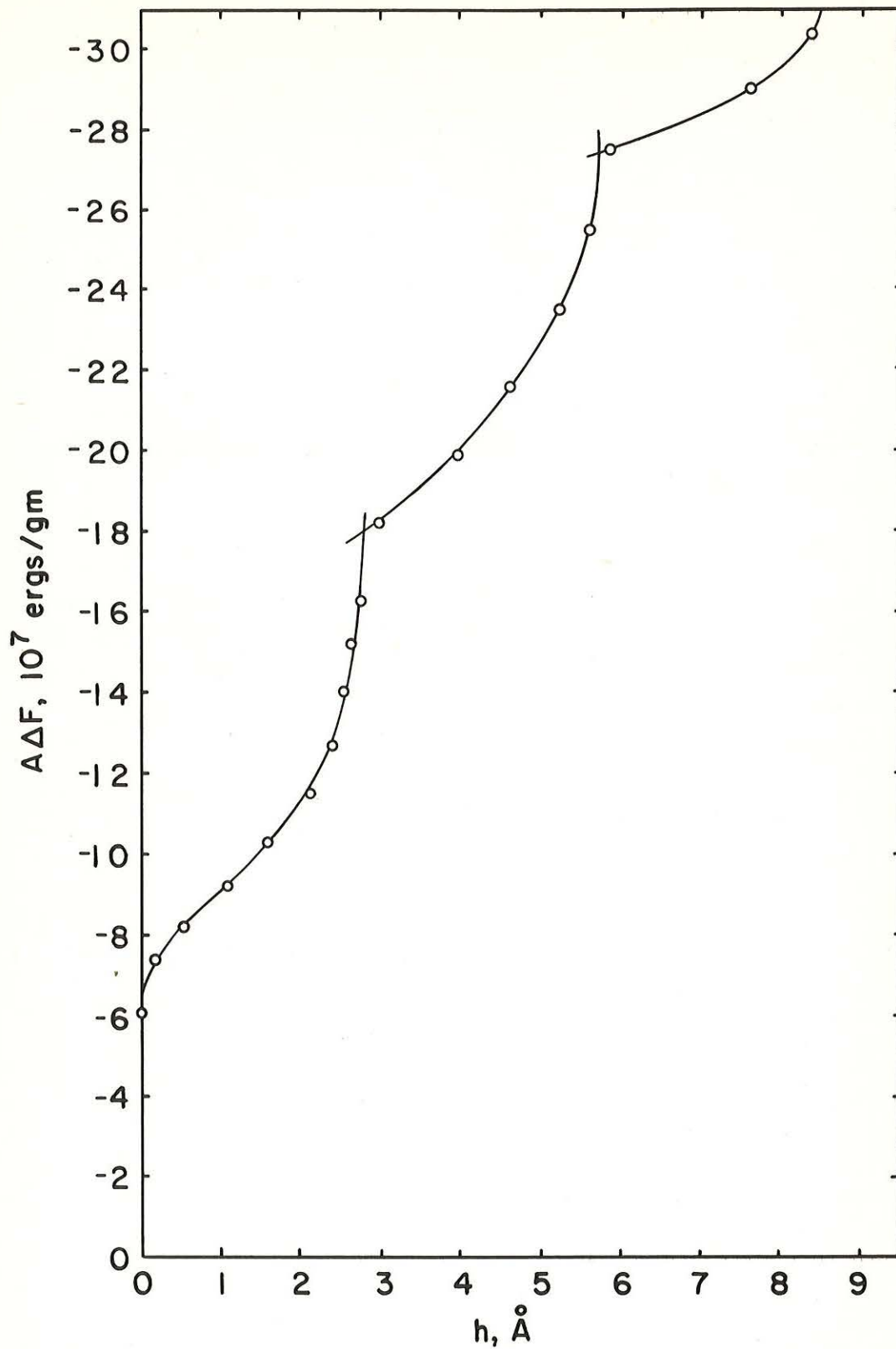


Fig. 11. Plot of total free energy change versus interlayer separation, first adsorption run

obtained from the X-ray diffraction data. ΔF data for the other adsorption runs produce very similar plots. Figure 11 shows sharp breaks which correspond closely with the slope changes noted in Fig. 10. Also, the breaks occur when h values are very nearly integral multiples of $2.8 \overset{\circ}{\text{A}}$, the thickness of a water molecule. This gives additional evidence that the interlayer water builds up in a laminar fashion.

Expansion energies

If the free energy changes could be divided into two components, one for adsorption on external surfaces and another for adsorption on internal surfaces, it would be possible to evaluate the expansion energies, i.e., the free energy change due to adsorption on and separation of the internal surfaces.

The free energy change brought about by the adsorption, on a solid surface, of a film at equilibrium with a vapor at some pressure p may be expressed as (27, p. 264):

$$\Delta F = \gamma_{sv} - \gamma_{so} \text{ ergs/cm}^2 \quad (1)$$

where γ_{so} is the surface free energy of the solid surface in vacuum and γ_{sv} is that of the solid-vapor interface in equilibrium at pressure p . When the solid-vapor interface is in equilibrium with the saturated vapor the free energy change is:

$$\Delta F = \gamma_{sv^0} - \gamma_{so} \text{ erg/cm}^2 \quad (2)$$

where γ_{sv0} is the surface free energy of the solid-vapor interface at the saturation pressure. According to Jura and Harkins (35), when the solid is wetted by the liquid, γ_{sv0} is equal to $(\gamma_{sl} + \gamma_{lv})$; γ_{sl} is the solid-liquid interfacial free energy and γ_{lv} is the surface free energy of the liquid in equilibrium with its own vapor. We have, therefore, at saturation:

$$\Delta F = \gamma_{sl} - \gamma_{so} + \gamma_{lv} \text{ ergs/cm}^2 \quad (3)$$

If capillary condensation occurs the γ_{lv} term drops out of Eq. (3). For the present system adsorption occurs only on the external surfaces of the clay at low relative pressures. Since only external areas, A_e , are involved, the free energy change is given by:

$$A_e \Delta F = A_e (\gamma_{sv} - \gamma_{so}) \text{ ergs/gm} \quad (4)$$

If only the external areas were available for adsorption over the entire relative pressure range it is proposed that the relationship $A_e \Delta F = \alpha(p/p_0)^\beta$ would continue to be obeyed. Under these circumstances, the linear portion of the $\log(A\Delta F)$ vs $\log(p/p_0)$ plot between p/p_0 of 0.05 to 0.18 would be extended to a p/p_0 of 1 as shown by the dashed lines on Fig. 10.

The free energy change at saturation would be:

$$A_e \Delta F = A_e (\gamma_{sl} - \gamma_{so} + \gamma_{lv}) \text{ ergs/gm} \quad (5)$$

If capillary condensation were to occur (still only external surfaces available) a behavior such as that observed by Fu and Bartell (34)

would be expected and the free energy change at saturation would be reduced by $A_e \gamma_{lv}$. With the present system this probably occurs very near the saturation pressure.

On the basis of the above discussion, the free energy changes due to adsorption on external and on internal surfaces were divided, at least to very near saturation, on Fig. 10 by extending the linear portions of the plots corresponding to adsorption only on external surfaces to the saturation pressure. The difference between $A\Delta F$ and $A_e \Delta F$ gives the free energy change $A_i \Delta F = A_i \phi$ where A_i is the internal surface area per gram and ϕ will be designated as the expansion energy per cm^2 of internal surface and given by:

$$\phi = \gamma_{sv} - \gamma_{so} + \Delta V \quad (6)$$

where ΔV is the free energy change per cm^2 of internal surface due to separation of layers against the force of interaction.

Figure 12 presents a plot of $A_i \phi$ for the first adsorption run versus platelet separation h . Values of $A_i \phi$ obtained from data of other runs produce very similar plots. Figure 12 shows that the free energy change due to adsorption of the second molecular layer of interlayer water is as great as or slightly greater than that for adsorption of the first layer. The free energy change for formation of the third layer of interlayer water is substantially less than for the other two. ϕ for adsorption of the first layer of interlayer water is the free energy change due to disappearance of a solid surface and the formation of a solid-film

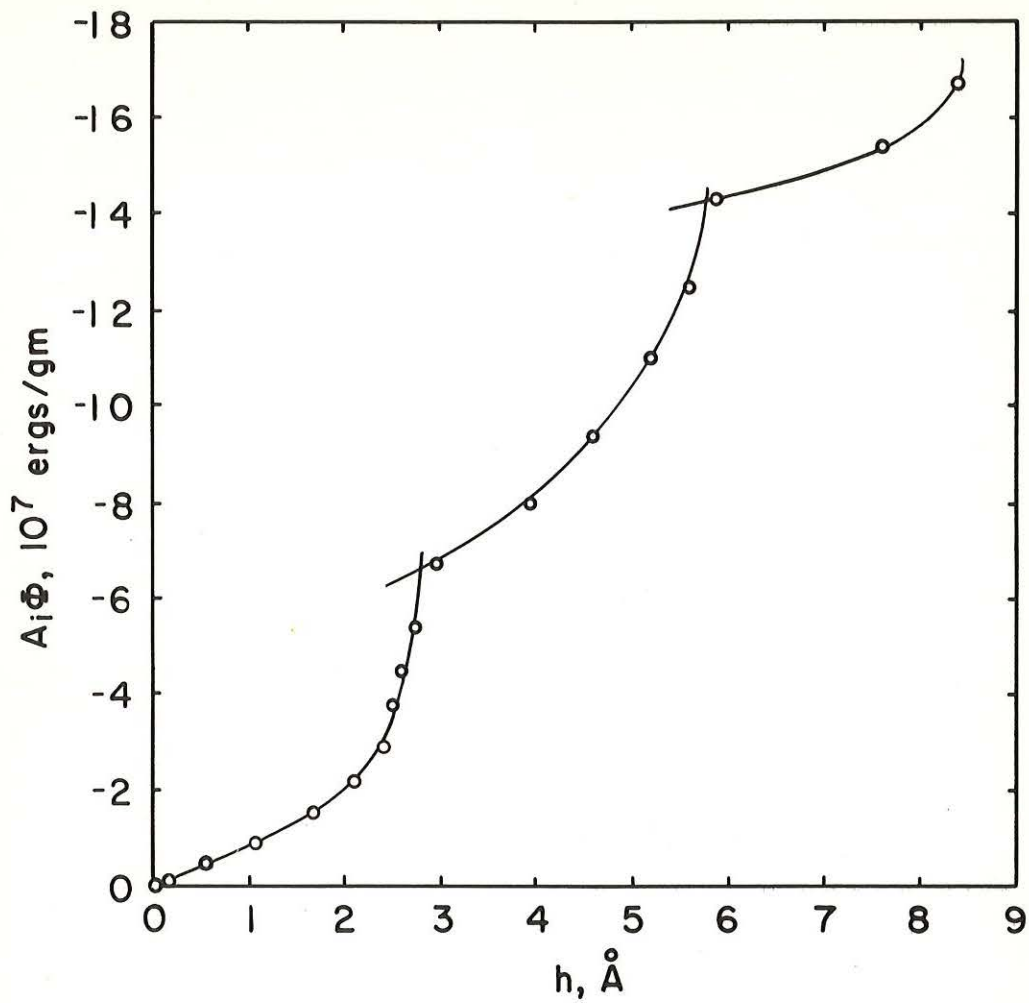


Fig. 12. Plot of free energy change due to adsorption on and separation of internal surfaces versus interlayer separation, first adsorption run

interface plus that due to separation against the force of interaction between platelets. The latter term will decrease the magnitude of the free energy change. The second layer of water must penetrate between the first and the clay surface. No new surfaces are formed nor do any disappear. The free energy change is due to extension of the film thickness and to expansion against the interaction forces. The free energy change due to extension of the film thickness is probably less than that for disappearance of solid surfaces and formation of solid-film interface; however, since the platelet separation is greater, the force of interaction is less and so the free energy change for formation of the second layer may be nearly the same as that for the first. The third layer of water may penetrate between the clay surface and existing inter-layer water, but most probably enters between the first and second layer. Again no new surfaces appear or disappear. The free energy change is due to extension of the film thickness and to expansion against forces of interaction further reduced by increased platelet separation. Since the free energy change on adsorption of the third layer is considerably less than that for the second, the change due to penetration between the first and second layers of water must be less than that for penetration between the clay surface and a water layer.

Swelling pressures

Roderick and Demirel (2), in an earlier study, suggested that there was a correlation between free energy data and swelling pressures

exerted by montmorillonites. An estimate of the pressure required to prevent separation of clay platelets due to penetration of water between layers (or the swelling pressure exerted by the clay on uptake of inter-layer water) was attempted using the basal spacing and free energy data of the present study.

At constant temperature and assuming all work to be pressure-volume work, we have for free energy:

$$dF = Vdp \quad (7)$$

where V is the molar volume and p is the external pressure. For the present system Eq. (7) becomes:

$$A_i d\phi = Vdp$$

Assuming water is incompressible the latter equation can be put into the following form:

$$d\phi = \frac{V}{A_i} dp = h_o dp \quad (8)$$

Where ϕ is the expansion energy (change in free energy due to adsorption on and separation of interlayer surfaces) per cm^2 , V is the total volume of interlayer water at saturation pressure per gram of sodium montmorillonite, h_o is the maximum platelet separation and p is the applied pressure. From Eq. (8) we obtain

$$A_i \int_{\phi = \phi_s}^{\phi} d\phi = A_i \int_{p=0}^p h_o dp \quad (9)$$

$$\text{or: } A_i \phi - A_i \phi_s = A_i h_o p \quad (10)$$

$$\text{or: } p = \frac{A_i \phi - A_i \phi_s}{h_o A_i} \quad (11)$$

where ϕ_s is the expansion energy when the clay is in equilibrium with saturated water vapor, p is the pressure required to prevent any platelet separation and $p = 0$ is the pressure when the maximum separation is reached. The platelet separation is a function of ϕ as shown in Fig. 12. The pressure required to prevent expansion beyond a certain separation h , when the sodium montmorillonite is in contact with saturated water vapor, may be obtained by determining the difference between $A_i \phi$ and $A_i \phi_s$ corresponding to separations h and h_o , respectively and dividing the difference by maximum separation h_o . The results determined have the dimensions $\frac{\text{ergs}}{\text{cm gm}}$ and must be divided by the internal surface area, A_i , to give the pressure in dynes/cm². Column 2 of Table 2 presents the external areas, A_e , determined for the first adsorption run by using various cross-sectional areas for the water molecule and the BET parameter q_m . Subtracting A_e from the total surface area of 748 m²/gm (from crystallographic data) gives the internal surface area A_i per gram. The values of A_i for the various water molecular areas were determined and used to calculate the swelling pressures at various interlayer spacings. The results are

presented in Table 3. Also presented are values for the expansion energy, ϕ , obtained from Fig. 12. The difference in the values obtained with various internal surface areas are probably less than the error due to the approximations of the methods for evaluation of the expansion energies and swelling pressures.

The expansion energy values at saturation may be due in part to

capillary condensation in external pores. This would tend to make the values given when three molecular layers of water are present somewhat larger than the actual case. The expansion energies given for the adsorption of the first two layers of water are not affected by capillary condensation since it occurs near the saturation pressure.

Since the swelling pressures were obtained from the saturation point, any capillary condensation effects would tend to make the listed values somewhat larger than those due only to adsorption on internal surfaces. This may affect the values of swelling pressure when two layers of interlayer water are present to some degree, but would probably be negligible when compared with the large swelling pressures at lower interlayer water contents. Mielenz and King (36) reported swelling pressures from 2 to 11 tons/ft² for sodium montmorillonite in consolidometer tests. The present data suggest the pressures they obtained were due to hydration above two layers of interlayer water.

It should be emphasized that the swelling pressures reported in Table 3 are those exerted when the sodium montmorillonite is in contact with saturated water vapor; the maximum observed interlayer separation is in equilibrium with the saturated vapor. If the sodium montmorillonite were in contact with liquid water further expansion would occur and comparatively smaller swelling pressures may develop. In this region, for separation beyond that for three or four molecular layers of water, the surface hydration energies are no longer important and the smaller

Table 3. Expansion energies and swelling pressures due to adsorption of water vapor on the interlayer surfaces of sodium montmorillonite (from the separation indicated from the maximum separation.)

	Area assigned to a water molecule, \AA^2	Internal surface area A_i , m^2/gm	Expansion energy, ergs/cm^2	Swelling pressure, p , $\text{dynes}, \text{cm}^2$	Swelling pressure, p , tons/ft^2
No interlayer water present	10.8	665	--	300×10^6	313
	11.5	660	--	302×10^6	315
	17.5	614	--	325×10^6	339
1 molecular layer of inter- layer water	10.8	665	- 9.8	181×10^6	190
	11.5	660	- 9.8	184×10^6	192
	17.5	614	-10.6	197×10^6	206
2 molecular layers of inter- layer water	10.8	665	-21.1	45×10^6	47
	11.5	660	-21.2	46×10^6	48
	17.5	614	-22.8	50×10^6	52
3 molecular layers of inter- layer water	10.8	665	-24.8	--	--
	11.5	660	-25.0	--	--
	17.5	614	-26.9	--	--

electrical double-layer forces become the major repulsive force between platelets (37). The further expansion exerting comparatively low additional pressure may be explained by attributing it to a low energy barrier (1).

CONCLUSIONS

The sorption isotherm data and X-ray diffraction data for water vapor adsorption and desorption by sodium montmorillonite, and data from the literature, indicate that:

1. The change in average basal spacings of sodium montmorillonite takes place in a continuous but non-uniform manner with changes in relative pressure. Continuity is due to the simultaneous existence of varying numbers of molecular layers of interlayer water. Expansion occurs in three increments. Basal spacing and line width data show average spacings correspond with an integral number of molecular layers of water just prior to each increment of expansion.

2. The relationship between relative humidity and the basal spacing of sodium montmorillonite is dependent on: a) the source and method of preparation of the sample; b) the initial conditions of the sample at the start of tests; and c) whether data is collected during adsorption or desorption.

3. Basal spacing, line width and free energy change data give evidence that the interlayer water builds up in a laminar manner.

4. Adsorption isotherms are more closely reproduced on successive adsorption-desorption runs than are desorption isotherms.

5. The hysteresis displayed by the sorption isotherms is due in part to the formation of a thixotropic structure at high relative pressures, and in part to attractive interaction forces between sodium montmorillonite platelets.

6. X-ray diffraction data and BET plots indicate that the BET parameter q_m obtained reflects adsorption only on the external surfaces of the sodium montmorillonite. Apparently sodium montmorillonite prepared from Wyoming bentonite is unique in this respect.

7. The relationship between free energy changes and relative pressure and the X-ray diffraction data for the adsorption of water vapor by sodium montmorillonite allows separation of the free energy change into two components; one due to adsorption on the external surfaces, and one due to adsorption on and separation of the internal surfaces.

8. Free energy data and X-ray data show that the expansion energy (free energy change due to adsorption on and separation of internal surfaces) during formation of the second layer of interlayer water is approximately the same as that for formation of the first layer. The change during formation of the third layer is substantially less than those for the other two.

9. Free energy data and X-ray data permit the estimation of swelling pressures exerted by sodium montmorillonite due to the uptake of interlayer water when the material is in contact with saturated vapor. The swelling pressure exerted when the platelet separation is zero is about 325 tons/ft^2 . The pressure exerted when one molecular layer of

water separates clay platelets is about 200 tons/ft². The pressure exerted when two molecular layers of water separate platelets is about 50 tons/ft².

ACKNOWLEDGEMENTS

The research reported herein was done at the Iowa Engineering Experiment Station, Iowa State University, under Project 505-S, Chemical stabilization and physico-chemical properties of soils. This project was sponsored by the Iowa Highway Research Board under Project HR-97 and was supported with funds from the Iowa State Highway Commission and the U.S. Bureau of Public Roads.

REFERENCES

1. Demirel, T. Adsorption of water vapor by sodium and calcium montmorillonite. Unpublished Ph.D. thesis. Ames, Iowa, Library, Iowa State University of Science and Technology. 1962.
2. Roderick, G. L. and Demirel, T. Expansion of montmorillonite due to adsorption of water vapor. Iowa Academy of Science Proceedings 70: 280-289. 1963.
3. Brunauer, S. The adsorption of gases and vapors. Physical adsorption. Princeton, N. J. Princeton University Press. 1943.
4. Klug, H. P. and Alexander, L. E. X-ray diffraction procedures for polycrystalline and amorphous materials. New York, N. Y., John Wiley and Sons, Inc. 1954.
5. Hendricks, S. B. and Jefferson, M. E. Structure of Kaolin and talc-pyrophyllite hydrates and their bearing on water sorption of clays. American Mineralogist 23: 863-875. 1938.
6. Hendricks, S. B., Nelson, R. A. and Alexander, L. T. Hydration mechanism of the clay mineral montmorillonite saturated with various cations. American Chemical Society Journal 62: 1457-1464. 1940.
7. MacEwan, D. M. C., Amil, A. R. and Brown, G. Interstratified clay minerals. In Brown, G., ed. The X-ray identification and crystal structures of clay minerals. pp. 393-445. London, Mineralogical Society. 1961.
8. Johns, W. D., Grim, R. E. and Bradley, W. F. Quantitative estimations of clay minerals by diffraction methods. Journal of Sedimentary Petrology 24: 242-251. 1954.
9. Milne, I. H. and Warshaw, C. M. Methods of preparation and control of clay mineral specimens in X-ray diffraction analysis. National Conference on Clays and Clay Minerals. Proceedings 4: 22-30. 1956.
10. Mooney, R. W., Keenan, A. G. and Wood, L. A. Adsorption of water vapor by montmorillonite. II. Effect of exchangeable ions and lattice swelling as measured by X-ray diffraction. American Chemical Society Journal 74: 1371-1374. 1952.
11. Gillery, G. H. Adsorption-desorption characteristics of synthetic montmorillonoids in humid atmospheres. American Mineralogist 44: 806-818. 1959.
12. Messina, M. L. Expansion of fractional montmorillonites under various relative humidities. Clays and Clay Minerals 19: 617-632. 1964.

13. Mooney, R. W., Keenan, A. G. and Wood, L. A. Adsorption of water vapor by montmorillonite. I. Heat of desorption and application of BET theory. *American Chemical Society Journal* 74: 1367-1371. 1952.
14. Grim, R. E. *Clay mineralogy*. New York, N. Y., McGraw-Hill Book Company, Inc. 1953.
15. Winterkorn, H. F. The science of soil stabilization. *Highway Research Board Bulletin* 108: 1-24. 1955.
16. Pauling, L. *The nature of the chemical bond*. Ithaca, N. Y., Cornell University Press. 1960.
17. Macey, H. H. Clay-water relationships and the internal mechanism of drying. *Ceramic Society Transactions* 41: 73-121. 1942.
18. Forslind, E. Crystal structure and water adsorption of clay minerals. *Swedish Cement and Concrete Research Institute Bulletin* 11: 1-20. 1948.
19. Barshad, I. The nature of lattice expansion and its relation to hydration in montmorillonite and vermiculite. *American Mineralogist* 34: 675-684. 1949.
20. Brindley, G. W. X-ray diffraction by layer lattices with random layer displacements. In Brown, G., ed. *The X-ray identification and crystal structures of clay minerals*. pp. 446-466. London, Mineralogical Society. 1961.
21. McBain, J. W. An explanation of hysteresis in the hydration and dehydration of gels. *American Chemical Society Journal* 57: 699-700. 1935.
22. Foster, A. G. The sorption of condensable vapors by porous solids. I. The applicability of the capillary theory. *Faraday Society Transactions* 28: 645-657. 1932.
23. Barrer, R. M. and MacLeod, D. M. Intercalation and sorption by montmorillonite. *Faraday Society Transactions* 50: 980-989. 1954.
24. Hirst, W. The mechanical interaction between mobile insoluble adsorbed films, capillary condensed liquid and fine-structured solids. *Faraday Society Discussions* 3: 22-28. 1948.
25. Johansen, R. T. and Dunning, H. N. Water-vapor adsorption on clays. *National Conference on Clays and Clay Minerals, Proceedings* 6: 249-258. 1959.

26. Brunauer, S., Emmett, P. H. and Teller, E. Adsorption of gases in multimolecular layers. *American Chemical Society Journal* 60: 309-319. 1938.
27. Adamson, A. W. *Physical chemistry of surfaces*. New York, N. Y. Interscience Publishers, Inc. 1960.
28. Orchiston, H. D. Adsorption of water vapor. III. Homoionic montmorillonites at 25°C. *Soil Science* 79: 71-78. 1955.
29. Emmett, P. H., Brunauer, S. and Love, K. S. The measurement of surface area of soils and soil colloids by the use of low temperature van der Waals adsorption isotherms. *Soil Science* 45: 57-65. 1938.
30. Zettlemoyer, A. C., Young, G. J. and Chessick, J. J. Studies of the surface chemistry of silicate minerals. *Journal of Physical Chemistry* 59: 962-966. 1955.
31. Clampitt, B. H. and German, D. E. Heat of vaporization of molecules at liquid vapor interfaces. *Journal of Physical Chemistry* 62: 438-440. 1958.
32. Takizawa, M. Mechanism of water vapor adsorption on bentonite. *Tokyo Institute of Physical and Chemical Research Scientific Papers* 54: 313-322. 1960.
33. Bangham, D. H. The Gibbs adsorption equation and adsorption on solids. *Faraday Society Transactions* 33: 805-811. 1937.
34. Fu, Y. and Bartell, F. E. Surface area of porous adsorbents. *Journal of Physical and Colloid Chemistry* 55: 662-675. 1951.
35. Jura, G. and Harkins, W. E. Determination of the decrease of free surface energy of a solid by an adsorbed film. *American Chemical Society Journal* 66: 1356-1362. 1944.
36. Mielenz, R. C. and King, M. E. Physical-chemical properties and engineering performance of clays. *State of California Department of Natural Resources, Division of Mines Bulletin* 169: 196-254. 1955.
37. van Olphen, H. *An introduction to clay colloid chemistry*. New York, N. Y. Interscience Publishers. 1963.

Appendix III

SOIL STABILIZATION WITH
EPOXY RESIN

by

Lin Lu

and

T. Demirel

January 1966

INTRODUCTION

Soil stabilization may be broadly defined as any regulated process that alters or controls soil properties for the purpose of improving their engineering performance. Processes by which soils may be stabilized include the use of other soil, chemical additives, cement, compaction, moisture control, or combinations of these.

The major applications of soil stabilization are as follows:

1. Stabilized soil provides bases or surfaces for secondary and farm-to-market roads where good primary roads are already in existence.

2. Stabilized soil provides for high type pavements where high-type rock and crushed gravel normally employed for such bases are not economically available.

3. For military and other emergencies where an area must be made trafficable within a short period of time.

4. For economic development, stabilized soil roads can lift underdeveloped areas out of the mud.

5. For city and suburban streets where the noise absorbing and elastic properties of certain stabilized soil systems process definite advantages over other construction materials.

Up to now, there has been no entirely successful method for stabilization of soils by the use of chemical admixtures. Although several materials are suitable under specific conditions or with particular soils, none have proved to be universally acceptable.

Portland cement is the most generally effective soil-stabilizing material. However, under certain conditions, especially where wide

temperature variation prevails, the cement treated soils have not always proven to be a durable admixture.

Many kinds of synthetic resins have been used for soil stabilization. Some of them have shown promising results. One of these synthetic resins, epoxy resin has never been tried as a stabilizing agent. Cured epoxy resin is an inert, tough solid. It can resist the penetration of water and the attacks of de-icing chemicals, oil gasoline and other materials commonly encountered on highways.

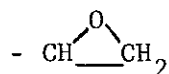
The objective of this research is to determine the effect of epoxy resin on soils which were treated by epoxy resin alone or epoxy resin with other additives. The other purpose is to give a tentative explanation of the mechanism of stabilization.

REVIEW OF LITERATURE

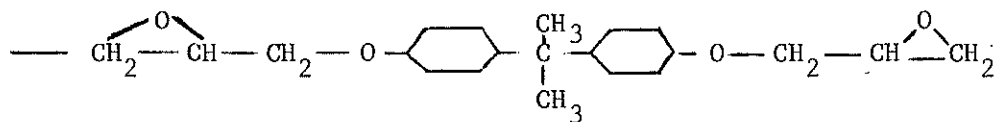
Epoxy Resin, Manufacturing Process and the Properties of its Polymers

The epoxy resin is one of the newest of the major industrial plastics. The resin cures into a thermosetting material which will retain its dimensional stability throughout its design range, i.e., they will not soften with heat or flow with pressure.

The epoxy-resin molecule is characterized by the reactive epoxy or ethoxyline groups (5)



An unusually tough, extremely adhesive and highly inert solid results when crosslinking or cure is accomplished through these groups. The epoxy molecule is represented by the diglycidyl ether of bisphenol A (15).



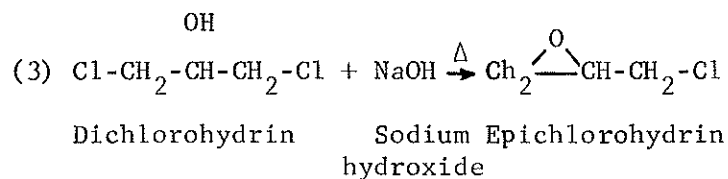
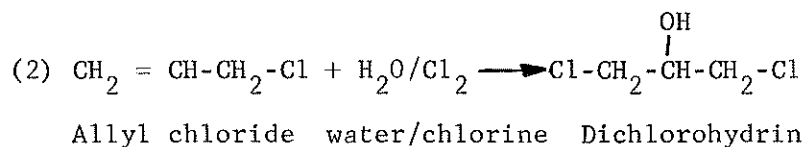
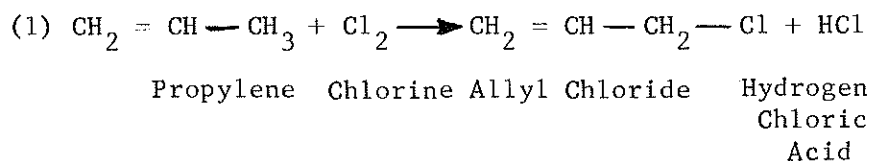
The epoxy resins which have viscosities in the 8,000 to 20,000-centipoise range are predominately of this structure (15). The usual raw materials for the synthesis of the diglycidyl ether of bisphenol A are epichlorohydrin and bisphenol A.

Epichlorohydrin is a colorless, mobil liquid having an irritating chloroform-like odor. It is represented by the formula:

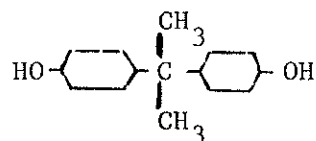


It is usually produced by the reaction of chlorine with propylene. The yielding allyl chloride is reacted with hypochlorous acid to produce dichlorohydrin which is exposed to sodium hydroxide at elevated temperature to strip off one hydrogen and one chlorine atom.

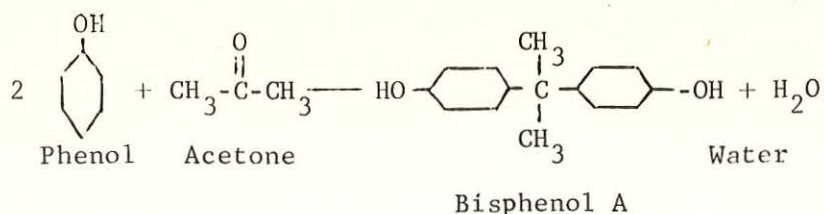
The three steps to yield epichlorohydrin from propylene can be expressed as follows:



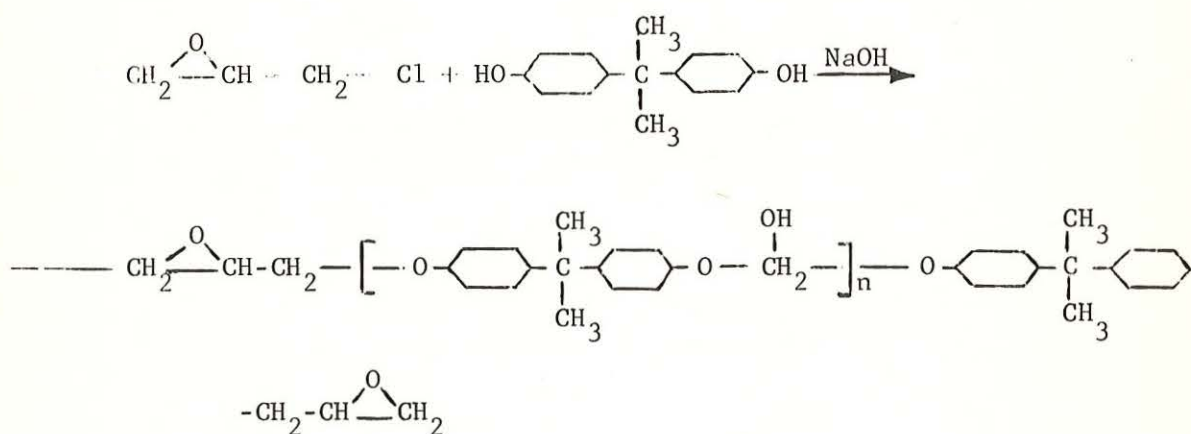
Bisphenol A or bis dimethylmethane:



It requires two basic intermediates for synthesis: acetone and phenol (15):



Diglycidyl ether of bisphenol A is produced by reacting epichlorohydrin with bisphenol A in the presence of a caustic (5):



Where n is the number of repeated units in the resin chain; when $n = 0$ the molecular weight is 340; when $n = 10$, it is about 3,000.

Epoxy resins in the pure or uncontaminated state possess indefinite shelf life. They are chemically stable at temperatures up to 200°C . The resins cure into thermoset compounds by three reactions (15): (1) direct linkage between epoxy groups; (2) linkage of epoxy groups with aromatic or aliphatic hydroxyls, and (3) cross-linkage with the curing agent through various radicals. Cured epoxy resins are very inert chemically. When the ether groups, the benzene rings and the aliphatic hydroxyls are present in the cured epoxy system, they are virtually invulnerable to caustic attack and extremely resistant to acids.

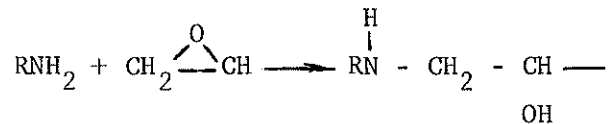
The epoxy resins which were used for this research were products of the Shell Chemical Company. They are furnished under the commercial names of Guardkote 120A and 120B. Guardkote 120A is composed of a diglycidyl ether of bisphenol A. 120B is a modified straight chain aliphatic amine containing both primary and secondary amine groups

(18). The physical properties of the cured system are as follows (20):

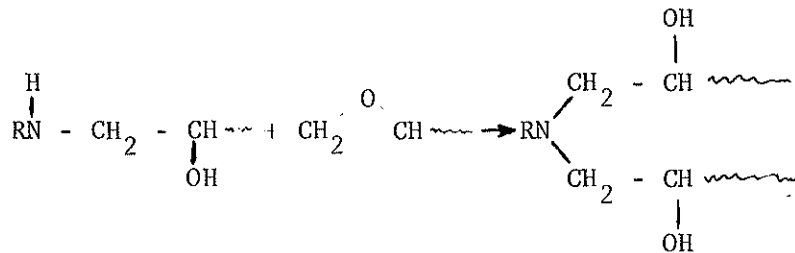
Tensile strength	4,900 psi
Tensile elongation	5%
Shore D hardness	77
Impact strength	0.6 ft - 16/in of notch
Flexural strength	8,600 psi
Flexural modulus	226,000 psi

The curing reactions possible with primary amines are (15):

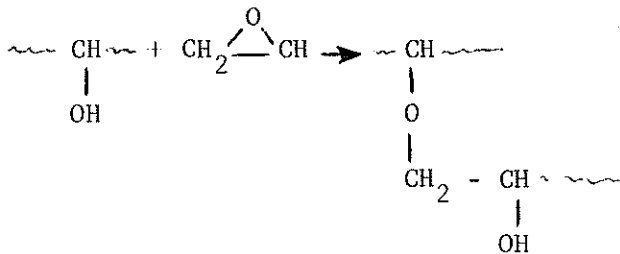
1. Reaction with an epoxy group to form a secondary amine



2. Another epoxy group is reacted to form tertiary amine



3. Reaction of hydroxyls so formed with epoxy



Review of Previous Work

Natural or synthetic resins which have been used for the purpose of soil stabilization may be divided into two groups: resinous waterproofing materials, and resinous waterproofing and bonding materials (16).

The chief function of resinous waterproofing materials is to maintain the moisture content of a soil at or below optimum moisture by preventing entry of water into the treated and compacted mixture. Very slight or no cementing action is obtained from the materials. Waterproofing agents usually attain maximum effectiveness when used in small quantities. Although imparting desirable characteristics to the soil, and providing considerable waterproofing effect under mild exposure, none of the water-repellent resins appears to be a suitable soil stabilizing agent at the present time. The most popular resinous waterproofing materials are Stabinol, Resin 321, Vinsol and NVX. Both Stabinol and Resin 321 were tested and reported by Mainfort (16) as soil stabilizing materials. Resin 321 in particular is the best waterproofing agent studied and its water-repellent characteristics can be utilized for improving the effectiveness of other stabilizing materials. In further studies by Mainfort (16), with more severe laboratory exposure and the use of a wide-range of soils, both stabinol and resin 321 were found to be ineffective under the more severe tests. Mainfort also indicated in his tests that Vinsol was superior to NVX but far inferior to both Stabinol and Resin 321.

Resin bonding materials, as used in soil stabilization, are con-

sidered to cement or bond the particles of soils with which they are mixed. The effectiveness of the resin treatment increases with the quantity used (16). This kind of treatment is still in experimental stages.

Mainfort (16) found aniline-furfural an effective bonding and waterproofing agent with the wide range of soils he used. Winterkorn (25) used aniline furfural as a soil stabilizer in his study for the Civil Aeronautics Administration. He found that the combination of either 70:30 or 35:65 parts by weight of aniline and furfural was a good resin binder. The 70:30 resin was the most effective of those tested for medium plastic soils with the small amounts of the chemicals used. The resin acted as both a binding agent and a waterproofing agent. But both combinations were found to be ineffective when used in alkaline mixes. Acid mixes resulted in maximum strengths.

Sheeler (19) used aniline furfural to stabilize Wisconsin loess with success. He found a ratio of 2 mol. aniline to 1 mol. of furfural produced the highest stability among the loess mixtures. The soil treated with aniline furfural was nearly dry after five days of air-curing and reached equilibrium after eight days regardless of the percentages of chemical content.

Hydrated lime has been tried as a catalyst to improve the strength of the loess soil. It was found that both immersed strength and dry strength were reduced by adding hydrated lime to the resin loess mixture. Either sodium hydroxide or aluminum chloride when added to the aniline-furfural-soil mixture resulted in increased strength. The immersed strength had a 28 percent increase by adding 0.3 percent aluminum

chloride to the mixture containing 5 percent aniline-furfural. He also found that the maximum strength occurred at 22 percent of 2 micron clay content. A maximum waterproofing at 3 percent resin content was obtained for loess soil; the moisture absorption increased with the increase of resin content. Aniline-furfural treated specimens were very resistant to freezing and thawing.

Mainfort (16) also found resorcinol-formaldehyde to be the best synthetic resin for hardening soil under moist-cure conditions at room temperature. The treated soil showed considerable promise under severe laboratory exposure. Mainfort showed this synthetic resin is suitable for improving other more economical admixtures; particularly the bituminous materials. Synthetic resins such as phenol-formaldehyde resin, urea-formaldehyde resin polystyrene and furfural alcohol have also shown promise for use as soil stabilizers (16,18).

Epoxy resins have never been tried in the field of soil stabilization; it has been used for surfacing and repairing Portland cement concrete (20). Burns (6) used epoxy resin as an additive in asphaltic concrete. The epoxy-asphalt concrete paving mixtures were tested in a field test section under jet blast and fuel spillage to compare the effectiveness of an epoxy-asphalt binder tack coat with that of a conventional asphalt tack coat. It showed that epoxy-asphalt concrete, properly designed and constructed would satisfactorily withstand jet blast temperatures in the order of 500^oF and is impervious to jet fuel. The epoxy asphalt binder tack coat resulted in a longer bond than the conventional asphalt tack coat.

MATERIALS USED

Soils

Four kinds of soils were used in this investigation; the choice of these soils depended on the amount of clay present. The soils were a friable Wisconsin age loess (Lab. No. 20-2), a plastic Wisconsin age loess (Lab. No. 528-4), a Kansan Gumbotil (Lab. No. 512-11) and a dune sand (Lab. No. S-6-2). All soils except the Kansan Gumbotil were grounded to pass a No. 10 sieve; while the Gumbotil soil passed the No. 4 sieve. The descriptions and properties of these soils are presented in Table 1.

Lime

The lime used in this study was a product of the U. S. Gypsum Co. It is a calcitic hydrated lime.

Epoxy Resin System

The epoxy system used in this research was a commercial product of the Shell Chemical Company. It is supplied under the name of Guardkote 120, in two components, Guardkote 120A and Guardkote 120B, which are individually stable. Guardkote 120A is an epoxy resin and Guardkote 120B is an amine hardener. The liquid Guardkote 120A can be cured at 80°F to become an unusually tough solid by adding Guardkote 120B to it at a weight ratio of 5 parts 120A to 1 part 120B as suggested by

the producer (18). Hand mixing for three minutes is usually required and an exothermic chemical reaction starts after 25 minutes. Therefore, the pure epoxy system should be used within about 15 minutes.

Table 1. Description and properties of soils used

Sample	Friable Loess (Lab. No. 20-2)	Plastic Loess (Lab. No. 528-4)	Kansan Gumbotil (Lab. 512-11)	Dune Sand (Lab. No. S-6-2)
Textural composition, %				
Gravel (>2.0 mm)	0	0	0	0
Sand (2.0-0.074 mm)	0.4	0.2	0.9	94
Silt (0.074-0.005 mm)	80.0	60.8	56.7	4
Clay (<0.005 mm)	19.6	39.0	42.4	2
Clay (<0.002 mm)	16.0	33.0	----	--
Predominant clay mineral	Montmorillonite	"	"	--
Physical properties				
Liquid limit, %	30.8	52.1	49.4	--
Plastic limit, %	24.6	20.0	25.9	--
Plasticity index	6.2	32.1	23.5	Non-plastic
Shrinkage limit, %	22.3	----	----	
Chemical properties				
Cat. ex. cap., m.e./100g	13.4	23.5	----	--
Carbonates, %	10.2	1.5	----	Non-calcareous
pH	8.7	5.6	----	--
Organic matter, %	0.2	0.2	----	--
Classification				
Textural	Silty Loam	Silty Clay	Silty Clay	Fine Sand
Engineering (AASHO)	A-4 (8)	A-7-6 (18)	A-7 (15)	A-3 (0)

METHOD OF PROCEDURE

Preparation of Specimen - Phase 1

The first phase of the investigation includes the molding of miniature soil specimens 1 inch high by 1/2 inch diameter. These specimens required much less preparation time, soil and epoxy than would be required if larger specimens were used. The results obtained for the different epoxy resin contents should show the relative effectiveness of epoxy-soil combinations.

Since significant amounts of water would probably tend to interfere with amine-epoxy reaction, it was decided that only dry soils should be used. However, the mixture was too dry to make a uniform mixture without adding extra water. Two ways of preparing the epoxy resin solution were tried. In the first method Guardkote 120A and 120B were dispersed in water individually by adding a dispersing agent with each. Sodium-montmorillonite was found to be the best dispersing agent for the epoxy-water suspension. The required epoxy and hardener were obtained from their respective suspensions. It was necessary to add additional distilled water to the soil-epoxy-mixture to insure uniform mixing.

In the second method, the epoxy and hardener were prepared by mixing without preemulsification. The mixture was hand-mixed three minutes before using.

Mixing

Soils passing the #10 sieve were used in this investigation.

About 40 grams of soil were placed in a porcelain dish and the required amount of resin mixture was added to give the desired percentages of resin. The soil and the resin mixture were then mixed with a spatula. Water was added during mixing to increase the volatile content to the estimated optimum. Different mixing orders, Table 2, showed that the immersed strengths were affected by the order of mixing.

Molding

Three 1 inch by 1/2 inch specimens were molded from each mixture. The required amount of the mixture to produce a 1 inch by 1/2 inch specimen having a specified dry density was placed in a cylindrical mold and compacted with static pressure. The molding apparatus was the same used and described by Roderick (18). Specimens with 9, 11, 13, 15 and 17 percent epoxy resin were molded for each mixture with the friable loess. Specimens with 5 percent resin but different volatile contents were molded for each mixture with dune sand.

Curing

All specimens of 1 inch by 1/2 inch were cured at room temperature for seven days. Each was completely immersed in distilled water for a 24 hour period before testing. The unconfined compressive strength of a certain mixture was obtained from the average of three specimens.

Testing

The miniature specimens were tested by a proving ring type hand-operated testing machine. Its maximum capacity for 1 inch by 1/2 inch specimens was 600 psi. Any specimens for which the unconfined compressive strength was higher than 600 psi were tested by another higher capacity proving ring machine. The load at which the specimen failed was divided by the cross-sectional area of the specimen to give the unconfined compressive strength of the specimen.

Preparation of Specimen - Phase 2

The epoxy resin mixture which was used in this phase was one part Guardkote 120A and 0.4 part 120B by weight. The epoxy mixture was prepared by the second method explained in the description of methods for the first phase of this study.

Mixing

The amount of the prepared epoxy solution required to give the desired amount of epoxy content was added to the soil. The following mixing procedure which was used for it was found to be the best in getting higher immersed strengths in phase 1 investigation (Table 2):

- A. The soil and the required amount of lime were mixed with a spatula for one minute (in case the second additive was used).
- B. The required amount of distilled water was added to the soil or soil lime mixture. It was then mechanically-mixed with a

Hobart Model C-100 mixer at low speed for one minute.

- C. It was then hand-mixed for one-half minute to assure proper distribution and pulverization of the soil.
- D. The epoxy-hardener mixture, which had been prepared by mixing thoroughly, was added to the soil, and the mixture was mixed by a Hobart mixer one and one-half minutes.
- E. The mixture was then hand-mixed for one minute.

The above procedure of mixing was used to prepare all specimens for the rest of this investigation.

Molding

Immediately after mixing, three specimens 2 inches in diameter by 2 inches high were molded with a drop-hammer apparatus developed by Davidson and Chu (8). The apparatus is shown in Figure 1. A predetermined quantity of soil-chemical-water mixture was placed in the cylindrical mold and the mixture was compacted by dropping a five pound hammer through a distance of one foot. After compacting the first blow, the temporary support was removed and four additional blows were given to the specimen. The reverse side of the specimen was given five blows in the same way. Specimens were removed from the mold by means of a hydraulic jack. They were then weighed to the nearest 0.1 gram and their heights measured to the nearest 0.001 inch. The height of all specimens were maintained at 2.000 ± 0.050 inches. Representative moisture samples were taken from the mixing bowl just prior to molding the first specimen and immediately after molding the third.

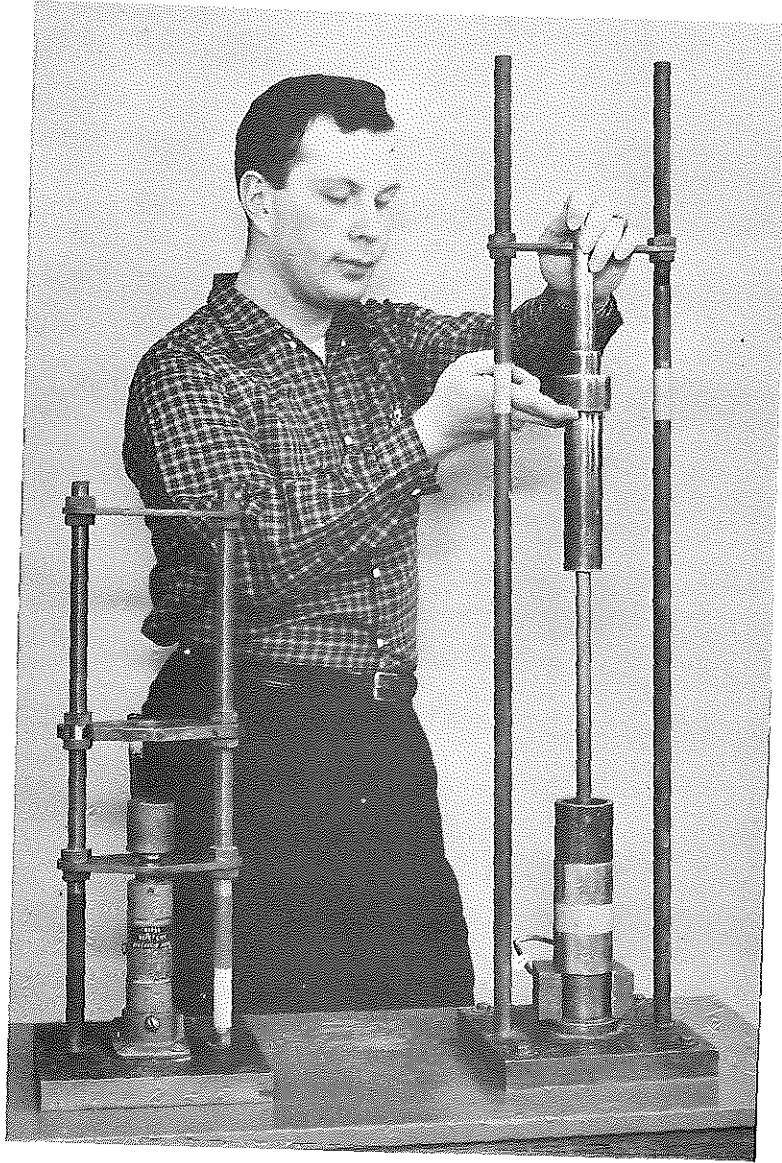


Figure 1. Apparatus for molding 2-inch diameter by 2-inch high test specimens. Drop hammer and molding cylinder shown in place.

The moisture samples were weighed to the nearest 0.01 gram, placed in an oven at 110°C for at least 16 hours and then weighed again. The moisture content for each mixture was determined to the nearest 0.1 percent on the basis of oven-dry weight of soil.

Curing

The specimens, prepared as above, were cured by air drying for various lengths of time at various temperatures. After curing, heights and weights were measured again. The specimens were then completely immersed in distilled water for a period of 24 hours. They were then weighed and measured again, and tested for unconfined compressive strength.

Testing

Unconfined Compressive Strength

The unconfined compressive strength was determined by the apparatus shown in Figure 2. Load was applied to the specimen at a deformation rate of 0.1 inch per minute until complete failure was attained. The maximum load in pounds divided by the cross-sectional area of the specimen was recorded as the unconfined compressive strength. The unconfined compressive strength obtained from specimens which were all immersed in distilled water for 24 hours after dry curing will be referred to as "immersed strength".

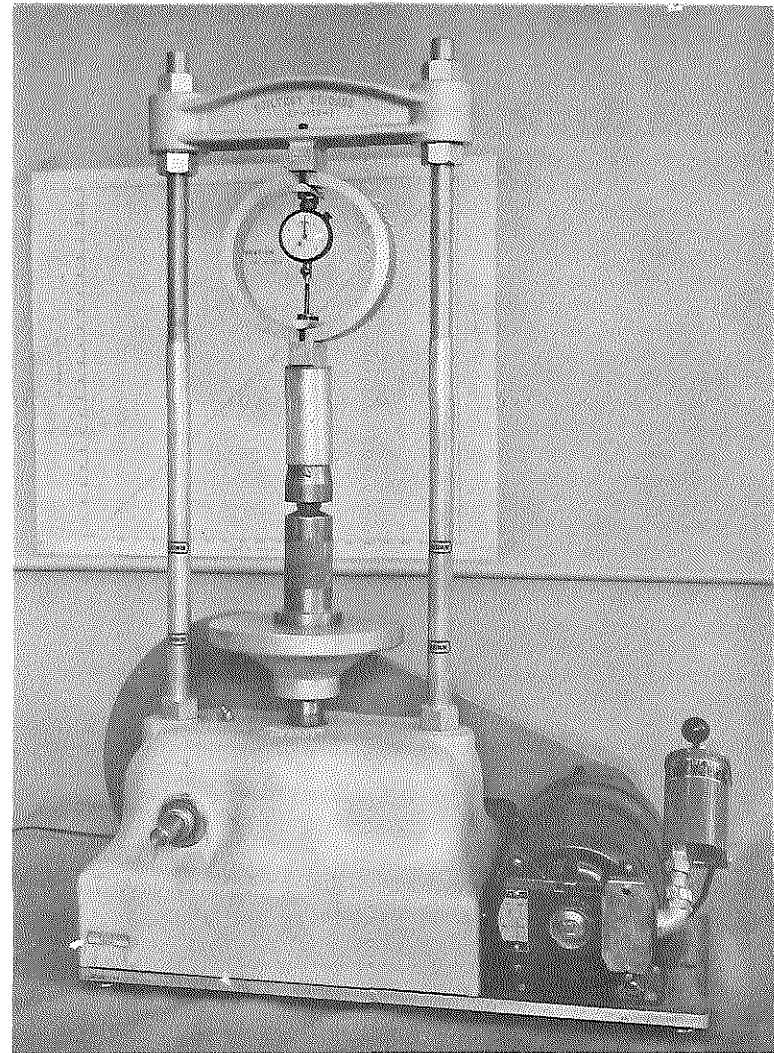
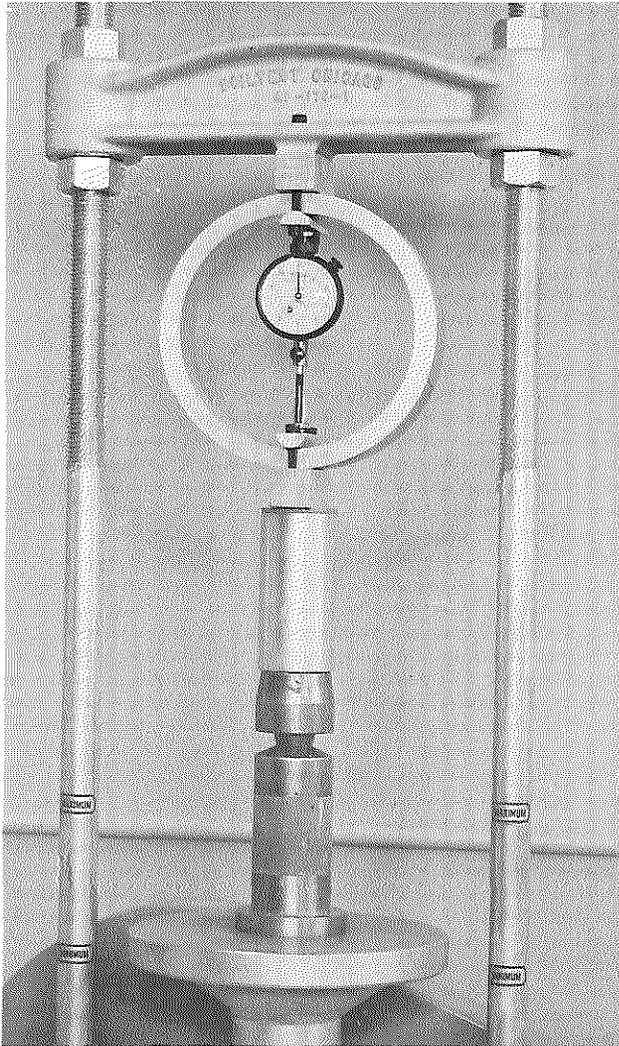


Figure 2. Two-inch diameter by 2-inch high specimen being tested for unconfined compressive strength.

Calculation of Dry Density

Dry density was calculated from the weight, height and volatile content determined at the time of molding.

$$\text{Dry density (pcf)} = \frac{\text{Wt. of specimen (gram)}}{\text{ht of specimen (inch)}} \times \frac{1.213}{1 + \frac{\text{volatile content (\%)}}{100}}$$

Calculation of Linear Shrinkage

Linear shrinkage was obtained after curing. It was calculated by comparison of the initial height and the height after curing

$$\text{Linear shrinkage (\%)} = \frac{\text{ht. after molding} - \text{ht. after drying}}{\text{ht. after drying}} \times 100$$

Calculation of Volatile Retention

After curing, the percentage of volatile which was retained in the specimen was calculated by the following formula

$$\text{Volatile retention \%} = \frac{\text{Wt. after curing} - \frac{\text{Wt. after molding}}{1 + \frac{\text{volatile at molding (\%)}}{100}}}{\frac{\text{Wt. after molding}}{1 + \frac{\text{volatile at molding (\%)}}{100}}}$$

Calculation of Linear Expansion

Linear expansion was obtained by comparison of the height after immersion and the height after dry curing

$$\text{Linear expansion \%} = \frac{\text{ht. after immersion} - \text{ht. after dry curing}}{\text{ht. after dry during}} \times 100$$

Calculation of Water Absorption

The amount of water absorption was calculated by the weight after

immersion, weight after molding, and the volatile content after molding.

$$\text{Absorption (\%)} = \frac{\text{Wt. after immersion} - \frac{\text{Wt. after molding}}{1 + \frac{\text{Volatile at molding (\%)}}{100}}}{\frac{\text{Wt. after molding}}{1 + \frac{\text{Volatile at molding (\%)}}{100}}} \times 100$$

Freeze-thaw Test

The following soil-epoxy resin admixtures were used in the Iowa

Freeze-thaw Test:

Soil 528-4	}	7 percent Guardkote 120A + 2.8 percent 120B + 2 percent calcitic hydrated lime
Soil 20-2		
Soil 512-11		
Soil S-6-2;		3 percent Guardkote 120A + 1.2 percent 120B + 2 percent calcitic hydrated lime.

Four specimens of 2 inch high by 2 inch diameter were molded at the optimum volatile content for maximum immersed strength for each of the above soil-additive mixes. The specimens were cured by drying 24 hours in a 104°F (40°C) oven. After curing they were tested by the Freeze-thaw test developed at the Iowa Engineering Experiment Station (12). Two specimens prepared from the same batch were completely immersed in distilled water for a period of 11 days. The remainder were given one day immersion and then followed by ten cycles of freezing and thawing. One freeze-thaw cycle consisted of 16 hours freezing at 20 ± 2°F and 8 hours thawing at room temperature. Sufficient water at a temperature of 35°F was maintained in the vacuum flask so that the specimen would contact water. At the completion of freeze thaw cycles and immersion,

all specimens were weighed, and their heights measured; the specimens were then tested for unconfined compressive strength.

Two specimens were molded from each of the raw soils at their optimum moistures. They were cured by drying at room temperature for seven days and were then subjected to several cycles of the freeze-thaw test. The specimens were not immersed in water because they would have slaked. The amount of expansion of those untreated specimens were compared with that of the resin treated specimens. Figure 14 shows the relative heaves of the treated and untreated specimens.

PRESENTATION AND DISCUSSION OF RESULTS - PHASE 1

The screening test is used to find what chemicals can be used to stabilize soil and what kinds of catalysts are feasible for the chemicals used in the laboratory test. Since the screening test specimens utilized less material and time than 2 inch by 2 inch specimens would require, the screening test is preferable when the effects of chemicals used as a stabilizing agent is not known. However, the immersed strength obtained from the screening tests were not always reproducible. The relationship of strength to percent chemicals added was not clearly defined by this kind of test. For this reason only friable loess (20-2) and dune sand (S-6-2) soils were investigated in phase 1 of the experiment.

Specimens containing 9, 11, 13, 15 and 17 percent epoxy were molded with friable loess (20-2). Epoxies pre-emulsified by using sodium montmorillonite as a dispersing agent were used. The results obtained from different combinations are presented in Table 2.

Since the specimens with pre-emulsified epoxy and hardener did not show higher immersed strengths than those with only mixed epoxies it was concluded that premulsification of epoxy and hardener was not necessary. The results showed that higher immersed strength would be obtained if the ratio for epoxy and hardener was 1 to 0.4 rather than 1 to 0.2. It was found that the extra water did not impede the adhesion between resin and clayey soil. On the contrary, a certain amount of water improved the interaction between the resin and soil. An optimum molding volatile content for immersed strength could be

Table 2. Effect of various epoxy resin contents on immersed strengths for friable loess and dune sand miniature specimens.

Soil	Epoxy 120A %	120B %	Molding Volatile Content %	Na Mont. %	Method of curing	Method of Mixing	Average immersed strength psi	
							A	B
20-2	9	3.6	17.0	1.0	A = 7 days of room temperature and 24 hours in immersed water	I	34	40
	11	4.4	20.5	1.0		I	77	98
	13	5.2	17.7	1.5		I	295	885
	15	6.0	18.3	2.0	B = 14 days at room temperature and 24 hours in immersed water.	I	394	545
	17	6.8	18.0	2.0		I	1325	1780
	17	6.8	16.5	2.0		I	2243	2243
	11	2.2	18.0	0			168	
	11	4.4	18.0	0		I	320	
	13	5.2	18.0	0	A	"	746	
	15	6.0	18.0	0		"	1140	
	17	6.8	18.0	0		"	1200	
	11	4.4	13.4	0		I	219	
	11	"	15.4	"		"	877	
	11	"	17.4	"	A	"	780	
	11	"	19.4	"		"	373	
	11	"	21.4	"		"	176	

Table 2
Cont.

Soil	Epoxy 120A %	120B %	Molding Volatile Content %	Na Mont. %	Method of Curing	Method of Mixing	Average immersed Strength, psi
20-2	17	6.8	18.0	0	A	II	746
	17	6.8	18.0	0	"	III	1711
	17	6.8	18.0	0	"	IV	1667
S-6-2	5	2.0	10	0	A	I	346
	5	2.0	0	0	"	I	266
	5	2.0	10	0	"	II	63
	5	2.0	10	0	"	III	346

Methods of Mixing

- I. Extra water was added to soil at the same time with the prepared epoxy.
- II. Extra water was added after the soil and the prepared epoxy had been mixed.
- III. Extra water was added and mixed with soil; the prepared epoxy was then added and mixed.
- IV. Extra water was added to the prepared epoxy; the mixture was then mixed with the soil.

found in the combinations of the same epoxy content with different percentages of volatiles at molding. Four different mixing orders were tried for 20-2 soil and the one in which extra water was added before the soil and the prepared epoxy had been mixed (mixing order III) proved the best in getting higher immersed strength.

Specimens containing only 5 percent epoxy with different mixing orders were prepared with soil S-6-2. Different mixing orders for the sandy soil also made the specimens fail at different immersed strengths. If the water and epoxy were added to the sandy soil at the same time or water was added to the sandy soil at the same time before adding of epoxy mixture, the immersed strengths would be higher than that of the specimens made by the mixing order II, (see Table 2). The conclusion is that the mixing water should never be added into the mixture after the epoxy and sand had been mixed. If water and epoxy were added to the sandy soil at the same time or sand was mixed with water first then the mixture was mixed with epoxy, the water might enable the epoxy to be more uniformly distributed. If the water were added after mixing the soil with epoxy only, the epoxy was unevenly distributed in the soil mass and it resulted in poor immersed strength.

The erratic results of this phase of the study were probably due to the dimensional effect of the miniature specimens. It was however, concluded that: (1) pre-emulsification of epoxy system was not necessary to incorporate the resin with wet soils; (2) water did not impede the adhesion between resin and soil, on the contrary a certain amount of water improved the resin-soil interaction and (3) the third mixing order (see Table 2) was best in getting higher immersed strength. Thus, this phase of the study laid the course for phase 2 study.

PRESENTATION AND DISCUSSION OF RESULTS - PHASE 2

Effect of Epoxies on Optimum Volatiles on
Immersed Strength and Dry Density

The percentages of epoxy added to the friable loess, based on dry weight of the soil were 7, 9, 11, and 13 percent in this investigation. Further tests were conducted by adding two percent lime to the friable loess-epoxy specimen containing 5, 7, and 9 percent epoxy. Tests were run for plastic loess and gumbotil soils. The mixtures of both soils contained 5, 7, and 9 percent epoxy and 2 percent lime. Two percent lime was also added to epoxy-sand mixtures which contained 2, 3, and 4 percent epoxy.

For each combination of those percentages, five or six sets of three specimens were prepared with different volatile contents. Each specimen of the same set was maintained within ± 1.0 percent in volatile content and ± 3 pcf in dry density according to ASTM Designation B 560-57 (1). Figure 3 shows the relationships of immersed strength versus days of dry curing for soil 20-2. With seven days dry curing at 80° F (room temperature) the maximum immersed strength for 7 percent resin content is 580 psi from Table 3. Tests showed that the immersed strength decreased with decreasing curing temperature.

It was found that the specimens of 20-2 soil with 7 percent epoxy content at optimum volatile content yielded the same immersed strength if they were cured in an oven at 104° F (40° C) for one day instead of seven days dry curing at room temperature. The oven curing not only

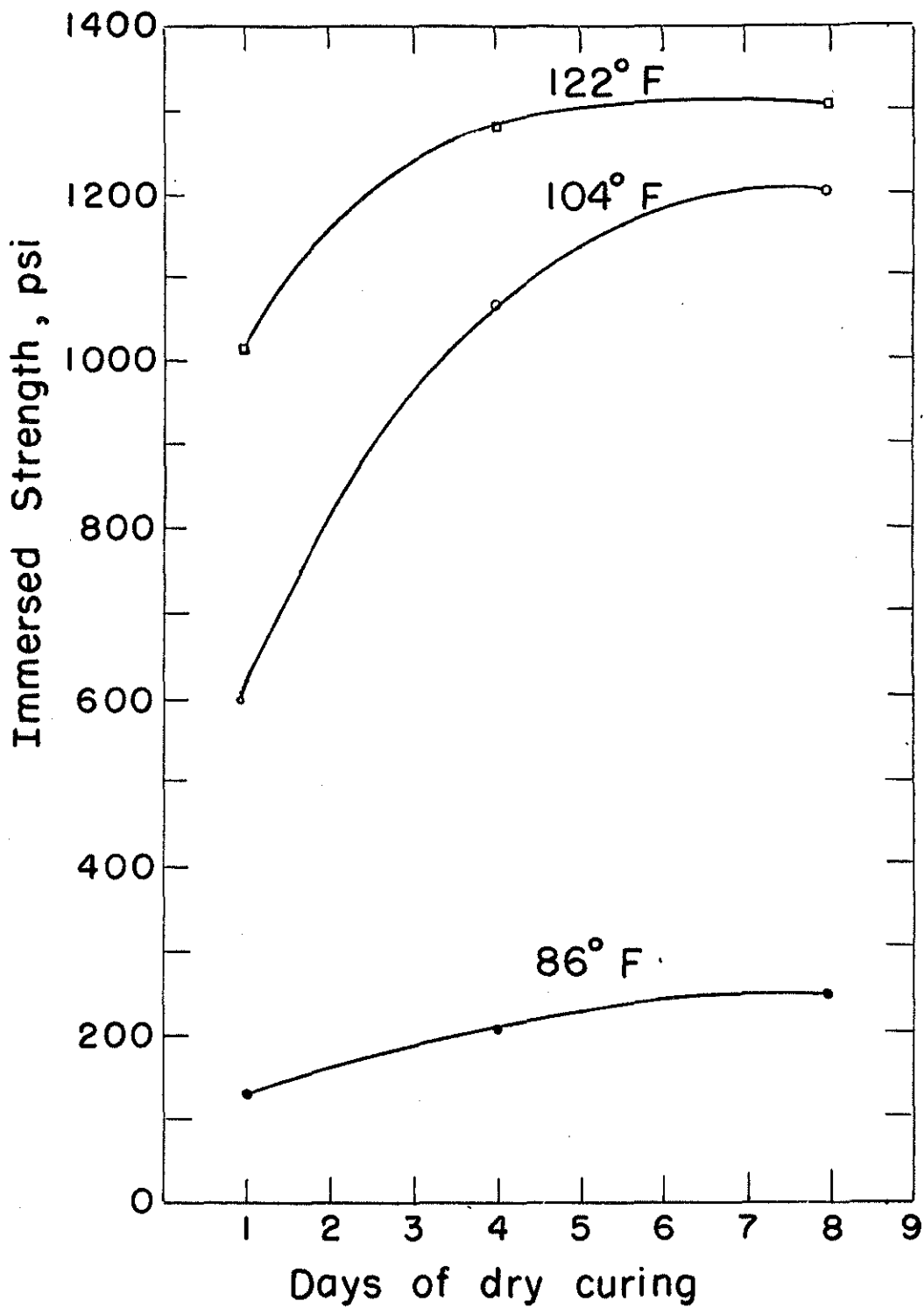


Figure 3. Effect of curing time on immersed strengths of epoxy resin-friable loess specimens.

shortens the curing time but also standardizes the curing temperature. All specimens with lime or other additives were cured under this condition.

All specimens were immersed in distilled water for 24 hours prior to testing for unconfined compressive strength. The strength of the individual specimens was maintained within 10 percent of the average value as required by ASTM Designation C109-54 (2).

The dry densities and immersed strengths obtained for different compositions are presented in Tables 3, 4, 5, and 6. The relationships between immersed strengths and molding volatile contents are shown in Figure 4, 5, 6, and 7. The dry densities versus molding volatile contents are shown in Figures 11, 12, and 13. From these density-volatile and immersed strength-volatile relationships the optimum molding volatile content for density and for strength were obtained and are tabulated in Tables 3, 4, 5, and 6.

Both Figures 4 and 5 show that the immersed strength of the friable loess increases with increasing epoxy content. The immersed strength gain from 7 percent to 9 percent epoxy content is 400 psi. However, if 2 percent of lime were added to the mixtures, the maximum strength gain would be approximately 850 psi. The epoxy-soil mixture yielded much greater immersed strength if 2 percent lime were added. The optimum molding volatile content for maximum immersed strength of epoxy-friable loess mixtures decreased 1.5 percent with every increase of 2 percent epoxy content from 7 percent epoxy content up to 13 percent epoxy content. For epoxy-lime-friable loess mixtures, the optimum volatile content for strength is seen to be nearly the

Table 3. Effect of Guardkote 120A and 120B on the properties of the friable loess (Lab. No. 20-2).

Guardkote 120 A %	120 B %	Molding Volatile Content %	Average Dry Density %	Optimum Volatiles for Density %	Maximum Dry Density pcf	Individual Immersed Strength psi			Average Immersed Strength psi	Optimum Volatile Content for Strength %	Maximum Immersed Strength psi	Average Linear Shrinkage	Average Volatile Retention %	Average Linear Expansion on Immersion, %	Average Moistures Absorption on Immersion, %
7	2.8	9.29	100.10			481	550	494	508			-0.13	2.1	-0.05	14.20
7	2.8	11.24	99.43			517	475	468	487			-0.12	3.0	-0.03	16.40
7	2.8	13.23	100.66			517	461	491	496			-0.17	3.3	0.00	15.15
7	2.8	14.17	101.54			554	593	563	570			-0.10	1.24	+0.25	10.48
7	2.8	14.21	100.18			485	524	718	576			-0.28	4.4	+0.39	14.12
7	2.8	14.96	100.55			606	633	517	586			-0.05	3.4	-0.06	11.66
7	2.8	19.93	97.91	15.00	100.10	356	366		361	14.00	580	+0.42	4.3	+0.15	17.84
9	3.6	7.85	98.77			639	633	596	623			+0.1	2.9	+0.31	18.00
9	3.6	9.52	100.77			833	850	814	832			+0.15	3.0	+0.30	15.22
9	3.6	12.21	102.00			993	896		945			+0.25	3.5	-0.05	9.23
9	3.6	14.90	102.15			590	656	1,011	752			-0.22	4.4	-0.07	10.89
9	3.6	15.82	102.40			465	478	774	572			+0.45	4.0	+0.03	13.28
9	3.6	18.15	99.66	14.50	102.50	567	567	685	606	12.50	1,000	+0.37	3.9	+0.07	11.52
11	4.4	5.05	99.58			814	929	902	882			-0.05	2.9	+0.48	13.53
11	4.4	6.93	100.30			994	863	797	885			+0.24	3.6	+0.39	16.36
11	4.4	8.70	102.40			922	1,126	1,116	1,055			+0.20	3.7	+0.26	10.40
11	4.4	12.10	101.70			1,153	1,093	1,086	1,110			-0.20	5.8	+0.19	11.10
11	4.4	14.45	103.87			823	837	892	851			+0.06	7.7	+0.25	13.39
11	4.4	15.18	103.32			748	837	1,017	867			+0.53	6.6	+0.05	12.32
11	4.4	18.00	98.71	13.50	104.0	445	475	649	523	10.50	1,135	+0.70	7.9	-0.20	15.04
13	5.2	5.66	103.87			1,120	1,289	955	1,121			+0.05	4.4	0.00	12.32
13	5.2	9.20	104.66			1,619	1,027	1,751	1,466			+0.40	6.7	+0.32	12.05
13	5.2	11.51	105.00			1,040	1,208	1,090	1,113			+0.89	8.7	+0.18	10.37
13	5.2	13.39	104.17			1,106	1,093	1,225	1,141			+0.47	9.2	0.00	12.42
13	5.2	13.72	103.34	10.50	105.2	781	856	948	862	9.00	1,490	+1.08	7.3	+0.02	11.96

Table 4. Effect of Guardkote 120A, 120B and lime on the properties of the friable loess (Lab. No. 20-2).

Lime %	120 A %	120 B %	Molding Volatile Content %	Average Dry Density pcf	Optimum Volatile for Density %	Maximum Dry Density pcf	Individual Immersed Strength psi		Average Immersed Strength psi	Optimum Volatile Content for Strength	Maximum Immersed Strength psi	Average Linear Shrinkage %	Average Volatile Retention %	Average Linear Expansion on Immersion, %	Average Moisture Absorption on Immersion, %
2	5	2.0	11.88	100.46			294	277	286			-0.60	1.8	+0.40	18.3
2	5	2.0	13.63	100.40			323	287	305			+0.40	2.2	+0.27	15.3
2	5	2.0	14.85	100.71			373	343	358			+0.10	2.8	+0.15	16.4
2	5	2.0	16.74	104.03	16.80	104.0	452	471	462	16.80	470	+0.40	4.4	+0.27	17.6
2	7	2.8	8.24	98.82			857	817	837			+0.45	1.8	+0.47	11.5
2	7	2.8	10.35	99.83			768	801	785			+0.43	2.6	+0.55	11.9
2	7	2.8	11.76	101.39			798	768	783			+0.35	2.7	+0.30	11.6
2	7	2.8	13.31	102.20			745	732	739			+0.17	5.0	+0.12	8.6
2	7	2.8	15.30	102.74			517	508	513			+0.12	7.5	-0.15	9.9
2	7	2.8	16.90	101.10	14.40	103.9	629	636	633	9.50	840	+1.30	4.8	+0.05	9.9
2	9	3.6	8.64	99.22			1,623	1,442	1,533			+0.50	2.7	+0.50	11.0
2	9	3.6	10.36	102.80			1,718	1,646	1,682			+0.33	3.7	+0.28	10.6
2	9	3.6	12.18	104.60			1,179	1,176	1,178			+0.15	6.0	+0.15	9.6
2	9	3.6	13.29	105.05			1,001	978	989			+0.13	7.3	-0.13	9.8
2	9	3.6	15.08	102.87	13.00	105.2	613	616	615	10.00	1,700	+0.90	8.7	0	13.0

Table 5. Effect of Guardkote 120A, 120B, and lime on the properties of the plastic loess (Lab. No. 528-4).

120 A %	120 B %	Lime %	Molding V. C. %	Average Dry Density pcf	Optimum Volatile for Density	Maximum Dry Density pcf	Individual Immersed Strength psi	Average Immersed Strength	Optimum Volatile Constant for Strength	Maximum Immersed Strength psi	Average Linear Shrinkage	Average Volatile Retention	Average Linear Expansion on Immersion, %	Average Moisture Absorption on Immersion, %
5	2.0	2.0	11.00	102.90			399	389			0.58	2.7	0.45	15.2
5	2.0	2.0	13.42	105.18			458	458			0.70	4.4	0.25	14.9
5	2.0	2.0	15.63	106.07			442	458			0.75	4.9	0.20	17.4
5	2.0	2.0	16.90	105.59			501	498			1.10	5.4	0.30	18.5
5	2.0	2.0	19.22	102.06	15.50	106.10	442	435	16.70	500	1.50	6.0	0.35	19.1
7	2.8	2.0	11.43	103.43			596	616			0.50	3.8	0.35	12.7
7	2.8	2.0	13.02	106.58			735	824			0.80	4.4	0.30	12.8
7	2.8	2.0	15.15	106.14			791	826			1.05	6.6	0.33	13.2
7	2.8	2.0	16.23	103.79			686	672			1.40	6.0	0.40	17.0
7	2.8	2.0	18.44	101.08	14.00	107.40	504	609	14.50	810	1.55	7.9	0.25	17.7
9	3.6	2.0	10.61	102.83			1,040	929			0.50	4.2	0.50	16.6
9	3.6	2.0	11.81	105.55			965	1,008			0.90	5.0	0.40	14.1
9	3.6	2.0	13.88	106.98			1,021	998			0.95	7.5	0.35	13.8
9	3.6	2.0	15.40	104.04	13.50	107.85	972	952	13.00	1,020	1.24	7.7	0.40	14.4

Table 6. Effect of Guardkote 120A, 120B and lime on the properties of the Kansan Gumbo (Lab. No. 512-11)

120A %	120B %	Lime %	Molding Volatile Content %	Average Dry Density pcf	Optimum Volatile For Density %	Maximum Dry Density pcf	Individual Immersed Strength psi	Average Immersed Strength psi	Optimum Volatile Content For Strength	Maximum Immersed Strength psi	Average Linear Shrinkage	Average Volatile Retention	Average Linear Expansion On Immersion	Average Moisture Assumption On Immersion, %	
5	2.0	2.0	12.81	97.55			241	248	245	20.0	429	0.60	2.6	0.70	20.7
5	2.0	2.0	14.51	100.22			264	251	258			0.65	3.6	0.65	20.0
5	2.0	2.0	16.90	100.90			277	300	289			0.70	3.7	0.55	20.4
5	2.0	2.0	18.20	99.82			356	290	323			1.20	3.7	0.50	19.4
5	2.0	2.0	20.06	98.09	16.40	101.00	471	386	429			1.45	4.2	0.50	20.0
7	2.8	2.0	14.18	95.60			501	458	479	18.0	600	0.75	4.3	0.55	18.5
7	2.8	2.0	15.76	98.26			471	524	498			0.60	4.6	0.25	20.0
7	2.8	2.0	17.90	99.36			642	554	598			0.85	5.9	0.40	19.1
7	2.8	2.0	19.11	98.00			461	465	463			1.15	6.5	0.35	19.8
7	2.8	2.0	22.90	94.33	17.40	99.60	491	501	496			2.05	7.3	0.25	21.4
9	3.6	2.0	14.67	98.44	16.5	101.85	846	732	789	17.0	850	1.10	3.9	0.80	19.3
9	3.6	2.0	16.35	101.74			853	791	822			1.40	4.4	0.75	17.2
9	3.6	2.0	17.93	99.05			846	824	835			1.15	4.9	0.65	17.7
9	3.6	2.0	19.32	97.28			682	577	630			1.50	6.6	0.55	18.9

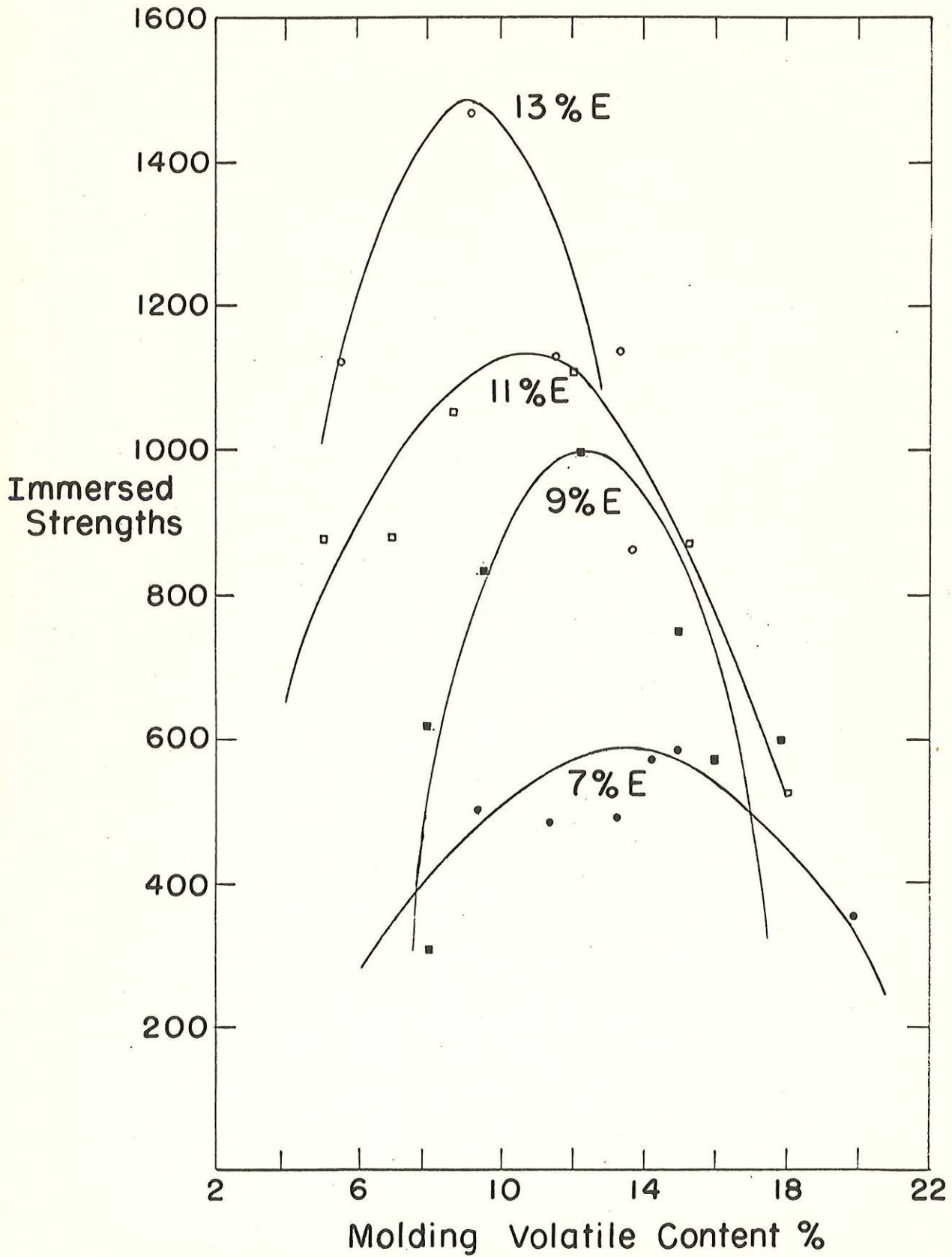


Figure 4. Molding volatile content -- immersed strength relationship for epoxy resin-friable loess mixtures.

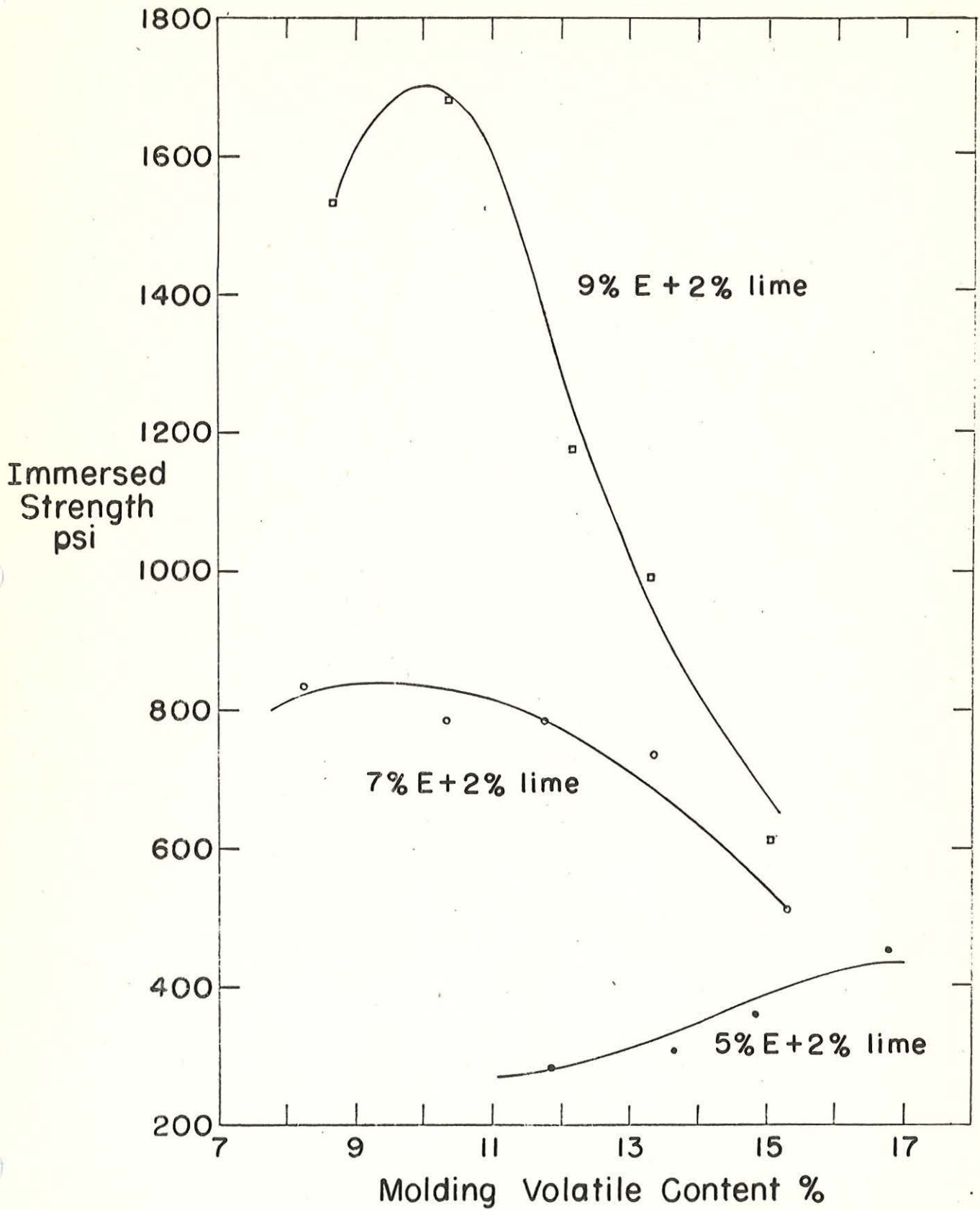


Figure 5. Molding volatile content -- immersed strength relationship for epoxy resin-lime-friable loess mixtures.

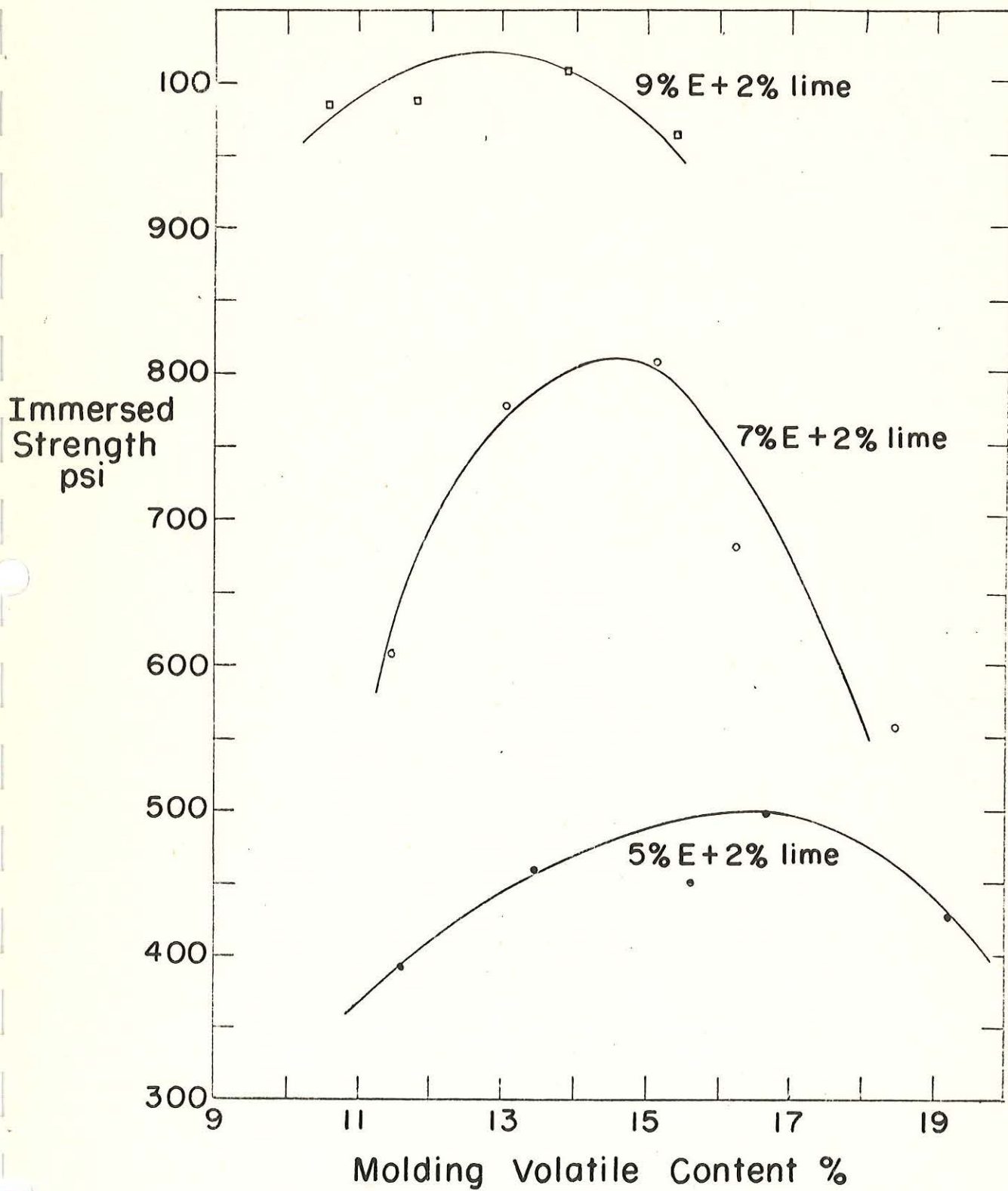


Figure 6. Molding volatile content -- immersed strength relationship for epoxy-lime-plastic loess mixtures.

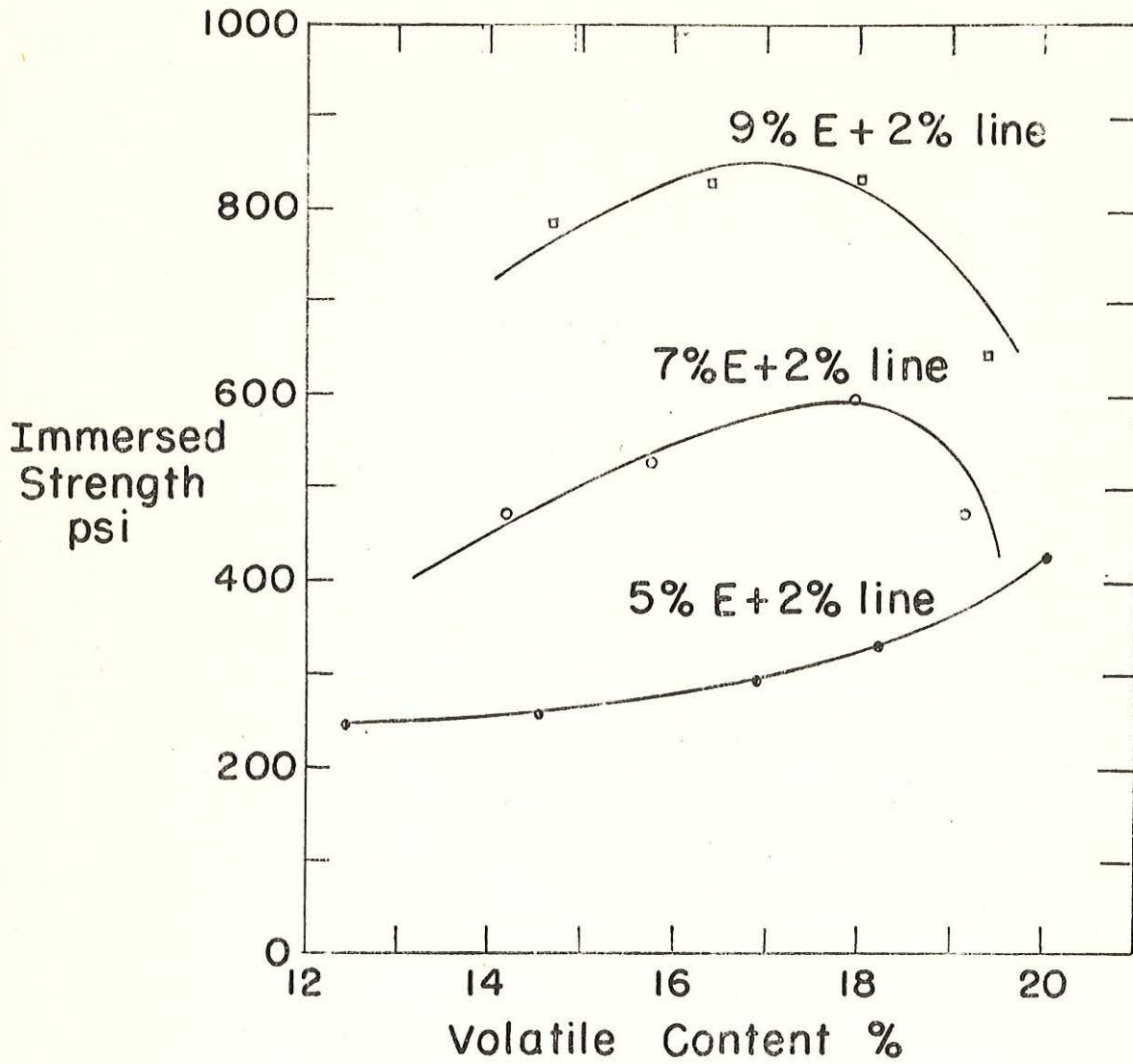


Figure 7. Molding volatile content -- immersed strength relationship for epoxy-lime-gumbotil mixtures.

same for 7 and 9 percent of epoxy content.

Figures 6 and 7 for plastic loess and gumbotil show the same pattern as that for friable loess, but when the epoxy content was increased to 9 percent the rate of strength change with increasing volatile content was less. At volatile contents higher than 20 percent the specimens would have many slickensides after compaction, so no more satisfactory specimens could be obtained. The plastic loess contained 39 percent clay and the gumbotil had 42.4 percent clay; both had higher clay contents than the friable loess, which had 19.6 percent. With 9 percent epoxy and 2 percent lime, the maximum immersed strength of the plastic loess and gumbotil specimens were 60 percent and 50 percent, respectively, of the maximum immersed strength of the friable loess specimens. Apparently, soils with heavy clay content are less effectively stabilized with epoxy-lime than other soils with less clay content.

Other additives, therefore, were tried to improve the stability of the epoxy-lime-gumbotil mixture. Table 7 and Figure 8 shows the strengths obtained with various chemicals, lime and cement. Lime still proved to be the best additive among all chemicals used in the epoxy-gumbotil mixture. Specimens with 2 percent lime and 5 percent epoxy had higher immersed strength than the specimens with 6 percent lime and 5 percent epoxy. With 4 percent lime, specimens showed higher immersed strength than the specimens with 2 percent lime after curing at 40°C oven for seven days; however the strength difference of the two mixtures was not significant after curing for one day. The increase in strength after seven days is probably due to the increase of lime content. Therefore, 2 percent lime, based on dry soil weight, was

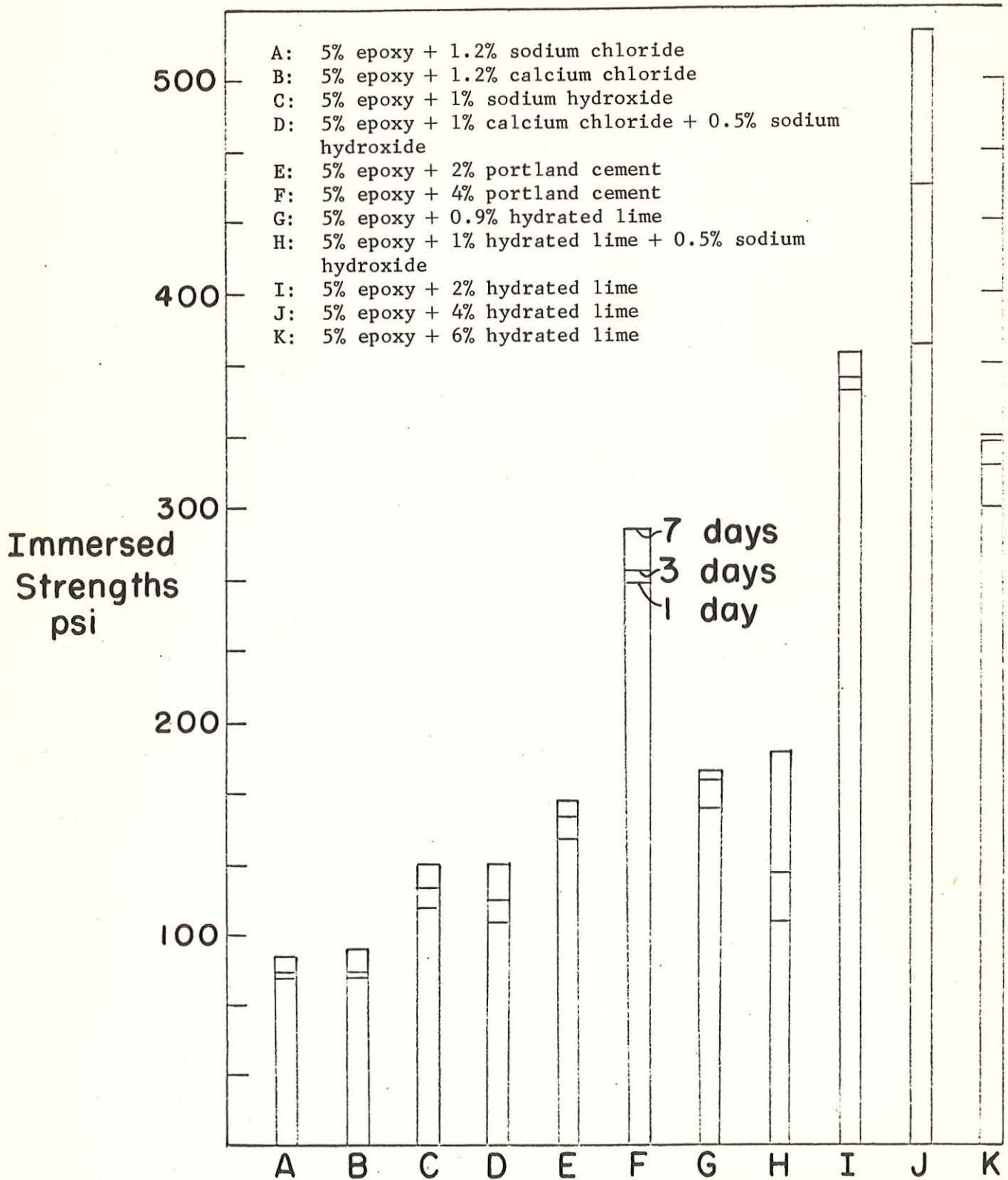


Figure 8. Effect of different additives on immersed strength of epoxy-gumbotil mixture.

Table 7. Effect of guardkote 120 A, 120 B and different additives on the immersed strengths of the Kansan gumbctil (Lab. No, 512-11)

120 A %	120 B %	V. C. %	Additives %	Curing Time	Ave. Strength psi
5	2.0	16.40	2% lime	one day	356
5	2.0	16.40	2% lime	three days	363
5	2.0	16.40	2% lime	seven days	373
5	2.0	17.36	4% lime	one day	376
5	2.0	17.36	4% lime	three days	452
5	2.0	17.36	4% lime	seven days	521
4%	1.6	17.84	6% lime	one day	297
4%	1.6	17.84	6% lime	three days	320
4%	1.6	17.84	6% lime	seven days	330
5%	2.0	16.00	1.2% NaCl	one day	80
5%	2.0	16.00	1.2% NaCl	three days	83
5%	2.0	16.00	1.2% NaCl	seven days	90
5%	2.0	16.00	1.2% CaCl ₂	one day	80
5%	2.0	16.00	1.2% CaCl ₂	three days	83
5%	2.0	16.00	1.2% CaCl ₂	seven days	96
5%	2.0	16.00	1% NaOH	one day	113
5%	2.0	16.00	1% NaOH	three days	123
5%	2.0	16.00	1% NaOH	seven days	133
5%	2.0	16.00	1% Ca(OH) ₂	one day	106
5%	2.0	16.00	0.5% Na(OH)	three days	116
5%	2.0	16.00	0.5% Na(OH)	seven days	133
5%	2.0	16.00	2% cement	one day	146
5%	2.0	16.00	2% cement	three days	156
5%	2.0	16.00	2% cement	seven days	162
5%	2.0	16.00	4% cement	one day	264
5%	2.0	16.00	4% cement	three days	271
5%	2.0	16.00	4% cement	seven days	290

Table 7 (continued)

120 A %	120 B %	V. C. %	Additive %	Curing Time	Ave. Strength psi
5%	2.0	18.00	0.9% lime	one day	159
5%	2.0	18.00	0.9% lime	three days	172
5%	2.0	18.00	0.9% lime	seven days	175
5%	2.0			one day	106
5%	2.0	16.00	2% lime and 0.5% NaOH	three days	129
5%	2.0			seven days	185
5%	2.0	18.00	1.8% lime	one day	231
5%	2.0	18.00	1.8% lime	three days	212
5%	2.0	18.00	1.8% lime	seven days	231
5%	2.0	18.00	3% lime	one day	251
5%	2.0	18.00	3% lime	three days	244
5%	2.0	18.00	3% lime	seven days	254
5%	2.0	18.00	4% lime	one day	261
5%	2.0	18.00	4% lime	three days	238
5%	2.0	18.00	4% lime	seven days	238
5%	2	18.00	5% lime	one day	281
5%	2	18.00	5% lime	three days	304
5%	2	18.00	5% lime	seven days	297

used as the secondary additive for the engineering evaluation of all epoxy-soil mixtures in the phase 2 investigation.

Figure 9 and Table 8 show that the maximum immersed strength obtained for dune sand is at the lowest volatile content. Those points were erratic rather than ordered and a smooth curve could not be drawn through the points. The maximum strengths obtained are approximately the same for 3, 4, and 5 percent epoxy contents. When the volatile content was increased by adding more water to the mixtures, the immersed strengths obtained would decrease. The rate of strength decrease with the increasing volatile content was greater for higher percentages of epoxy. The minimum immersed strength for 4 and 5 percent epoxy was at a volatile content of approximately 6 percent; while for 3 percent epoxy, the volatile content is 8 percent for minimum strength.

Both lime and cement were tried as additives for the sand-epoxy mixture in order to make higher immersed strengths. Figure 10 and Table 9 show the immersed strengths obtained with different combinations. The maximum immersed strengths of epoxy-sand specimens in Figure 9 and Table 8 were obtained from mixtures in which no extra water was added during mixing. However, the same rule could not apply to the epoxy-lime sand mixtures; if no extra water was added to the epoxy-lime-sand mixtures, the specimens would slake after immersing in water. The experiment showed that 1 or 2 percent water was necessary for the epoxy-lime-sand mix. Further tests indicated that the water should be added and mixed with lime-sand mixture before the prepared epoxy was used. This is the same procedure of molding specimens suggested at the end of presentation and discussion of results in phase 1. The specimens

Table 8. Effect of guardkote 120 A, 120 B and lime on the properties of the dune sand (Lab. No. S-6-2).

120A %	120B %	V. C. %	Ave. Dried Density pcf	Method of Curing	Individual Strength	Immersed psi	Ave. Immersed Strength psi	Optimum V. C. for Strength %	Maximum Immersed Strength psi	Ave. Linear Shrinkage %	Ave. V. C. Retention %	Ave. Linear Expansion on Immersion %	Ave. Moisture Absorption on Immersion %
3	1.2	2.88	110.5	Seven days in room temp. and one day in distilled water.	337	264 337	313	1.2 (no extra water was added)	353	-1.15	1.2	+0.20	16.7
3	1.2	5.14	110.9		330	386	358		-0.70	0.6	0.00	12.5	
3	1.2	6.74	111.5		353	356	354		-0.80	1.0	-0.15	10.3	
3	1.2	8.20	112.3		198	205 159	184		-0.77	0.9	-0.65	9.4	
3	1.2	11.53	112.3		238	238	238		-0.60	1.6	-0.10	7.8	
4	1.6	3.61	110.9	"	287	271 294	384	1.6 (no extra water was added)	356	-0.70	1.3	-0.13	14.6
4	1.6	5.92	112.4	"	225	238	232		-0.43	1.4	-0.13	9.5	
4	1.6	8.62	112.1	"	376	264 330	323		+0.40	1.3	-0.23	7.2	
4	1.6	10.68	114.0	"	310	205 271	262		-0.45	1.7	-0.18	3.3	
5	2.0	2.13	112.5	Seven days in room temp. and one day in distilled water.	320	327 320	323	2.12 (no extra water was added)	353	-1.00	2.0	+0.10	15.8
5	2.0	3.58	112.6		146	182 195	141		-1.00	2.5	+0.05	14.2	
5	2.0	5.49	111.2		93	80 100	91		+0.40	1.7	0.00	12.9	
5	2.0	9.43	113.6		179	133 159	157		-0.20	1.7	-0.20	7.2	
3	1.2	1.16	108.7	"	379	353 337	353	1.2 (no extra water was added)	353	-0.44	0.7	+0.02	17.2
4	1.6	1.49	109.4	"	337	386 346	356		-0.25	1.3	+0.33	17.8	
5	2.0	1.80	110.3	"	346	379 379	368		-0.57	1.4	+0.35	17.6	

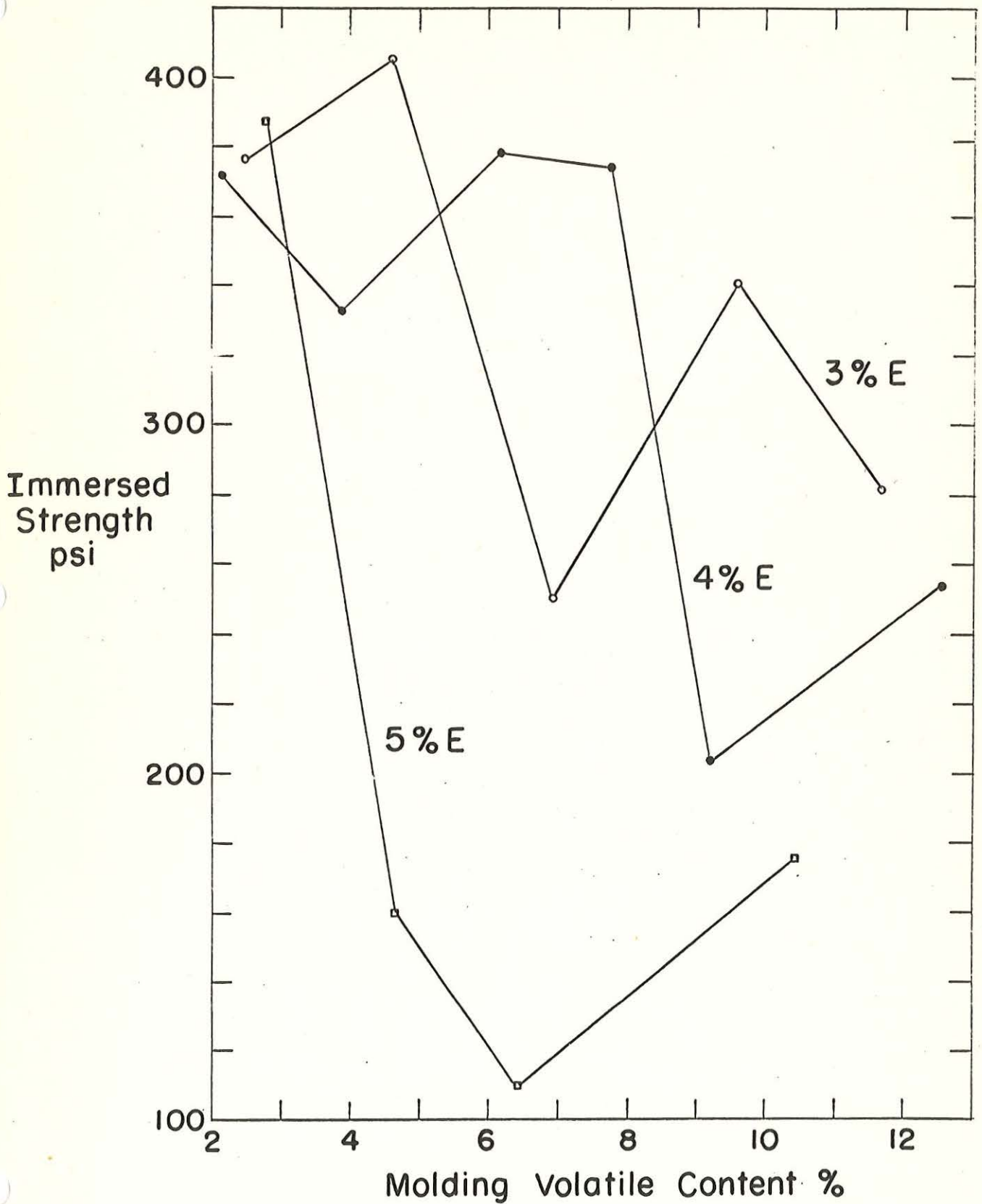


Figure 9. Molding volatile content -- immersed strength relationship for epoxy-dune sand mixtures.

Table 9. Effect of Guardkote 120 A, 120 B and different additives on the average immersed strengths of the dune sand (Lab. No. S-6-2).

120 A	120 B	Additive	Method of Curing	Ave. Immersed Strength, psi	V. C. %
3%	1.2%	2% lime	1 day in 40° oven, 1 day in distilled water	684	2.20
3%	1.2%	2% cement	"	532	1.70
3%	1.2%	3% cement	"	573	2.20
3%	1.2%	3% cement	1 day in 100% humidity rm. 1 day in distilled water	655	2.20
2%	0.8%	2% lime	1 day in 40° oven 1 day in distilled water	318	1.80
2%	0.8%	3% lime	"	373	2.80
2%	0.8%	4% lime	"	176	3.80

with 3 percent epoxy would have their strength increased by 92 percent if 2 percent lime was added as a second additive. The results are given in Table 10 and Figure 10.

A tentative explanation is given for the mechanism of the epoxy and epoxy lime stabilization based on the test results of the loess, gumbotil and sand specimens. Uncured epoxies are either honey-colored liquids or brittle-amber solids which become liquid when heated. Enlarged 10 million times, the molecules of resin might resemble short pieces that vary in length from one half inch in some of the liquid to several inches in the solids (21). These threads are joined together at the ends and along the sides to form large cross-linked structures after curing. Each molecule is tied to several others like the ropes of a fish net or the filaments of a spider's web, but in an irregular rather than uniform pattern. Since the epoxy resins are cured only by aromatic or aliphatic hydroxyls and various other organic radicals, it is believed that no chemical reaction has taken place between epoxy resins and various kinds of soil particles. But the epoxy resins successfully stabilize soils which have either ion exchange capacity or no ion exchange capacity; therefore there is evidence of attraction between the soil and the polymer. This attraction (14) could be caused by the electrically unsaturated ions on the surface of the soil particle attracting the ionic polymer (amine groups), aided by a secondary valence force between the soil and the polar groups of the polymer (epoxy and hydroxyl groups).

When the epoxy resin mixture alone is mixed with the dune sand, a coating of individual particles with resin solution is attained. The

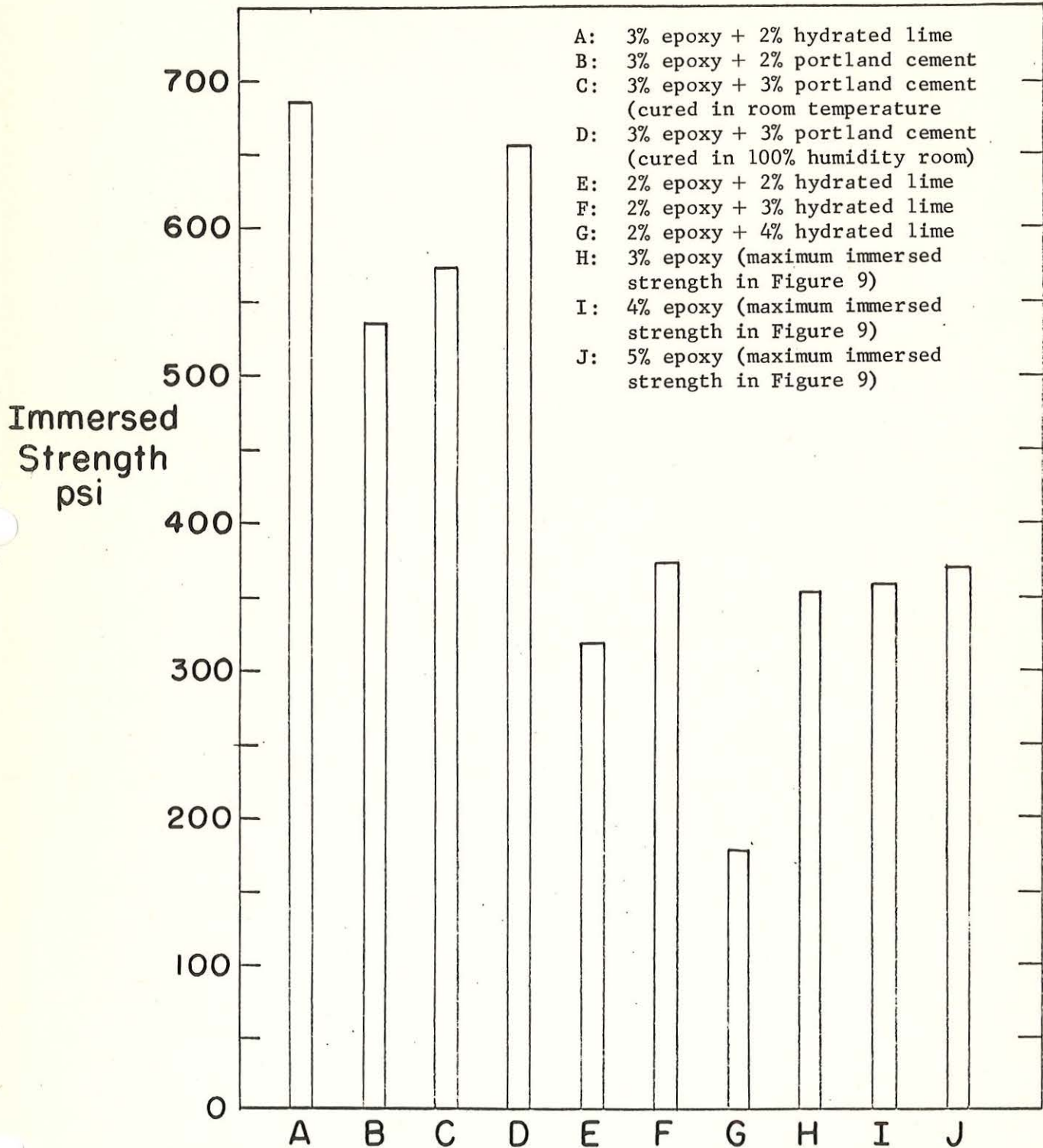


Figure 10. Effect of different additives on immersed strength of epoxy-sand mixture.

Table 10. Effect of Guardkote 120B and lime on the curing time and relative hardness of the cured epoxy resin.

T = 80°F	120A parts by weight	120B parts by weight	Lime parts by weight	Curing time minutes	Relative hardness (by Shore Cleroscope)
	10	1	0	100	6
	10	2	0	25	550
	10	3	0	23	510
	10	4	0	20	350
	10	1	0.5	26	270
	10	1	1	22	510
	10	1	2	22	550
	10	1	3	22	170
	10	4	0.5	10	210
	10	4	1	10	250
	10	4	2	9	220
	10	4	3	7	330
	10	2	0.5	13	600
	10	2	1	13	620
	10	2	2	15	650
	10	2	3	15	610

epoxy is in contact with and adheres to the sand grains. When the cured epoxy hardens, it becomes a solid and binds the sand grains together.

The sand specimens yield a decreasing strength when water is added during mixing. Water is a non-solvent for epoxy mixtures. Tests showed that the addition of water to a prepared epoxy makes the epoxy gel float on the water surface. The individual sand grains will be surrounded by a film of water due to the hydrophilic character of grains, so the epoxy globules are prevented by the water film from coming in contact with and adhering to the sand grains. By the time the mixing water evaporates, the epoxy globules will already have set-up and the viscosity is so great it will stay somewhere between the sand grains which are less effectively bound than for the epoxy-sand specimens without the addition of water. If more water is used, thicker water films around the sand grains will be formed. This further reduces the probability of epoxy coming in contact with and adhering to the sand grains and it results in further strength decreases.

The maximum immersed strengths of dune sand specimens did not increase with increasing epoxy contents. The specimens containing 4 and 5 percent epoxy had approximately the same immersed strengths as the specimens with 3 percent epoxy content. Probably, 3 percent epoxy is enough to coat the individual sand grains with epoxy film. More epoxy makes the thickness of film increase, but it would not help the increase of strength.

When the epoxy is mixed with the friable loess, the volatile-strength relationship follows the usual pattern of increasing strength with increasing volatile content until a maximum is attained. Tests

in phase 1 have indicated that pre-emulsification of epoxy and hardener was not absolutely necessary; probably the clay fraction of soil acts as an emulsifying agent and thus aids the distribution of the resin in the water; thus the extra water mixed with soils prior to the addition of the prepared resin, enables a more thorough distribution of the dispersing epoxy resin particles through the mixture. After the epoxy resin particles set up, the solid epoxy adheres to soil grain or agglomerates of grains and bind them together. With higher volatile content the strength values will decrease due to the less effective compaction.

Hydrated calcific lime has been found to be a very beneficial additive to improve the epoxy-soil mixture with higher immersed strengths. The friable loess specimens with 5 percent epoxy content would slake in water; they would give 470 psi maximum immersed strength when 2 percent hydrated lime was added. Specimens with 7 percent epoxy content had a 45 percent immersed strength increase after adding 2 percent lime to the mixture and those with 9 percent epoxy contents had a 70 percent strength increase.

The volatile-strength relationships of lime-epoxy-clayey soil mixtures follow the same patterns as the specimens of epoxy-clayey soil mixtures. The optimum volatile content for strength decrease with the increasing epoxy content. Soils which have higher clay contents require a higher optimum volatile content for strength. Each soil has a maximum volatile content beyond which satisfactory specimens cannot be molded. The limitations increase with the proportion of clay content.

When lime alone was used as a stabilizing agent with the friable loess, 2 percent hydrated calcitic lime gave 75 psi maximum immersed strength after seven days moisture curing. However, the specimens with 7 percent epoxy would have a 250 psi strength gain if 2 percent lime was added to the mixture and the specimens with 9 percent epoxy content would have a 700 psi strength increase. The effect of lime is therefore believed to be due to its effects on both soil minerals and the epoxy-hardener system. Lime may be expected to attack soil mineral surfaces and render them electrically more unsaturated and more polar; the properties of cured epoxy might also be changed by the action of lime; all resulting in better bonding and in an increase in strength.

The effect of lime on pure epoxy systems was investigated briefly by determining setting time, relative hardness and X-ray diffraction pattern of various epoxy, hardener and lime mixes. Results obtained (Table 10) indicated that setting time decreases in proportion to the percentage of lime. Relative hardness on the other hand increased markedly with lime for 10:1 epoxy hardener system, meaning savings from hardener can be realized by using a few parts of lime. For 10:2 epoxy hardener system, however, increase in hardness with lime was not so pronounced; whereas hardness of the 10:4 epoxy hardener system showed a significant decrease with lime producing set epoxy systems with moderate hardness. In the screening tests 10:4 epoxy hardener system was found most suitable for soil stabilization (Table 2). This combination when used for soil stabilization in conjunction with lime was found to produce higher stability. It may therefore be concluded that a moderate hardness results in better bonding. A possible explana-

tion for this follows:

The majority of resins and polymers show little or no crystalline nature in X-ray diffraction analysis (13). These substances formed with less degree of crystallization are called amorphous solids. In Figure 11, curve (a) shows the cured epoxy-hardener specimen has fair crystallinity, while curve (b) shows the same specimen with lime has less crystallinity. As the peak appearing in curve b was identified as Ca(OH)_2 according to the ASTM index (3), we can anticipate that lime affects the polymerization reaction and makes the epoxy resin less crystalline, and low hardness points out that the polymer has high ductility. A more ductile material is thus formed which can deform plastically to a greater extent than the epoxy resin specimen without lime. The higher ductility of resin could partially be responsible for increases in immersed strength of soil specimens. The lime left which shows in X-ray diffraction, becomes available for soil-lime reaction which gives rise to added strength.

Figure 12 shows volatile-dry density relationships for the friable loess-epoxy combinations. The optimum volatile contents for maximum dry densities are, on the average, 1 to 1.5 percent more than the optimum volatile content for strength. The maximum dry densities are seen to increase with increasing epoxy content. Figure 13 shows the relationships for volatile content-dry density for the friable loess-epoxy-lime combination. The optimum volatile contents for density and for strength are approximately the same for 5 percent epoxy content. For higher epoxy contents, the value of optimum volatile content is higher than that for immersed strength. An increase of 2 pcf in dry

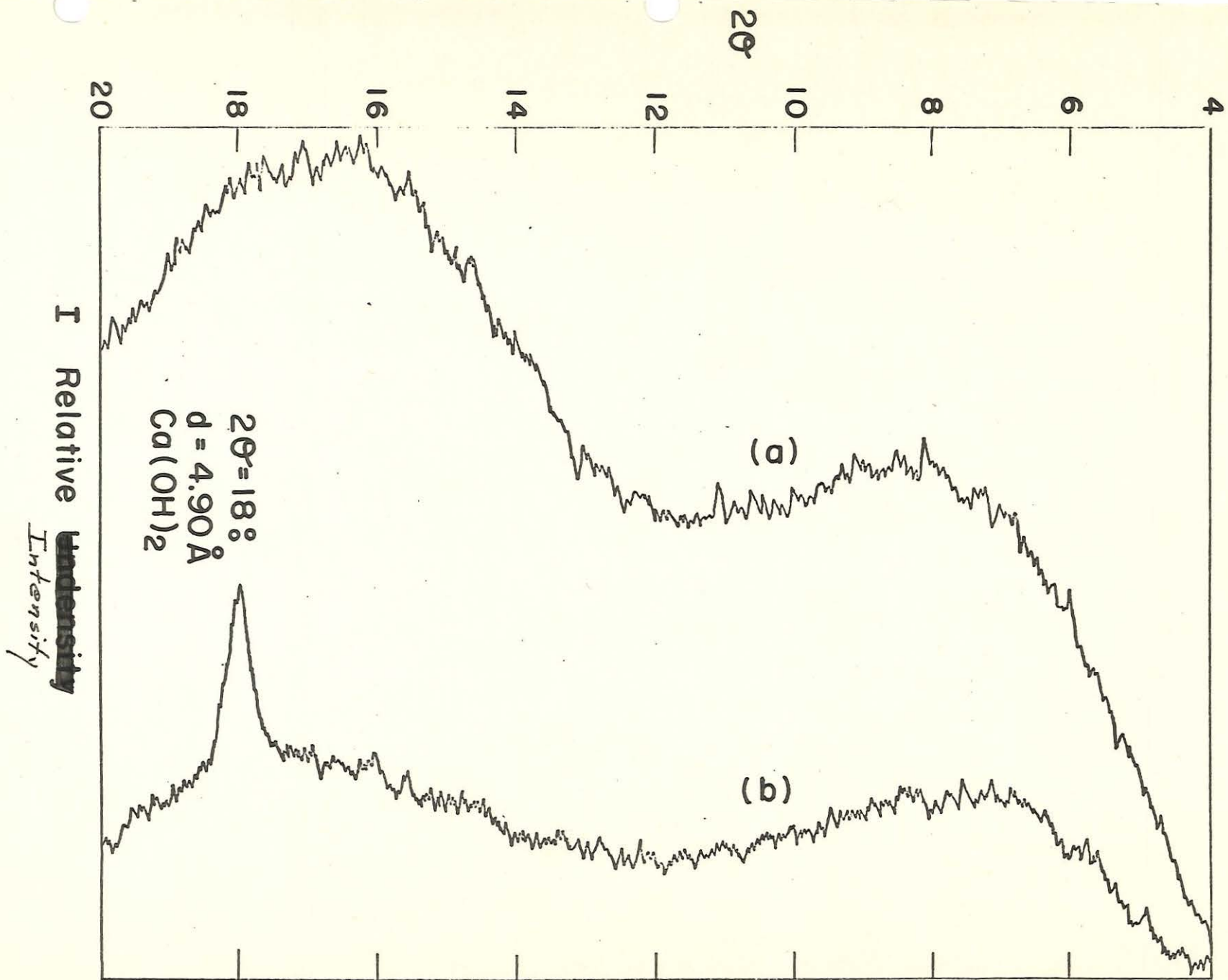


Figure 11. X-ray diffraction curves for: a) Epoxy: hardener 5:1 by weight, b) Epoxy: hardener: lime: = 5:1:1 by weight.

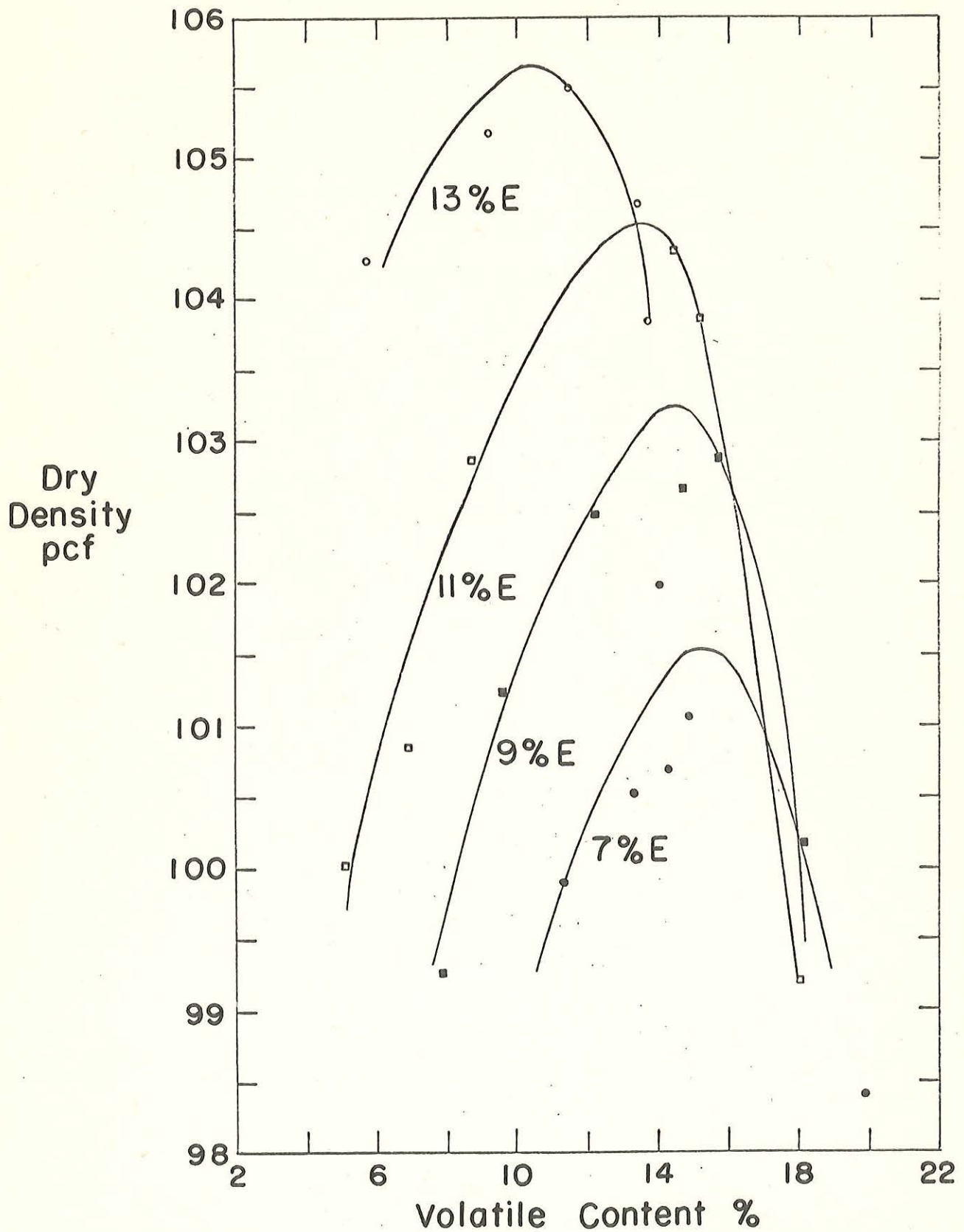


Figure 12. Molding volatile content -- dry density relationship for epoxy-friable loess mixtures.

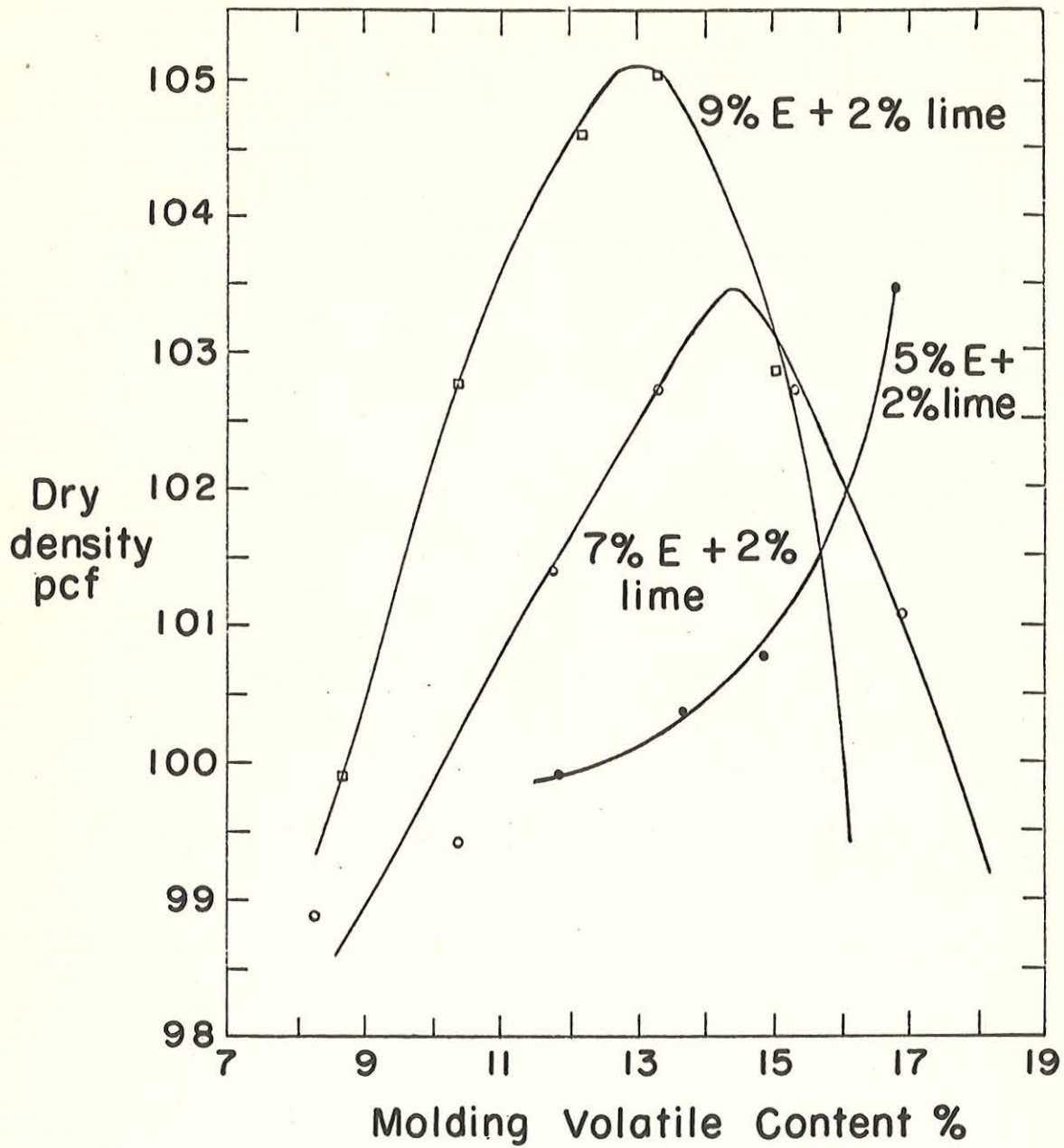


Figure 13. Molding volatile content -- dry density relationship for epoxy-lime-friable loess mixtures.

density is obtained if 2 percent lime is added to the epoxy-soil mixture.

The volatile content-dry density relationships for the plastic loess and gumbotil stabilized by epoxy and lime are presented in Figure 14. It was found that the maximum dry densities for different epoxy contents were approximately the same for plastic loess soil; while the relationships for gumbotil shows that the maximum dry density for the specimen with 5 percent epoxy content is greater by 2 pcf than that of the specimen containing 7 percent epoxy.

Effect on Shrinkage, Swelling and Moisture Absorption

The immersed strength, the shrinkage upon drying, and the expansion upon wetting are all important criteria of the engineering stability of a soil. Excessive deformations from drying, wetting and alternative freezing and thawing are symptoms of instability of soils. If these happen to a base or a subbase material, the excessive deformation can cause the road surface material to be damaged or cracked.

According to Roderick (18), allowable maximum linear expansion of the stabilized soil, used as a flexible highway base course, is 1.64 percent.

The data presented in Tables 3, 4, 5, 6, and 8 show that the four soils gave average linear expansion values which are far less than the 1.64 percent maximum allowed after immersion for one day. On the viewpoint of the allowable linear expansion upon immersion in water, they would be suitable as base course material when stabilized with the amount of epoxy used.

The absorption of water by cohesive soils causes swelling and conversely drying causes shrinkage. These volume changes have been studied for cohesive soils (11). It shows that the maximum changes in volume due

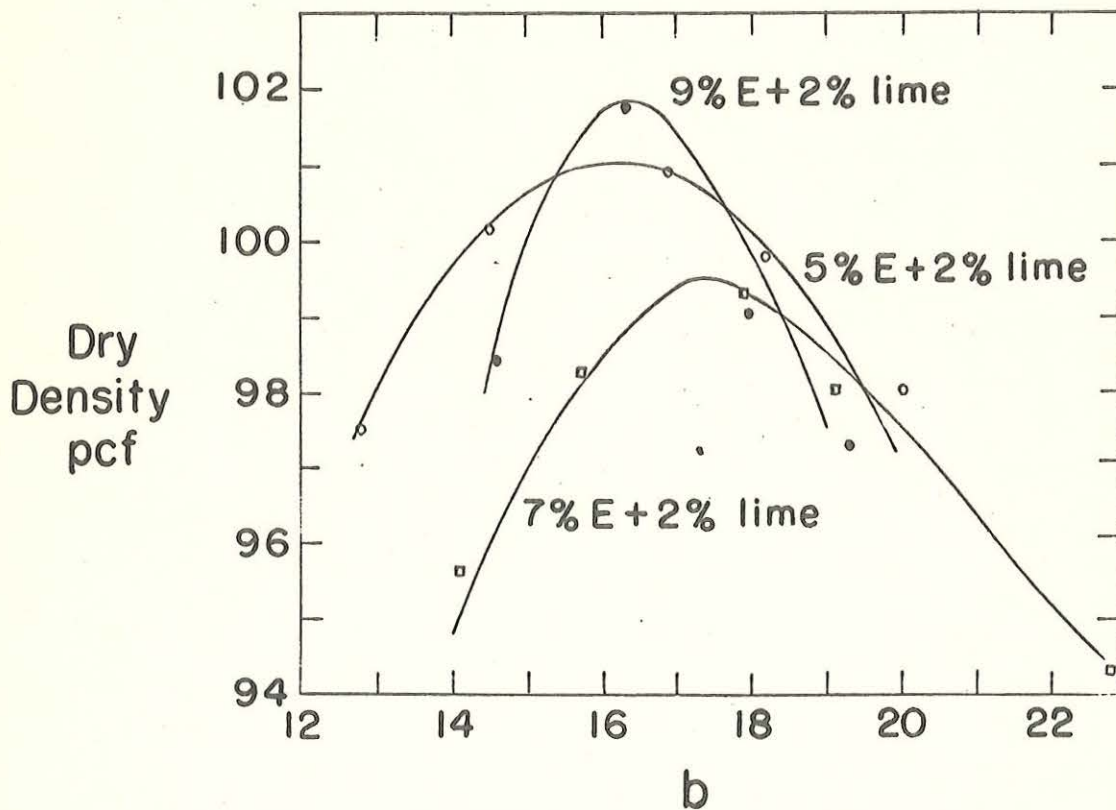
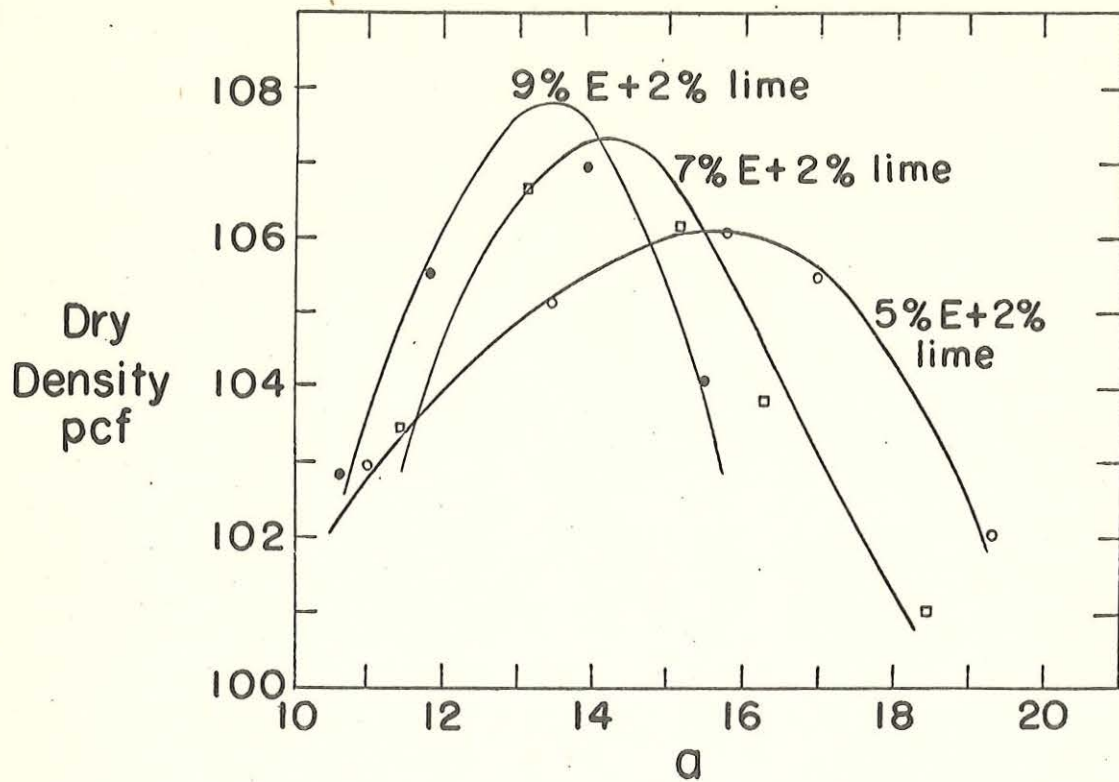


Figure 14. Molding volatile content-immersed strength relationship for epoxy

- Resin-lime-plastic loess mixtures
- Resin-lime-gumbotil mixtures.

to drying occurred when the specimens were made up in a saturated condition. But the minimum changes in volume due to swelling occurred when the specimens were made up in saturated condition. It is therefore considered advisable to compact cohesive subgrades below their optimum moisture content in cases where they are likely to be subject to evaporation of moisture during the life of the road and above their optimum moisture content in case the ingress of moisture is likely to occur during the life of road.

The results presented in Tables 3, 4, 5 and 6 show that the average linear shrinkages of the three soils are less when their volatile contents are at or below optimum for strengths; the average linear expansions on immersion are less when their optimum volatile contents are at or above optimums for strength. It is concluded that the same rules which were suggested above should be applied to the epoxy-lime stabilized soils during construction.

For cement stabilized soils used as a paving material, a recommended requirement with respect to absorption is that the maximum moisture content at any time during wet-dry or freeze-thaw tests shall not exceed the quantity which will completely fill the voids of the specimens at time of molding. The maximum dry density of the friable loess specimen containing 9 percent epoxy, from Figure 10, is about 106 pcf. The specimens would weigh $\frac{A \cdot h}{12^3} \times 106 \times 454$ gram. Where A is the cross-sectional area of the specimens in square inches, h is the height of the specimen in inches. Therefore, the 2 by 2 inch specimen would weigh $\frac{\pi(2)^2 \times 2}{4 \times (12)^3} \times 106 \times 454 = 175$ gm. If the specific gravity of the soil is assumed to be 2.65, the solid space of the soil in 2 by 2 inch specimen would be equal $\frac{175}{2.65} \text{ cm}^3$. In case the void space is filled with water, the maximum water content should be equal to $\frac{37}{175} = 21$ percent.

The average moisture absorptions are all less than 21 percent after immersion. They are suitable as paving materials on the basis of absorption of water.

Frost Susceptibility

The deformation and the reduced strength caused by alternative freezing and thawing tests are the main measurements in the evaluation of frost susceptibility. The Iowa Freeze-Thaw Test (12) was used with specimens prepared from the raw soil and the selected mixtures. All raw soils except sand bulged and were completely destroyed at the end of the 10th cycle. Figure 15 shows the treated and untreated specimens after three cycles of alternative Freeze-Thaw Test. The treated soils contained 7 percent epoxy and 2 percent hydrated lime except dune sand which was stabilized by 3 percent epoxy and 2 percent lime. The results of the test are tabulated in Table 11. There was almost no detectable heaving of epoxy-lime dune sand specimens after 10 freeze-thaw cycles. Both linear expansion and the strengths obtained from freeze-thaw specimens were affected by the percentage of clay content. The specimens with more clay yielded more linear expansion and lower strength than those with less clay content. The linear expansion for the freeze-thaw specimens were 0, 0.25, and 3.17 percent for the friable loess, plastic loess and the gumbotil, respectively. When subjected to the freeze-thaw test, specimens for friable loess, plastic loess, gumbotil and dune sand had average strengths of 820, 677, 366, and 672 psi, respectively. These are 97.5, 83.5, 61 and 98.5 percent of maximum immersed strengths

Table 11. Effect of freezing and thawing on untreated and treated soils.

	Friable Loess 2% Lime + Epoxy Resin Content, %		Plastic Loess Epoxy Resin Content % + 2% Lime		Gumbotil Epoxy Resin Content % + 2% Lime		Dune Sand Epoxy Resin Content % + 2% Lime	
	0	7	0	7	0	7	0	7
	Molding volatile content, %	18.85	9.66	15.09	15.03	20.35	18.44	3.64
Dry density, pcf	106.06	100.65	106.45	105.75	104.87	99.48	105.27	111.70
Linear expansion after 10 cycles of freeze-thaw, %		0		0.25		3.17		0
Linear expansion after 11 days immersion, %	--	0.40	--	0.73	--	0.80	--	0.30
Volatile after 10 cycles of freeze-thaw, %	31.25	2.25	29.54	4.07	32.03	3.48	20.85	1.82
Volatiles after 11 days immersion	--	16.80	--	18.17	--	21.05	--	17.67
Unconfined compressive strength after 10 cycles of freeze-thaw (Pf) psi	--	820 (840)	--	677 (810)	--	366 (600)	--	672 (684)
Unconfined compressive strength after 11 days immersion (Pc) psi	--	708	--	730	--	463	--	598
Index of resistance to freezing $R_f = \frac{P_f}{P_c} \times 100\%$	--	115.8	--	92.7	--	79.1	--	112.4

obtained by these soils (Tables 4, 5, 6, and 8) at identical epoxy contents. Gumbotil was affected most severely both in expansion and unconfined compressive strength when subjected to alternate freezing and thawing.

California Bearing Ratio

The California Bearing Ratio test, usually shortened to CBR, is another way to determine the stability of the base course for flexible pavements. The main purpose of a base course in flexible pavement design is to provide a stress-distributing medium which will spread the load applied to the surface, so that shear and consolidation deformations will not take place in the subgrade. Table 12 shows the results of CBR tests performed on untreated 20-2 soil and on soil 20-2 treated with epoxy. The CBR value of the untreated specimen was 10. The CBR value of the specimen treated with 7 percent epoxy and 2 percent lime is approximately 40 times that of the untreated specimen.

The linear expansion for the treated specimen was constant after soaking 25 hours in water. Linear expansion of the untreated specimen was approximately 27 times that of the treated specimens after soaking 96 hours in water; the small linear expansion shows that water proofness was obtained by the treatment.

California Bearing Ratio values for lower epoxy contents were estimated by assuming proportionality between CBR values and epoxy contents. The assumption was based on observed proportionality between unconfined compressive strengths and epoxy contents.

Table 12. Effect of epoxy resin on California Bearing Ratio and related properties of the friable loess.

Epoxy 120 A %	120 B %	lime %	Dry density of molded specimen pcf	Volatile content during molding, %	Moisture retention after curing %	Moisture absorption after 4 days soaking %	Expansion of specimens during 4 days soaking		CBR at 0.1 penetration after 4 days soaking
							elapsed time, %	hours	
0	0	2	10664	17.88	*16.02	18.19	0	0.000	10
							1	0.007	
							25	0.038	
							48	0.047	
							72	0.053	
7	28	2	106.75	9.80	**7.94	13.78	96	0.055	410
							0	0.000	
							1	0.001	
							25	0.002	
							48	0.002	
							72	0.002	
							96	0.002	

* The specimen was cured at room temperature for one day period.

** The specimen was cured at 104°F oven for one day period.

The estimated CBR values for 1 and 2 percent epoxy content are given below.

Soil	Epoxy content %	Lime content %	CBR
20-2	1	2	50
20-2	2	2	100

THE APPLICATION OF EPOXY STABILIZATION TO PAVEMENT CONSTRUCTION

Pavements may be classified as flexible or rigid. The main difference between the two types of pavements is the manner in which they distribute the load over the subgrade. Due to the rigidity and high modulus of elasticity the rigid pavement tends to distribute the load over a relatively wide area of soil. A major portion of the structural capacity is supplied by the slab itself. The flexible pavement, on the contrary, distributes the load over a relatively small area and consists of layers which will resist the load distributed through them; therefore the highest quality materials are near the surface.

If soil (20-2) stabilized by epoxy and lime is considered to be the material for a flexible pavement (subbase, base and surface course material), the pavement may be designed by the following criteria:

I. Unconfined Compression Test Design

The thickness of flexible pavements are built to such a depth that stress on any given layer will not cause undue rutting, shoving and other differential deformations resulting in an uneven surface. In other words, the thickness is determined by the total load applied at the surface and in part by the strength characteristics of the subgrade. A formula derivable from Boussinesq's equation for thickness design is given below (10)

$$T = \left[\left(\frac{q}{q - p} \right)^{2/3} - 1 \right] \pi Z^2$$

where T = the steel load

q = load intensity on loaded area

p = the vertical pressure transmitted to the surface at depth Z.

Assuming $q = t = 70$ psi where t is inflation pressure, the above equation then becomes*:

$$T = 220 \left[\left(\frac{70}{70 - p} \right)^{2/3} - 1 \right] z^2$$

The maximum immersed strength for the specimen of 20-2 soil containing 5 percent epoxy and 2 percent lime is 470 psi. Taking the immersed strength proportional to the epoxy content the specimen of 20-2 soil with 1 percent epoxy and 2 percent lime would have 94 psi immersed strength. According to Terzaghi (23), the ultimate bearing capacity for cohesive soil in footing design is approximately 3.5 times that of pressures which cause the specimen to fail. Therefore, the bearing capacity for 1 percent epoxy and 2 percent lime combination for 20-2 is 320 psi. If the highway is constructed within Iowa, the bearing capacity should be reduced to $320 \times 97.5 = 320$ psi according to the reduction from Iowa Freeze-Thaw Test results. Further, if the factor of safety for bearing capacity is 5 the maximum bearing capacity of 20-2 after stabilizing with 1 percent epoxy and 2 percent lime is 64 psi. Then from the formula given above (10) setting $p = 64$ the protective layer for 16,000 wheel load (T) is 4 inches.

II. CBR Design

Base materials for flexible pavements are required to have design CBR values not less than 80 (26). If a 16,000 lb wheel load is selected

* The formula is not applicable beyond $t = 70$ and $z = 0$.

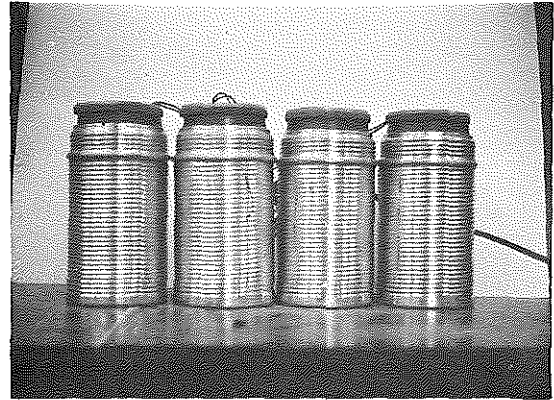
as a maximum wheel load for commercial vehicles on highways and if the natural subgrade at construction site has a CBR value of 6, the thickness of the required protective layer lying above the natural subgrade is 19 inches. The thickness was obtained from Figure 15 which was developed by the Corps of Engineers for the design of flexible highways. The CBR value of the natural subgrade would rise up to 10 after compaction (Table 12). Then the protective layer above the compacted subgrade would require 14 inches. The relative thickness is shown in Figure 17. The thickness design may be latered if different materials are available at the construction sites. They are discussed in the following different cases.

a. If subbase material with a CBR value of 40 is available near the construction site, or if the subgrade soil can be stabilized up to a CBR of 40 by adding 1 percent epoxy and 2 percent lime, the necessary protective layer would be 7 inches over the subbase as shown in Figure 18a.

b. According to the predictions of the CBR test, 2 percent epoxy and 2 percent lime can bring 20-2 soil up to a CBR value of 100. If this stabilized soil were used as a base material, the necessary surface thickness is 4 inches. When compared with unconfined compression test design this result corresponds to a safety factor of 5. The cross-section is shown in Figure 18b.



(a) Friable loess -- the two specimens on the right were untreated; the other 2 specimens contained 7 percent epoxy and 2 percent lime.



(b) Plastic loess -- the 2 specimens on the right were untreated; the other specimens contained 7 percent epoxy and 2 percent lime.



(c) Kansas gumbotil -- the 2 specimens on the right were untreated; the other 2 specimens contained 7 percent epoxy and 2 percent lime.



(d) Four pairs of the treated specimens from four kinds of soils remained intact in the water after immersing 11 days.

Figure 15. Effect of three cycles of alternal freezing and thawing on untreated and treated soil specimens.

Pavement thickness (inches)

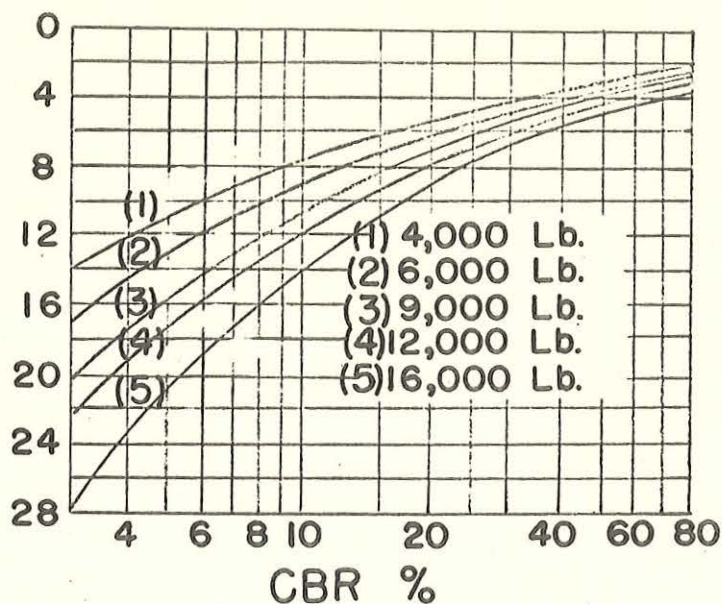


Figure 16. Design curves for flexible highways by Corps of Engineers (from Yoders, Principles of Pavement Design) (21).

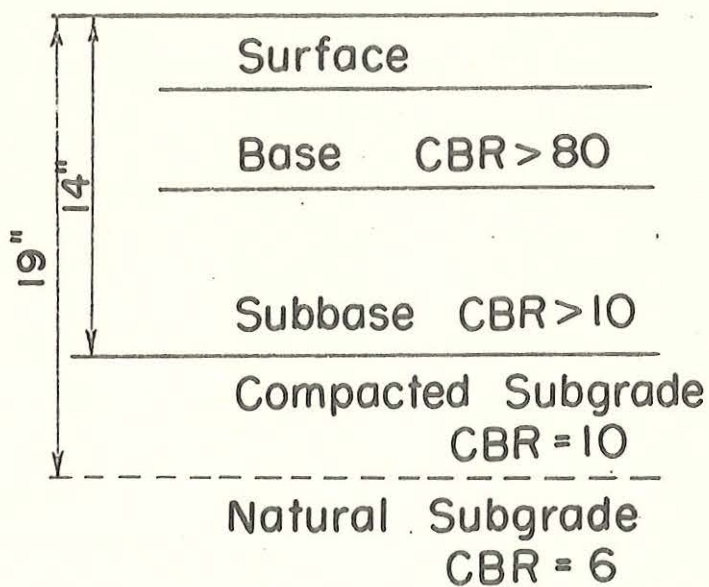


Figure 17. Pavement thickness for 16,000 wheel load, based on CBR value.

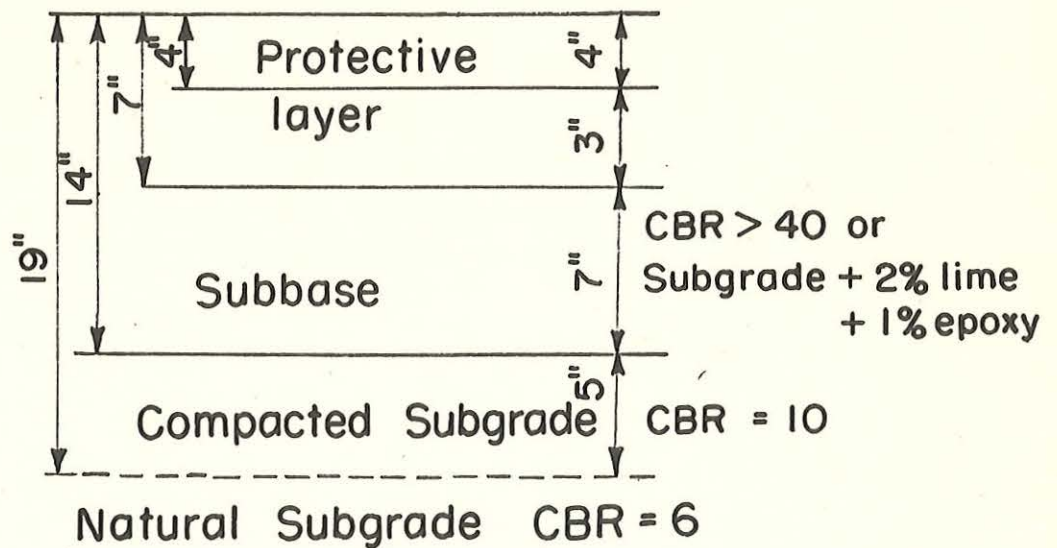


Figure 18a. Pavement thickness for 16,000 lb. wheel load on friable loess based on CBR value of epoxy -- lime stabilized subbase.

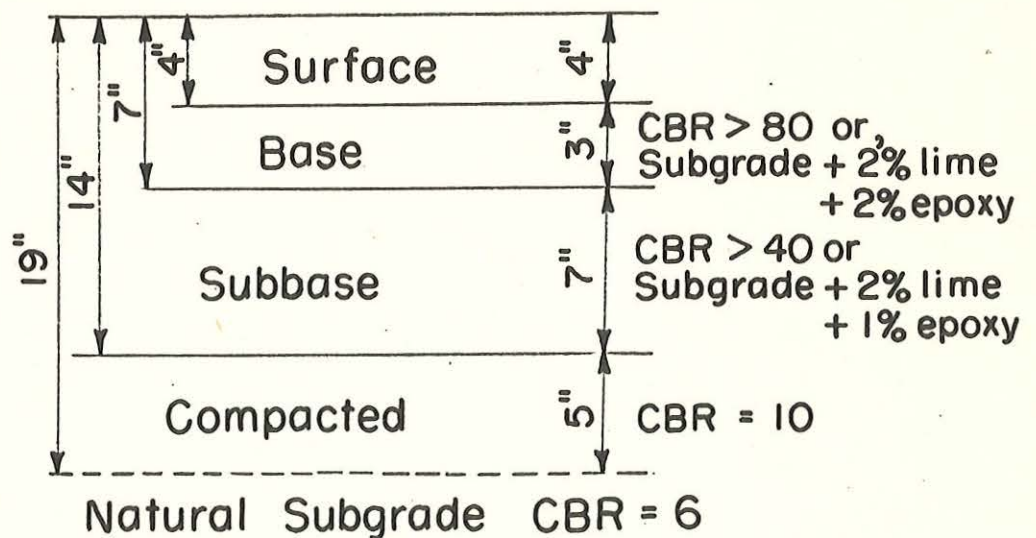


Figure 18b. Pavement thickness for 16,000 lb. wheel load on friable loess based on CBR value of various epoxy-lime contents.

Wearing Surface Material

The data obtained with epoxy-lime-soil specimens in unconfined compression and CBR tests suggested the evaluation of the mixtures' suitability as wearing surface materials. The chief function of a surface course is to provide a smooth surface resistant to traffic and to impart some shearing resistance to the pavement with added resistance to deformation.

The Hveem Test, developed by the California Division of Highways, utilizes a stabilometer and a cohesiometer to test the friction and cohesion of flexible-pavement materials. The deformation in the stabilometer test is expressed as a function of the ratio of the transmitted lateral pressure to that of the applied vertical pressure. With selected epoxy-lime contents, mixtures were molded and tested according to the specification of test method No. Calif. 301-A (22). The compaction of the test specimen was accomplished by means of the mechanical compactor which imparts a kneading action consisting of a series of individual impressions made with a ram having a face shaped as a sector of a 4 inch diameter circle. A 350 psi pressure was applied with a kneading action one hundred times to each 2 1/2 by 4 inch specimen. The specimens were cured by the method described in phase 2 and immersed in 140^oF water for half an hour prior to testing.

Cohesion was measured by means of the Cohesiometer test. The test was run according to the specifications of No. Calif. 306-A (22).

The results of the two tests are presented in Table 13. The suitability of the plant-mixed surfacing by the Hveem method is deter-

Table 13. Effect of epoxy and lime on Hveem Test and related properties of friable loess

Epoxy 120A %	120B %	Calcitic hydrated lime %	Volatile content during molding %	Dry Density pcf	Stabilometer value R	Cohesimeter C
9	3.6	2	10	115	96	grams per inch width with corrected to a 3 inch height
				115	95	
				117	66	1085
				116	78	950
						--

* from formula $R = 100 \frac{100}{\frac{2.5}{D} \left(\frac{P_v}{P_h} - 1 \right) + 1}$ for soil only

P_v = 160 psi vertical pressure

D = turns displacement reading

P_h = horizontal pressure during 160 psi vertical pressure

** from formula $R = \frac{22.2}{\frac{P_h D}{P_v - P_h} + 0.222}$

P_v = 400 psi vertical pressure

P_h = horizontal pressure during 400 psi vertical pressure

mined on the basis of whether or not the asphalt content and aggregate grading will satisfy the following requirements (4).

	Light Traffic	Medium Traffic	Heavy Traffic
Stabilometer Value R	30+	35+	37+
Cohesimeter Value C	50+	50+	50+

No specification has been established for epoxy-stabilized mixtures. However, both R and C values obtained from epoxy stabilized soil mixtures are far greater than the values presented above for heavy traffic conditions for asphalt surfacing courses.

Traffic Simulator for Checking Behavior of Epoxy-Lime-Soil Mixtures

The Traffic Simulator test was devised primarily as a check on the behavior of paving mixes under a moving load. The equipment was developed by the Bituminous Research Laboratory, I.S.U. (7). The six specimens used in this test were identical with those used in Hveem stability tests. An oscillating carriage provided loading on the test specimens with a moving wheel. Only one way traffic over the test specimens was simulated. Forty pounds load was used in the tests conducted because this load provides an equivalent of 80 psi tire loading on the specimens. Generally, evaluations and comparisons of the behavior of mixes have been based on the specimens after 5,000 passes. Mixes that show a displacement of more than 1/8 inch at or before 5,000 passes are arbitrarily deemed suspect to distress under traffic. The test was conducted at room temperature. Distilled water was sprayed, by hand, on the tops of No. 1 and No. 2 specimens shown in

Figure 15 during operation in order to investigate whether or not the specimens would be affected by a moving load during wetting.

Since the inside diameters of the specimen holding rings were slightly over 4 inches, the specimens fitted loosely in the rings. The No. 2 and No. 6 specimens were tightened by inserting metal shims around their sides. The other four samples were tightened by nails, as shown in Figure 19. When the carriage rebounded due to the thrush springs in the ends, the specimens tightened by nails gradually loosened and hit the cover. After 8,550 passes the surfaces of the loose test specimens deteriorated to the point of failure. Tight specimens (No. 2 and No. 6), however, remained intact with no evidence of failure. The average deformations of No. 1 and No. 2 specimens, measured by Ames dials, were 0.03 and 0.025 inches after 8,550 and 5,000 passes (corresponding to 1.2 and 1.0 percent deformations), respectively. In comparison with the results obtained by Csanyi (7), the specimen with 9 percent epoxy had less deformation than those asphalt Ocheydan aggregate mixes containing 4 to 8 percent asphalt.

Flexural Strength

If epoxy-soil mixes are treated as rigid pavement materials, the flexural strength, or the modulus of rupture, for each specimen might be determined by the beam breaking test. The molding and testing procedure was based on the method of test for flexural strength of soil cement, using a simple beam of 3 by 3 by 11 1/4 inch size with third point loading, suggested by Felt and Abrams in ASTM (1). The beam was molded with a dry density of 106 pcf which is the maximum

dry density of the 20-2 specimen containing 9 percent epoxy obtained in the phase 2 investigation. The beam was cured one day in a 104^oF oven and soaked in water for 24 hours prior to testing. The modulus of rupture for the specimen of 20-2 soil with 9 percent epoxy content was calculated to be 225 psi after testing. A specimen of the same soil with 15 percent Portland cement, molded and tested as a dry soil beam by Tinoco (24) yielded a modulus of rupture of 140 psi. The value of modulus of rupture from the epoxy-lime-soil beam was inferior when compared with that of concrete pavement material which ranges from 600 to 750 psi (17).

The results of Hveem, traffic simulation, and flexural strength tests suggest that epoxy stabilized soil may be used as a semi-rigid surface coarse material.

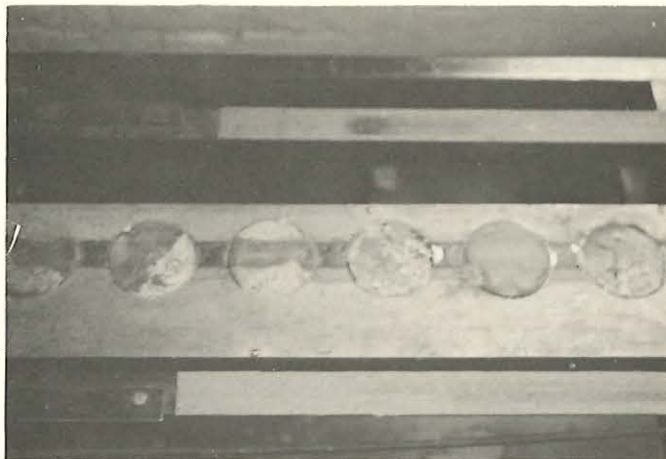


Figure 19. Effect of 8,500 passes of the Traffic S. T. on six specimens, which were numbered from the right specimen to the left.

FURTHER INVESTIGATION OF MIXING ORDER

When lime was mixed directly with a prepared epoxy-hardener solution prior to adding the mixture to the soil, the specimen would yield greater immersed strength than the specimen molded with the mixing order presented in the phase 2 investigation. In other words, the following mixing order for soil-epoxy-lime mixes was the best one so far investigated for getting good immersed strength.

1. Air dry soil with the required amount of distilled water was mixed with a Hobart model C-100 mixer at low speed for one minute and was then hand-mixed.

2. Two percent calcitic hydrated lime based on the oven dry soil weight was added to the prepared epoxy-hardener mixture. The mixture was then stirred with a spatula to insure a uniformity before using.

3. The soil-epoxy-lime mixture was then mechanically mixed for two minutes, followed by hand-mixing for a minute.

A preliminary investigation showed that the specimens of friable loess containing 7 percent epoxy and 2 percent lime had 22 percent strength gain if the above mixing order was used rather than the mixing order presented in phase 2 investigation. This procedure of mixing is suggested for further study on epoxy-lime stabilization.

CONCLUSIONS

The following conclusions were reached on the basis of this investigation on four different soils:

1. After the soils were stabilized with various percentages of epoxies, all were found suitable as base course materials. Traffic Simulator Tests have shown that the resistance of epoxy-treated soils against the abrasive action is excellent, therefore epoxy or epoxy-lime stabilized soils may be tried as a road surface material.
2. The effectiveness of epoxy treatment depends on the clay content. High clay contents give the least satisfactory results. The epoxy stabilization is most effective for the friable loess.
3. All soils used in this investigation were improved in immersed strengths by the addition of lime to the soils to be stabilized by epoxy.
4. Epoxy affects soils in two ways: (1) it reduces the moisture affinity of clays by surface chemical action, and (2) it imparts cementation, thereby producing a semirigid soil framework. The lime is believed to be an agent which causes the cured epoxy to be a more ductile material. This may be responsible for increased immersed strengths of soil specimens.
5. The higher the curing temperature, the faster the setting of epoxy stabilized soil. Curing temperatures between 30°F and 104°F were found most practical for curing epoxy stabilized soil specimens. The short curing time for epoxy makes it an ideal stabilizing agent for emergencies. The epoxy dune sand mixtures with lime could be hardened

at 80°F in half an hour.

6. Because of the high-cost epoxy (\$0.60 per pound) compares unfavorably with other methods of soil stabilization. However the cost of epoxies has shown a very rapid decline. If this trend continues epoxy may be an economic stabilization agent for future.

ACKNOWLEDGEMENTS

This research was done at the Iowa Engineering Experiment Station, Iowa State University, under Project 505-S, Chemical Stabilization and Physico-Chemical Properties of Soils. This project was sponsored by the Iowa Highway Research Board under Project HR-97 and was supported with funds from the Iowa State Highway Commission and the U. S. Bureau of Public Roads.

LITERATURE CITED

1. American Society for Testing Materials. Standard methods of freezing-and-thawing tests of compacted soil-cement mixtures. A.S.T.M. Standards Designation D 560-57. Philadelphia, Pennsylvania. Author. 1958.
2. _____ . Tentative method of test for compressive strengths of hydraulic cement mortars. A.S.T.M. Standards. Part 3, Designation C 109-54T. Philadelphia, Pennsylvania. Author. 1955.
3. _____ . Index to the X-ray power data file. Philadelphia, Pennsylvania. Author. 1959.
4. The Asphalt Institute. Mix design methods for asphalt concrete and other hot-mix types. College Park, Maryland. Author. 1963.
5. Billmeyer, F. W., Jr. Textbook of polymer science, New York. Interscience publisher. 1962.
6. Burns, C. D. Laboratory and field study of epoxy-asphalt concrete. U. S. Army Corps, Engineer Waterways Experiment Station, Tech. Rept. No. 3-638, Jan. 1964.
7. Csanyi, L. H. and Fung, H. P. Traffic Simulator for checking mix behavior. Bituminous Research Laboratory, Iowa Engineering Experiment Station, Iowa State University of Science and Technology, Ames, Iowa. 1963.
8. Cotton, M. D. Early soil-cement research and development Portland Cement Association and Development Laboratories. p. 12. Bulletin D 42 Skokie, Illinois. 1959.
9. Davidson, D. T. and Chu, T. Y. Some laboratory tests for the evaluation of stabilized soils. Unpublished paper presented at the 58th Annual Meeting of the American Society for Testing Materials, Atlantic City, N. J. Mimeo. Ames, Iowa. Engineering Experiment Station, Iowa State University of Science and Technology. 1955.
10. Demirel, T. Use of calcium lignosulfonate with aluminum sulfate for soil stabilization. Unpublished M.S. thesis. Ames, Iowa, Library, Iowa State University of Science and Technology. 1959.
11. Department of Science and Industrial Research Road Laboratory. Soil Mechanics for road engineering. Harmondsworth, Middlesex, England, 1951.

12. George, Kalankamary P. Development of a freeze-thaw test for evaluating stabilized soil. Unpublished M.S. thesis. Ames, Iowa, Library, Iowa State University of Science and Technology. 1961.
13. Klug, H. P. X-ray diffraction procedurers. New York, John Wiley & Sons, Inc. 1954.
14. Lambe, T. W. Stabilization of soils with calcium acrylate. Boston Society of Civil Engineers 38 127-154, 1951.
15. Lee, H. and Neville, K. Epoxy resins. New York, N. Y. McGraw-Hill Book Company, Inc. 1957.
16. Mainfort, R. C. A summary report on soil stabilization by the use of chemical admixtures. U. S. Civil Aeronautics Administration Technical Development and Evaluation Center. Technical Development Report No. 136, February 1951.
17. Portland Cement Association. Concrete paving design for roads and streets carrying all classes of traffic. Chicago, Illinois. Author. 1951.
18. Roderick, G. L. Use of polystyrene for soil stabilization. Unpublished M.S. thesis. Ames, Iowa, Library, Iowa State University of Science and Technology, 1963.
19. Sheeler, J. B. Stabilization of loess with aniline-furfural. Highway Research Board proceeding 36. Jan. 1957.
20. The Shell Chemical Company. The properties of cured epoxy resin. Private Communication Union, New Jersey. 1963.
21. Skeist, I. Epoxy resins. New York, N. Y. Reinhold Publishing Corporation. 1958.
22. State of California Department of Public Works Division of Highways. Materials and Research Department Laboratory, Manual of California Standard Test Procedures, California. 1955.
23. Taylor, L. D. Fundamentals of soil mechanics. New York, N. Y. John Wiley and Sons, Inc. 1958.
24. Tinoco, F. H. Structural properties of cement stabilized soils. Unpublished M.S. thesis. Ames, Iowa, Library, Iowa State University of Science and Technology, 1963.
25. Winterkorn, H. F. A laboratory study of the soil stabilizing effectiveness of artificial resins with special emphasis on the aniline-furfural resins. U. S. Civil Aeronautics Administration Tech. Development Note 43. January 1947.

26. Yoder, E. J. Principles of pavement design 3rd. ed. New York, N. Y. John Wiley and Sons, Inc. 1964.

AMENDMENT TO THE FINAL REPORT

Results of Screening Studies

Preliminary screening of urea-formaldehyde, urea-formaldehyde-spent sulfite liquor, polystyrene-spent liquor, reclaimed rubber, and reclaimed rubber-spent sulfite liquor were done by using the screening test developed earlier at Iowa State.¹

Sample:

The test utilizes 1 inch high by 1/2 inch diameter test specimens. This small size results in considerable savings of time and materials, and is sufficiently large for clays, silts, and fine sands. Only the portion of the soil which passes the No. 40 sieve is used, since large particles and conglomerates would unduly influence the characteristics of the specimens. The minus No. 40 portion, with its higher percentages of clay-size material and increased surface area, provides a more rigorous test of effectiveness.

Apparatus:

The molding apparatus consists of a lever arrangement by which the soil mixture is compressed by hand into a cylindrical mold.

The unconfined compression testing machine automatically plots stress versus strain by means of a lever system which is controlled by the relative motion of parts of the machine during loading. This machine was modified after the British Building Research Station apparatus.

Procedures:

The soil, additives, and enough water to bring the sample approximately to optimum liquid content, are thoroughly mixed by hand with a spatula. The required amount of the mixture to give a 1" by 1/2" specimen of the desired

¹Roderick, G. L. Demirel, T. and Davidson, D. T., Use of phosphoric acid and furfuryl alcohol for soil stabilization. Proc. Iowa Academy of Science, V. 69, pp. 370-379, 1962.

density is placed in the mold and compressed by static pressure on the lever. The sample is then extruded and cured. After curing, one-half of the samples are tested for unconfined compressive strength; the other half are immersed in water for 24 hours and tested.

Results:

The results obtained primarily reflect the cohesive strength of the soil-additive system. The test after immersion reflects waterproofing ability of the stabilizer.

Soil: The soil subjected to the screening tests was a silty clay loess. It contained 80 percent silt and 20 percent clay.

Urea formaldehyde: The liquid urea-formaldehyde resin used in this study was Foramine 21-019 produced by Reichhold Chemicals, Inc. Catalysts used were ammonium chloride and phosphoric acid. Satisfactory and consistent strengths were obtained with 9 percent urea formaldehyde and 1 percent phosphoric acid (average dry strength 300 psi, average immersed strength 200 psi) and 9 percent urea formaldehyde and 2 percent ammonium chloride (average dry strength 500 psi, average immersed strength 200 psi). Samples made with lower percentages of these additives showed sudden drops in strength. Addition of spent sulfite liquor (from 2 to 8 percent) lowered both the dry and the immersed strengths as much as 50 percent. Further investigation of urea-formaldehyde, soil systems is suggested.

Polystyrene-spent sulfite liquor: Earlier investigations at Iowa State had shown that a benzene solution of polystyrene to be an effective soil stabilization agent¹. The purpose of the present screening investigation

¹Roderick, G. L. and Demirel, T. Soil stabilization with polystyrene. Proc. Iowa Academy of Science, V. 71, pp. 369-376. 1964.

was to find out if spent sulfite liquor could replace part of the polystyrene. The polystyrene used was plaspan 8 produced by The Dow Chemical Company. Plaspan 8 was desolved in benzene before adding it to the soil. Addition of spent sulfite liquor increased the dry strength slightly but reduced the immersed strength. Addition of 4 percent spent sulfite liquor increased the dry strength of the soil stabilized with 9 percent polystyrene from 1400 psi to 1700 psi but reduced its immersed strength from 500 psi to 300 psi. On the basis of results obtained detailed investigation of spent sulfite liquor as a secondary additive with polystyrene stabilization is not recommended.

Reclaimed Rubber: The reclaimed rubber used in this study was obtained from Midwest Rubber Reclaiming Company. It was desolved in Creosote oil prior to addition to the soil. The solution consisted of 1 part reclaimed rubber and 3 parts Creosote oil. The percentages of reclaimed rubber and creosote oil added to the soil were 2, 4, 6 percent rubber and 6, 12, 18 percent creosote oil. A third combination tried consisted of 4.5 percent reclaimed rubber 13.5 percent Creosote oil and 4.5 percent spent sulfite liquor. None of the strengths obtained with these formulations gave satisfactory strengths; all dry strengths were about 100 psi and all immersed strengths were about 20 psi. On the basis of these results a detailed investigation of these additives is not recommended.